Charles University in Prague

Faculty of Science

Department of Biochemistry

Mgr. Zdeněk Kukačka

Characterization of protein structures using chemical cross-linking and mass spectrometry

Charakterizace struktury proteinů pomocí chemického zesítění a hmotnostní spektrometrie.

Ph.D. Thesis

Supervisor: RNDr. Petr Novák, Ph.D.

Prague 2015

To my dearest wife Karolína Kukačková

Declaration

I declare that I have worked on this thesis under the guidance of my supervisor and that all sources of the previous knowledge are properly cited. No part of this work was used and will not be used for obtaining any other academic degree than Ph.D. from Charles University in Prague.

Prague .....

.....

Mgr. Zdeněk Kukačka

Declaration of authorship

I declare that Zdeněk Kukačka contributed significantly (25 – 70%) to the experiments and to all 3 scientific publications contained in this Ph.D. thesis. He performed most of the experiments, substantially contributed to their planning, and took a significant part in the primary data interpretation and their preparation for the publication.

Prague .....

.....

RNDr. Petr Novák, Ph.D.

Acknowledgements

First, I would like to thank my family, especially my wife for her endless support and tolerance during all of my overnight and weekend experiments.

Next, I would like to thank my supervisor, Petr Novák for guidance, valuable advice, patient support and almost unfettered freedom during the work on this thesis. In addition, I really appreciate that he opened to me the scientific world not only in his laboratory but also during the conferences, meetings and fellowships.

Many thanks belong also to Petr Man and Petr Pompach who helped me always, not only at the time when I was in MS trouble.

Very special thank goes to Ljubina Ivanova and Daniel Kavan for her big support and understanding and his advices. The doors of their labs were always open when I needed anything.

Thanks belong also to my other former and current colleagues, classmates or labmates from the Laboratory of Structural Biology and Cell Signalling and Laboratory of Protein Structure Characterization for many advices and creating great atmosphere at the Institute, namely to Lucie Hernychová, Eliška Pospíšilová, David Adámek, Josef Chmelík, Alan Kádek, Hynek Mrázek, Daniel Rozbeský and Pavel Talacko.

I should not forget to thank my bachelor and later diploma student Michal Rosůlek, who considerably helped me with the preparation of many experiments.

Last but not least I would like to thank Renata Ptáčková for her advice and support at times when I prepared this Ph.D. thesis.

Finally, this research would not have been carried out without the financial support from the Grant Agency of Charles University (800413 and 644313), Grant Agency of Czech Republic (P207/10/1934), Institutional Research Concept of the Institute of Microbiology RVO61388971, Ministry of Education, Youth and Sports of the Czech Republic and European Regional Development Funds (CZ.1.07/2.3.00/20.0055, CZ.1.07/2.3.00/30.0003 and CZ.1.05/1.1.00/02.0109). Access to instrumental and other facilities was supported by EU (Operational Program Prague – Competitiveness project CZ.2.16/3.1.00/24023).

Abstrakt

Některé bílkoviny k plnění své funkce vyžadují přítomnost specifického ligandu, kofaktoru nebo prostetické skupiny. Vazba této specifické molekuly může v molekulách bílkovin způsobit konformační změny. V některých případech může charakterizace takovýchto konformačních změn představovat velmi náročný úkol. V předkládané práci je popsán nový přístup sloužící ke sledování těchto změn pomocí kombinace chemického zesítění a hmotnostní spektrometrie s vysokým rozlišením. Na modelovém systému, kterým byl zvolen protein kalmodulin, je ukázáno, že analýza pomocí izotopově značených síťovacích činidel umožnuje získat přehled o změnách struktury způsobených přítomností nebo nepřítomností ligandu. Byly rovněž popsány potenciální nedostatky metody, které tkví především v nedostatečné proteolýze proteinu.

Tato nová metoda, která zároveň umožňuje kvantifikaci strukturních změn proteinů, byla použita spolu s dalšími technikami k charakterizaci neutrální trehalasy Nth1 v komplexu s proteinem Bmh1 (kvasinková forma proteinu 14-3-3). Výsledky odhalily, že vazba proteinu Bmh1 vyvolává přeskupení molekuly Nth1 se změnami především v tzv. “EF-hand“ podobném motivu, který je nezbytný pro aktivační proces.

Abstract

Some proteins require presence of their specific ligand, cofactor or prosthetic group for their activity. Binding of this specific molecule can cause conformational changes which permit to perform their function. In some occasions the identification of conformational changes could be really challenging task. In this thesis we describe the novel approach for monitoring structural changes in proteins using chemical cross-linking and high resolution mass spectrometry and its application on model calmodulin system. It is demonstrated that analysis using isotope-labelled cross-linking agents enabled us to get insight into the structural rearrangement caused by presence or absence of the protein ligand. However, it is shown that the method has potential drawback due to limited enzymatic proteolysis.

The novel approach that also makes it possible to quantify the changes in protein structure was used together with other methods for characterization of the neutral trehalase Nth1 in complex with Bmh1 protein (yeast isoform of protein 14-3-3). The results revealed that Bmh1 induce structural rearrangement of Nth1 molecule with changes within the EF-hand like motif which is essential for the activation process.

CONTENTS

ABBREVIATIONS

AP-MALDI	Atmosperic pressure - Matrix-Assisted Laser Desorption/Ionization
BDP-NHP	Biotin Aspartate Prolin-PIR-N-hydroxyphtalimide
CCS	Collision Cross Section
CD	Circular Dichroism
CID	Collision Induced Dissociation
DSG	DiSuccinimidyl Glutarate
DSS	DiSuccinimidyl Suberate
ECD	Electron Capture Dissociation
EDC	1-Ethyl-3-(3-dimethylaminopropyl)carbodiimide
EM	Electron Microscopy
ESI	ElectroSpray Ionization
ETD	Electron Transfer Dissociation
FTICR	Fourier Transform Ion Cyclotron Resonance
FPOP	Fast Photochemical Oxidation of Proteins
H/D	Hydrogen/Deuterium
ICAT	Isotope-Coded Affinity Tags
IM-MS	Ion Mobility Mass Spectrometry
IRMPD	InfraRed Multiphoton Dissociation
LC	Liquid Chromatography
MALDI	Matrix-Assisted Laser Desorption/Ionization
MS	Mass Spectrometry
MS/MS	Tandem mass Spectrometry
NMR	Nuclear Magnetic Resonance
PIR	Protein Interaction Reporter
PKA	cAMP-dependent Protein Kinase
RP-HPLC	Reverse Phase High-Performance Liquid Chromatography
SDS-PAGE	PolyAcrylamide Gel Electrophoresis in presence of Sodium Dodecyl Sulfate
TOF	Time Of Flight
X-Ray	Roentgen crystallography

1 INTRODUCTION

1.1 Protein structure and methods of its determination

1.1.1 Proteins and their role in metabolism

Proteins are one of the building blocks of body tissue. They like other biological macromolecules (biomacromolecules) are essential parts of organisms and participate in all biological processes within cells. Proteins have many crucial roles in all living organisms ranging from bacteria and viruses, through fungi to plants and animals including humans. They function as catalysts, transporters and storage of other molecules as well as provide immune response, generate movement, transmit nerve impulses or control growth and differentiation. [Berg 2002, Whitford 2005].

Proteins are linear polymers that are formed from amino acids. The individual amino acid residues are linked with adjacent residues by peptide bond into long chains (called polypeptides). Although all proteins are composed of the only 20 (excluding selenocysteine and pyrrolysine) L-α-amino acids, these molecules are very complex and differ in size, number of subunits, function and other properties. In addition, proteins could be posttranslationally modified (phosphorylation, glycosylation, disulphide bonds etc.) or covalently/noncovalently bound to other molecules (iron ions, organic molecule, heme group etc.). Each of these modifications can alter chemical and physical properties, stability, activity and ultimately folding and function of proteins [Berg 2002, Voet 2011].

1.1.2 Protein structure

After unravelling the sequence of the genome in many organisms, the number of known proteins rapidly increased. However, most of their structures are still unknown. Unfortunately, the determination of the amino acid sequence is not sufficient for elucidation of three-dimensional protein structure. In terms of structure the above noted amino acid sequence (order of residues in polypeptide chain) is called as “primary structure”. Folding of polypeptide chain into regular structure such as alpha helix, beta sheet, turn or loop is denoted as “secondary structure” and the overall shape of single molecule is referred as “tertiary structure”. If protein assembly consists of more than one molecule then the spatial arrangement of all subunits is referred to as “quaternary structure” (Fig. 1) [Berg 2002, Voet 2011].

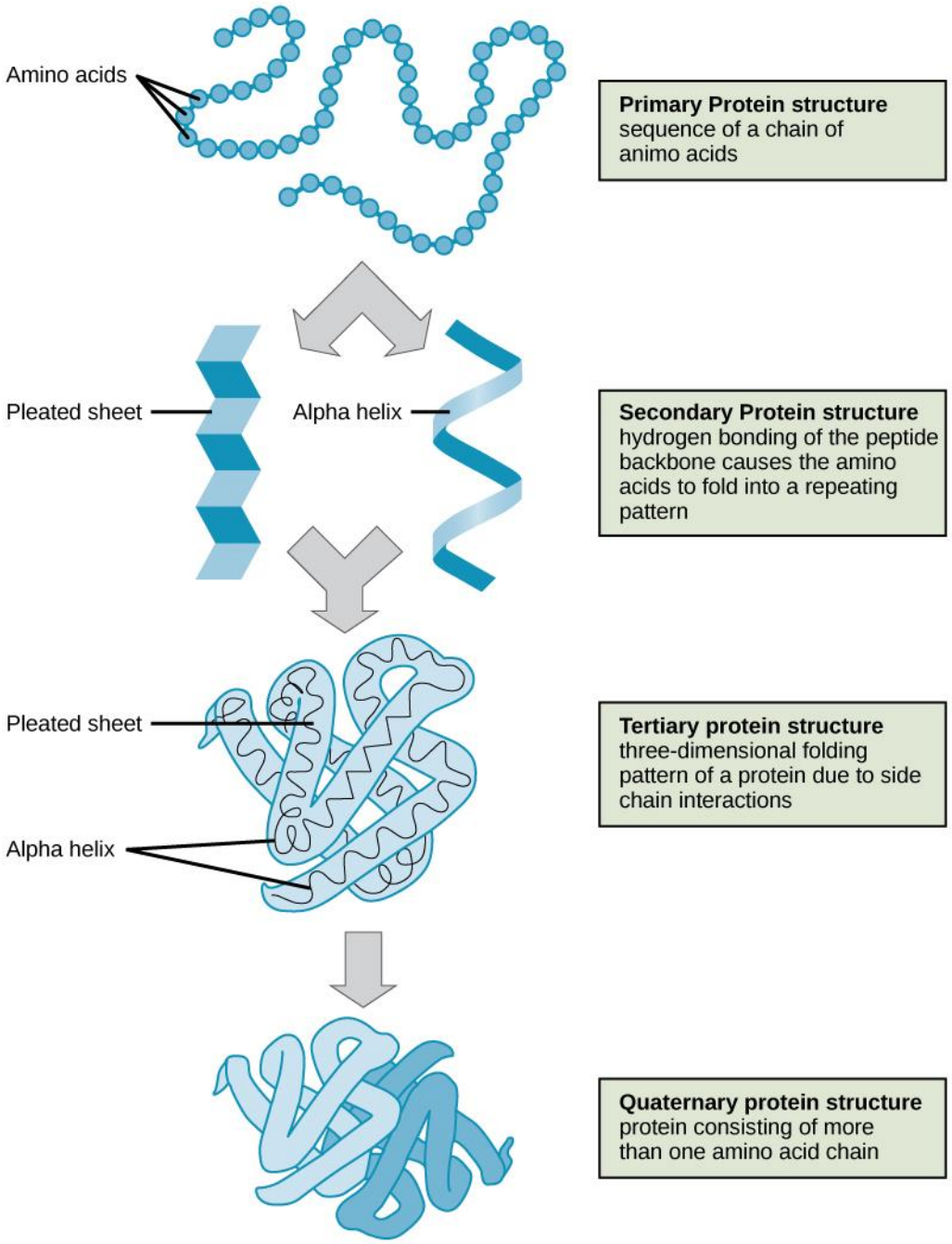

Fig. 1: Different levels of protein structure [Boundless 2014].

Physiological function of proteins in organisms is directly dependent on their three-dimensional structure and therefore elucidation of protein structure may also uncover its physiological function. This is reason why the research of protein structures and development of methods for its determination is still an attractive scientific field.

1.1.3 Determination of protein structure

A number of methods have been employed to address the question of tertiary protein structure, and as a consequence, the mechanisms of complex formation. The most often used techniques are X-ray crystallography (also called Roentgen crystallography) [Parker 2003], and Nuclear magnetic resonance spectroscopy (NMR spectroscopy) [Mittermaier 2006].

X-ray crystallography is a method that helped in solving the three-dimensional structure of proteins in a crystal at atomic level. Its principle is based on the diffraction of X-ray beam on the crystal atoms. The positions of individual atoms in the crystal are determined from the picture of electron density, which is produced by measuring the intensities and angles of diffracted beams. The protein crystal is bombarded with a focused monochromatic X-ray beam, producing a diffraction pattern of "reflections" (regularly spaced spots). The final three-dimensional model of electrons within the crystal is converted from the two-dimensional images taken at different rotations using Fourier transform. X-ray crystallography can provide detailed information about protein complexes but it is difficult to use for analysing large protein assemblies. Also, complexes cannot be always reconstituted from recombinant components. A considerable disadvantage of this method is crystal preparation that requires large volumes of highly concentrated protein and usually takes a lot of time. Moreover, crystals hardly represent a natural solution environment [Ilari 2008, McPherson 1990].

NMR spectroscopy is another method which can be used for determination of tertiary structure of the proteins. It relies on the phenomenon of nuclear magnetic resonance in which electromagnetic radiation energy is adsorbed and re-emited by nuclei which have nonzero spin number and which are placed in a strong magnetic field. The radiation energy is used at a specific resonance frequency (usually 400-1000 MHz) which depends on the strength of the applied magnetic field and the magnetic properties of the studied atoms. The nuclei under study are isotopes that have an intrinsic magnetic moment and angular momentum (nonzero spin) for example ^{1}H or ^{13}C. In contrast to X-ray crystallography, NMR spectroscopy can provide detailed information not only about the structure of molecules but also about their dynamics and reaction states in solution. Unfortunately, the interpretation becomes difficult with the increasing size of the molecules or protein complexes. Although larger structures have been solved, structure determination using NMR spectroscopy is usually limited to proteins or protein assemblies smaller than 40

kDa. Considerable amounts of material that have to be isotopically labelled are required, and the resulting structure is an average of various conformations that might exist in solution, which significantly reduces the quality of the information [Marion 2013, Markwick 2008].

Due to limitations of the above described techniques, alternative methods are increasingly used. They include, e.g., cryo-Electron Microscopy (cryo-EM) [Milne 2013], Small-Angle X-Ray Scattering (SAXS) [Glatter 1982], InfraRed Spectroscopy (IR spectroscopy) [Barth 2007], Surface Plasmon Resonance (SPR) [Schuck 1997], thermophoresis [Jerabek-Willemsen 2011], analytical ultracentrifugation [Schuck 2003] or mass spectrometry (MS) that cannot give information about positions of all atoms but can provide information about shape, interaction partners, solvent accessibility or distance constraints between atoms of studied molecule[Kaltashov 2013]. However, from the above mentioned methods only mass spectrometry techniques represent efficient strategy to study the tertiary structure, different conformation states and dynamics of proteins together under physiological conditions. Moreover, mass spectrometry has a very low consumption of sample and time the required for data interpretation is very short [Sinz 2007, Schmidt 2014].

1.2 Characterization of proteins by mass spectrometry

1.2.1 Principle of mass spectrometry

Mass spectrometry is an analytical method that is used to study chemical substances in miscellaneous types of sample. That is why it has spread to the various scientific disciplines. The analytes are during the MS process are ionized, separated in electric and magnetic field and finally detected. From this it is apparent that ionization, separation and detection are crucial processes for this analytical technique and therefore each of them will be described in detail later. For individual ions in the gas phase, mass spectrometers accurately measure so called “mass-to-charge (*m/z*) ratio” where *m* represents the ion’s mass and *z* represents its charge. The result of mass spectrometry measurement is a plot in which *m/z* ratio is on the x-axis whereas on the y-axis is abundance of measured ions. These plots are called mass spectra [Dass 2007].

1.2.2 Ion sources

The first necessary step in mass spectrometry is ionisation (conversion of analytes into gas phase ions) that occurs in ion source. Nowadays there exists a plethora of ion sources each of which is suitable for a specific application. One of from the commonly used ionisation technique is Electron Impact (EI). EI is performed by volatilizing analyte directly in the source that is directly linked to the analyser. During the ionisation process the molecules of samples in gas phase are bombarded by a beam of electrons that is directly formed by heating a filament bias at a negative voltage compared to the source. The beam of electrons is accelerated to 70 eV. Positive molecular ion is formed by removing electron from the highest energy orbital. The series of fragment and radical ions are produced in addition to the molecular ions. The molecular weight of analysed sample can be determined whereas from the fragment ions can be determined the structure of sample. EI is typically used for GC-MS analyses. The big disadvantage of EI is the fact that it cannot be used for ionisation of biomacromolecules [Dass 2007].

1.2.3 Soft ionisation techniques

Although the beginnings of mass spectrometry go back to the end of nineteenth century, the soft ionization techniques for the identification of biomolecules were invented at the end of the twentieth century [Fenn 1989, Karas 1988, Tanaka 1988]. Nobel Prize was awarded for invention of these ionisation techniques in 2002. Only soft ionization techniques such as ElectroSpray Ionization (ESI) and Matrix-Assisted Laser Desorption/Ionization (MALDI) enable the transfer of the high mass biomolecules into ions in the gas phase without undesirable fragmentation. Into the group of soft ionization techniques belong also Fast Atom Bombardment (FAB), Atmospheric Pressure Chemical Ionization (APCI) or Atmospheric Pressure Photo-Ionization (APPI).

The mechanisms of the two main soft ionisation methods are completely different. In the ESI, the liquid, which contain the studied substance, is dispersed by electrospray into an aerosol. This very fine aerosol is sprayed into the vacuum space using a thin capillary which carries a large potential difference (approximately 3000 eV) and which can also be heated to increase evaporation of the solvent from creating droplets (Fig. 2). The size of a charged droplet is steadily decreasing via solvent evaporation to the point when the droplet reaches the so-called Rayleigh limit. At this moment the electrostatic repulsion becomes more powerful than the surface tension that causes that the droplet holds together. This

action leads to Coulomb fission and when the original droplet is broken, forming many smaller but more stable droplets. The new smaller droplets continue in decreasing their size and the process of Coulomb fissions is repeated until the point when the solvent is completely evaporated [Fenn 1989]. The common solvents for ESI are mixtures of water with methanol, acetonitrile or other volatile organic compounds. Volatile substances are used because the ion formation is connected with intensive evaporation of the electrospray solvent. Because with increasing conductivity of the solvent the size of droplet decreases, organic acids (formic acid, acetic acid etc.) in positive mode or bases (ammonium, urea etc.) in negative mode are usually added to the electrosprayed solution. In addition, the acids and bases are an essential source of protons to facilitate the ionization process. To increase sensitivity modern mass spectrometers are equipped with nanospray, i.e. electrospray with a thinner capillary adapted for lower flow rates [Wilm 1994, Wilm 1996]. ESI has many various applications; however, it is typically used for the study of biomolecules in cases when the mass spectrometry is combined with separation by liquid chromatography [Chaurand 2012, Inutan 2012]. In terms of mass spectrometry ESI could be combined with various types of mass analysers.

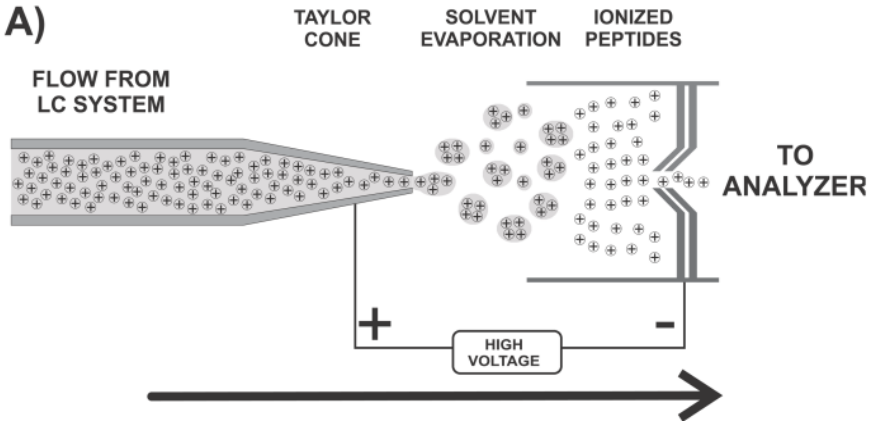

Fig. 2: Principle of ESI (ElectroSpray Ionization) [Demartini 2013].

In the case of MALDI, the sample is first mixed with a solution of a suitable matrix and dried on a special plate. The resulting crystallized mixture is irradiated by laser which leads to the ablation and desorption of the matrix (including sample) that absorbs the energy of the laser (Fig. 3). Finally, molecules of the sample are ionized by de/protonation in the hot plume of ablated gases. The de/protonation occurs due to the transfer of charged particles from the matrix to the sample. [Knochenmuss 2003, Dreisewerd 2003, Karas 2003] Unfortunately, the detailed mechanism is still unclear. Forming charged ions are

accelerated by high electric field into mass analysers where are further processed. MALDI ionisation occurs in vacuum. However, an atmospheric pressure-MALDI (AP-MALDI) technique recently described shows the MALDI can operate also under atmospheric pressure. Unfortunately, the process of ionisation in AP-MALDI is less effective than in vacuum MALDI and therefore this ionisation is not commonly used.

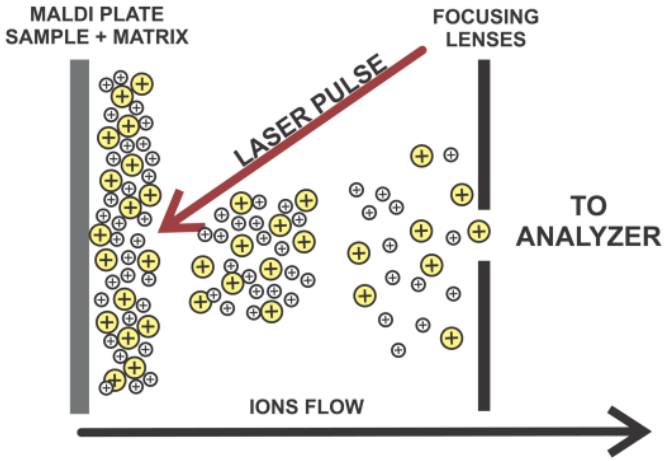

Fig. 3: Principle of MALDI (Matrix-assisted laser desorption ionisation) [Demartini 2013].

As it is apparent from the above facts, the selection of the matrix is a crucial step. The suitable matrices are selected so as strongly and efficiently absorb the laser energy and crystallize with samples without side reaction. They are mostly low mass aromatic acids, for example α-cyano-4-hydroxycinnamic acid (CHCA) or 2,5-dihydroxybenzoic acid (DHB) that cannot to evaporate during the sample preparation. MALDI commonly employs the use of UV lasers such as nitrogen lasers (337 nm), Nd:YAG lasers (266 nm and 355 nm) or IR lasers such as Er:YAG lasers (2.94 mm) and CO_2 laser (10.6 mm). In contrast to ESI that produces multicharged ions, MALDI mostly produces positive or negative ions with one or two charges, which simplifies data interpretation. Typical molecular ions are $[M+/-H]^{+/-}$ or $[M+Na]^{+}$. The relative advantage of MALDI over ESI is the purity of studied samples because the presence of contaminants (salts, detergents) in electrospray significantly decreases the sensitivity of measurement and contaminants also could form adducts with the sample. MALDI is mostly combined with mass analysers with a wide mass range such as TOF (Time of flight) [Aeberslod 2003]. MALDI-TOF and MALDI-TOF/TOF instruments are useful and powerful tools for peptide fingerprinting and proteomic applications generally. Modern mass spectrometers with high resolution (orbitrap, FT-ICR) are usually equipped for both ionisation techniques ESI and MALDI.

1.2.4 Mass analysers

Generally, mass analyser is a component of mass spectrometer which separates the ions in vacuum according to their *m/z* ratio. As previously described, the suitable combination of ion source with mass analyser is a necessary step to achieve satisfactory results. The parameters describing analyser characteristics are resolving power (ability to distinguish signals for samples with similar *m/z* value), mass accuracy (ability to determine correct *m/z* value to the signal), *m/z* range (range of m/z values that can be measured by analyser), linear dynamic range (range over which the signal of an ion is linear with analyte concentration) and acquisition speed (time necessary for measurement; its value is specified in Da/s, Hz or number of measurements) (Table 1) [Holcapek 2012].

Table 1. Common parameters of mass spectrometers used in LC–MS [Holcapek 2012].

Mass analyser type	Resolving power [$\times 10^3$]	Mass accuracy (ppm)	m/z range [$\times 10^3$]	Acquisition speed (Hz)	Linear dynamic range
Q	3–5	Low	2–3	2–10	10^5–10^6
IT	4–20	Low	4–6	2–10	10^4–10^5
TOF	10–60	1–5	10–20	10–50	10^4–10^5
Orbitrap	100–240	1–3	4	1–5	5×10^3
ICR	750–2500	0.3–1	4–10	0.5–2	10^4

Q - quadrupole analyser, IT - ion trap, TOF - time of flight, ICR - ion cyclotron resonance

The principle of ion separation is different for each mass analyser. With sector mass analysers the path and/or velocity of the charged particles are affected using an electric and/or magnetic field. The trajectories of the ions are bent according to their *m/z* ratios. The electric field plays a crucial role also in quadrupole mass analysers because oscillation of electric field is used to affect ions passing through a 4 parallel rods (at any time one pair is positive and the other negative) between which a radio frequency field is also formed. Quadrupole mass analyser works as selective mass filter. Only the ions with certain *m/z* value are passed through the field at a defined potential and frequency on the rods. Similar principles as quadrupole are employed by ion traps (linear ion trap, cylindrical ion trap) that differ only in the arrangement of the system. Other mass analysers, TOF and Fourier Transform - Ion Cyclotron Resonance (FT-ICR) [Comisarow 1974] were used for the measurement of proteins in this Ph.D. thesis and therefore will be described in detail.

TOF mass analyser uses an electric field to accelerate the ions through the same potential, and then measures how long it takes to travel from the source to the detector (Fig. 4) [Stephens 1946]. The separation is based on the kinetic energy and velocity of the ions in a drift tube. Ions of the same charges have equal kinetic energies; therefore their velocities will therefore depend only on their masses. Ions with low *m/z* reach the detector faster than ions with high *m/z*. The time, which the ions spend in drift tube is in the range of ns-µs. TOF analysers, which are typically used with MALDI, have theoretically unlimited *m/z* range, very high sensitivity and mass accuracy, but a limited dynamic range and not so high resolving power. The resolving power can be increase if the TOF instrument is equipped with a reflector. The reflector is an ion mirror with constant electrostatic field that is attached to drift tube and that reflects the ion beam toward the detector. The reflector is used to correction of kinetic energy distribution. Ions with same *m/z* value and different kinetic energy spend a different time in the reflector. Ions with higher kinetic energy penetrate deeper into the reflector, and thus take longer path to the detector. Arrangement of TOF mass spectrometer with reflector is beneficial by increasing the ion flight path.

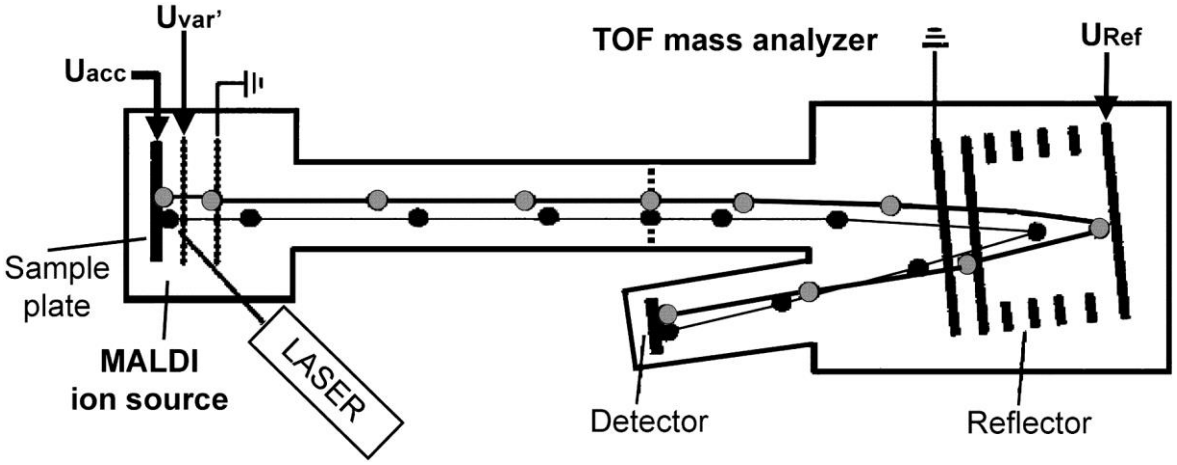

Fig. 4: Scheme of MALDI-TOF instrumentation with reflector. Grey and black dots represent ions with same *m/z* value and different kinetic energy ("black ions" have lower kinetic energy). [Hirsch 2004].

Ion Cyclotron Resonance with Fourier transform for measuring *m/z* value uses the movement of ions in a magnetic field. The ions are accelerated and trapped into a Penning trap (a static electric/magnetic ion trap) where they are effectively excited at their resonant cyclotron frequency. The excitation is caused by an oscillating electric field which is

orthogonal to the magnetic field. Excited ions move in a circular path with increasing size of the orbit. The *m/z* value is determined by detecting the image current produced by cyclotroning ions. Detectors at fixed positions in space measure the electrical signal of ions which pass near them over time, producing a periodic signal. The frequency of an ion's cycling is determined by its mass to charge ratio [Comisarow 1974]. Final mass spectrum (frequency- domain spectrum) is obtained from current image (time domain signal) by performing a Fourier transform (Fig. 5) [Marshall 1998, Marshall 2002, Heeren 2004]. FTICR is a mass analyser with high sensitivity, highest resolving power and thus outstanding mass accuracy [Marshall 2000]. In addition, FTICR is a non-destructive mass analyser.

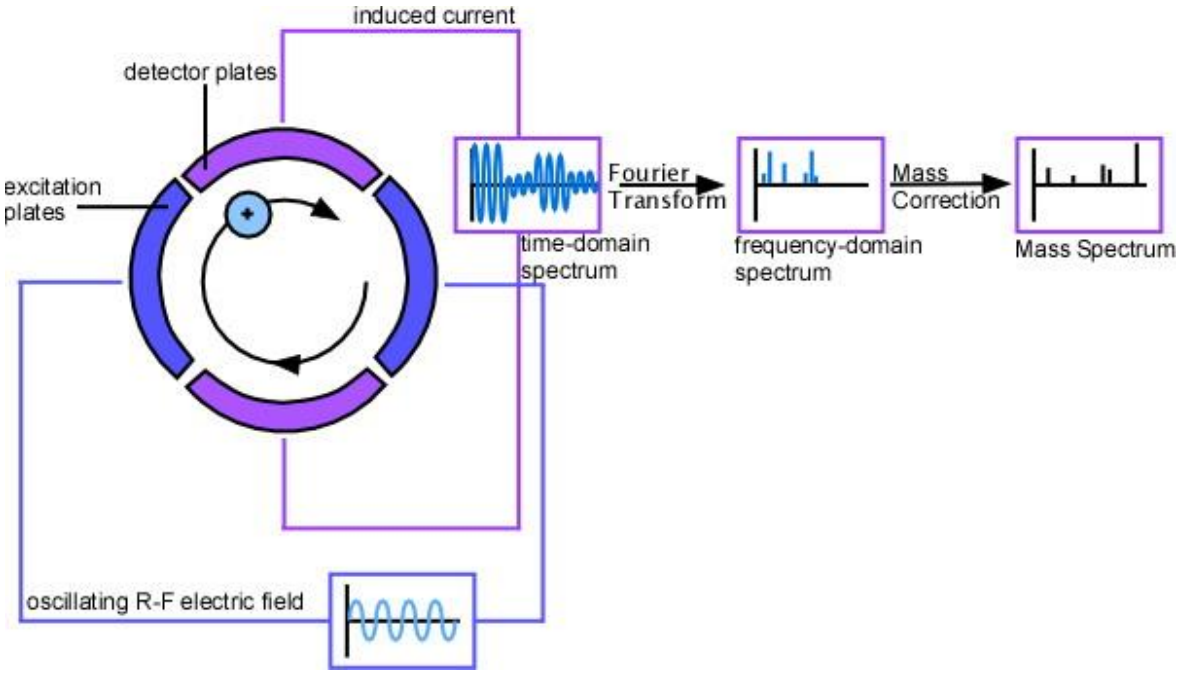

Fig. 5: Principle of FT-ICR mass analyser. [Dunnivant 2014].

Hybrid mass spectrometers consisting of two or more different types of analysers are often used in order to improve device characteristics. Arrangement of at least two mass analysers in series also allows us to carry out MS/MS experiments due to which we can determine the amino acid sequence of peptides and determine the exact location of a modification. The principle of tandem MS is fragmentation of analyte ions, mostly due to collisions with inert gas. The first step of MS/MS experiments is a selection of an ion with certain *m/z* whose fragmentation spectrum we would like to acquire. This so-called precursor ion is subjected to fragmentation using any of the many techniques and

subsequently the spectrum of ions, which are formed from a selected precursor, is subsequently measured. The MS/MS spectrum contains characteristic signals for a series of complementary ions. Mostly it is possible to see b- and y- ions because fragmentation occurs preferably at the peptide bond (Fig. 6). Each signal from b- or y- ion series corresponds to loss of one, two, three etc. amino acids from the peptide C- or N-terminus [Aebersold 2003]. The presence of the amino acid can be determined based on the differences in the value of *m/z* between two consecutive y- or b-fragments can be determine.

Commonly used fragmentation techniques are Collision Induced Dissociation (CID) [McLuckey 1992, Paizs 2005], Electron Capture Dissociation (ECD) [Zubarev 2008] Electron Transfer Dissociation (ETD) [Coon 2009]or InfraRed Multiphoton Dissociation (IRMPD) [Little 1994].

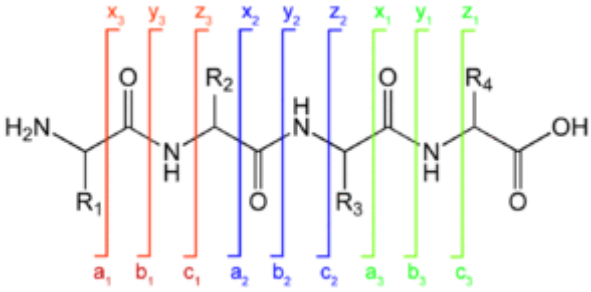

Fig. 6: Fragmentation of precursor ion during MS/MS analysis.

1.3 Mass spectrometry techniques for structural biology

In order to study protein (or generally biomacromolecules) three-dimensional structure, shape, dynamics and interaction of proteins in solution, mass spectrometric approaches seem to be a promising technology where a standard high resolution technique fails. These mass spectrometric approaches can be divided into techniques such as native mass spectrometry and ion mobility, which are not based on covalent modification, and into techniques which use covalent modification. The techniques which are based on covalent modification can be further divided to methods which can be used to monitor changes of protein backbone such as hydrogen/deuterium exchange, and methods which can be used to monitor changes of protein side chains such as covalent labelling or hydroxyl radical labelling. Results obtained from mass spectrometric approaches do not represent spatially high resolution data but can form a basis for generating three dimensional models, mapping protein interaction interface/landscape or refinement of earlier resolved structures, and thus indirectly lead to the elucidation of physiological function [Konijnenberg 2013,Konermann 2014].

1.3.1 Native mass spectrometry and ion mobility

Native mass spectrometry is a relatively new approach for determining intact structure of biomacromolecules and their complexes in the gas phase in the near-native state. The basis of this expanding approach is the theory that the structure of molecules in solution can be identical to their structure in the gas phase [Wyttenbach 2011, Skinner 2012].. The theory is based on previously published papers and studies describing that overall size of a studied molecule and its noncovalent interactions can be conserved in the gas phase. Overall, it is apparent that biomacromolecular ions after desolvation in electrospray can be preserved in a state of local energy minimum under properly optimized conditions the molecular structure retains short-time (in millisecond range common for native MS experiments) stability in properly optimized conditions. Even so it is undisputed that in some cases the transition of biomacromolecules from physiological conditions in solution to the gas phase can affect the native assembly of the studied molecule or complex. For successful native MS it is necessary to perform nanoESI ionization of the sample in a suitable volatile buffer such as ammonium acetate. The characteristic feature of protein conformation in native MS is different distribution of charge states. ESI-MS spectra with higher charge states of ions (lower *m/z*) are typical for unfolded or unstructured proteins because their backbone is more accessible to solvent [Kaltashov 2005]. Opposite are ESI-MS spectra of proteins with native conformation in the gas phase in which lower charge states are presented. Based on the distribution of charge states it is therefore possible to study the dynamics of proteins [Robinson 2007, Robinson 2011].

Additional structural information can be obtained by combining native MS and ion mobility (IM-MS, Ion Mobility Mass Spectrometry) [Bohrer 2008]. The IM-MS investigates the movement of ions in an electric field in the presence of inert gas. The behaviour of ions in an inert gas is characterized by their effective Collision Cross Section (CCS). Via the CCS IM-MS provides information about the size and shape of the analysed biomacromolecules. Noncovalent complexes can be dissociated into individual components using fragmentation techniques in the gas phase. After dissociation, the effective CCS for individual subunits of a complex can be also determined. Subsequent comparison of CCS for the complex and for individual subunits can provide valuable information about the composition and stoichiometry of protein complexes [Sobott 2003, Hyung 2009].

1.3.2 Hydrogen/deuterium exchange

One of the first techniques which utilized covalent modification of proteins for their structural study was hydrogen/deuterium exchange. In the early period, this method was frequently combined with NMR. However, currently it is mostly connected with mass spectrometry, which has several advantages (low sample consumption, no size limitation and rate of interpretation) over NMR. Indeed, the H/D exchange is a time-resolved monitoring of replacement of covalently bonded hydrogen atoms by deuterium atoms and vice versa. The source of deuterium in solution is D_2O solvent in which the studied protein is located. Exchange rate depends on the accessibility of the solvent and the involvement of hydrogen atoms in the hydrogen bonding, which are the main stabilizing factors of the protein secondary structure. H/D exchange represents a very gentle method, since replacement of deuterium atoms for hydrogen has no effect on the tertiary structure. Amide hydrogens which are part of the polypeptide backbone are monitored during the H/D exchange. Hydrogen atoms of functional groups in the side chains are also replaced by deuterium atoms, but their exchange rate is very high and therefore cannot be detected during the measurement. On the contrary, hydrogen atoms of the peptide bond are exchanged very slowly and this is the reason why the exchange also cannot be detected during the measurement. This technique provides information about the surface accessibility of studied molecules [Iacob 2013, Konermann 2011]. Based on the obtained data, it can be deduced which part of the molecule is in the interaction with a ligand or which part of the molecule changed its conformation. A big disadvantage of H/D exchange is the so called back exchange. Back exchange is a phenomenon in which deuterium atoms are back replaced by hydrogen atoms. Temperature and pH of solution have a crucial effect on back exchange (Fig. 7).

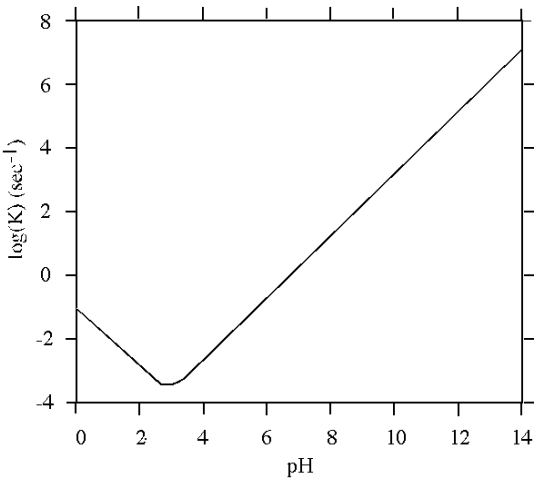

Fig. 7: A plot describing the dependence of exchange rate constant on reaction pH [Bai 1993].

The dependence of the exchange on pH rate can be expressed by the equation

$$k_r = k_{H^+} 10^{-pD} + k_{OH^-} 10^{(pD - pK_D)} + k_{H_2O}$$

where k_r is the rate constant of exchange, K_D represents the constant of D_2O dissociation, pD is pH value correlated for deuterated buffer, k_{H+} and k_{OH-} are rate constants for acid and base catalysis, k_{H2O} is a rate constant of exchange catalysed by water [Bai 1993]. Temperature dependence for a model peptide at 20°C can be expressed by the equation

$$k_r(T) = k_r(293) e^{\frac{-Ea\left[\frac{1}{T} - \frac{1}{293}\right]}{R}}$$

where k_r is the rate constant of exchange, T represents reaction temperature, Ea is activation energy of reaction and R is universal gas constant. The above equation implies that the kinetics of replacement is the slowest at 0°C and pH 2.5-3.0 (Fig. 7) [Bai 1993].

1.3.3 Covalent labelling and hydroxyl radical labelling

Covalent labelling (also referred to as "footprinting") is a technique that provides information about the solvent accessibility of side chains. Exposed regions can react with a covalent probe, whereas regions inside the molecule are protected. Side chain modifications formed during covalent labelling are highly stable and therefore the back exchange is not possible. Unfortunately, interpretation of acquired LC-MS spectra can be complicated because digestion of labelled peptides can be altered and also differentially labelled peptides are eluted from the LC system at different retention times.

A really broad range of chemical probes have been developed during the last twenty years including isotope-coded affinity tags (ICAT) or probes that can absorb UV light pulse, thus enabling the specific photo-dissociation of labelled peptides. Beside the determination of structure and interactions of proteins and protein complexes, the covalent labelling techniques have been successfully applied for exploring nucleic acids.

A special type of covalent labelling is labelling by hydroxyl radical (•OH). Hydroxyl radical labelling utilizes the highly reactive •OH which causes oxidative modifications of solvent exposed side chains. Although hydroxyl radical react with all types of residues, sulphur-containing and aromatic residues react significantly faster than aliphatic or negatively charged side chains (**Chyba! Nenalezen zdroj odkazů.**).

Table 2. A list of reaction rates of hydroxyl radical labelling for all amino acid residues [Chen 2012].

	HO^-	
substrate	rate (M^{-1} s^{-1})	pH
Cys	3.5×10^{10}	7.0
Trp	1.3×10^{10}	6.5–8.5
Tyr	1.3×10^{10}	7.0
Met	8.5×10^{9}	6–7
Phe	6.9×10^{9}	7–8
His	4.8×10^{9}	7.5
Arg	3.5×10^{9}	6.5–7.5
cystine	2.1×10^{9}	6.5
Ile	1.8×10^{9}	6.6
Leu	1.7×10^{9}	~6
Val	8.5×10^{8}	6.9
Pro	6.5×10^{8}	6.8
Gln	5.4×10^{8}	6.0
Thr	5.1×10^{8}	6.6
Lys	3.5×10^{8}	6.6
Ser	3.2×10^{8}	~6
Glu	2.3×10^{8}	6.5
Ala	7.7×10^{7}	5.8
Asp	7.5×10^{7}	6.9
Asn	4.9×10^{7}	6.6
Gly	1.7×10^{7}	5.9

The reaction rate is naturally affected by ambient conditions (pH, temperature etc.). Various methods can be used for •OH formation; for example, synchrotron radiolysis [Wang 2011], γ-irradiation [Schorzman 2011], pulsed electron beams, electrochemical flow cells or FPOP (Fast Photochemical Oxidation of Proteins) [Chen 2012]. In the case of FPOP, •OH is produced by UV laser photolysis of dilute H_2O_2 inside a continuous-flow capillary tube. Labelling by •OH is extremely fast. It has been estimated that oxidation occurs on a microseconds and is thus faster than most conformational changes. Therefore FPOP provides the opportunity to gain insight into the structures of short-lived folding intermediates (Fig. 8). However, this approach can also be used for monitoring protein–protein interactions, protein–DNA complexes, epitope mapping or integral membrane protein studies [Fabris 2012, Konermann 2010, Kiselar 2010, Takamoto 2006].

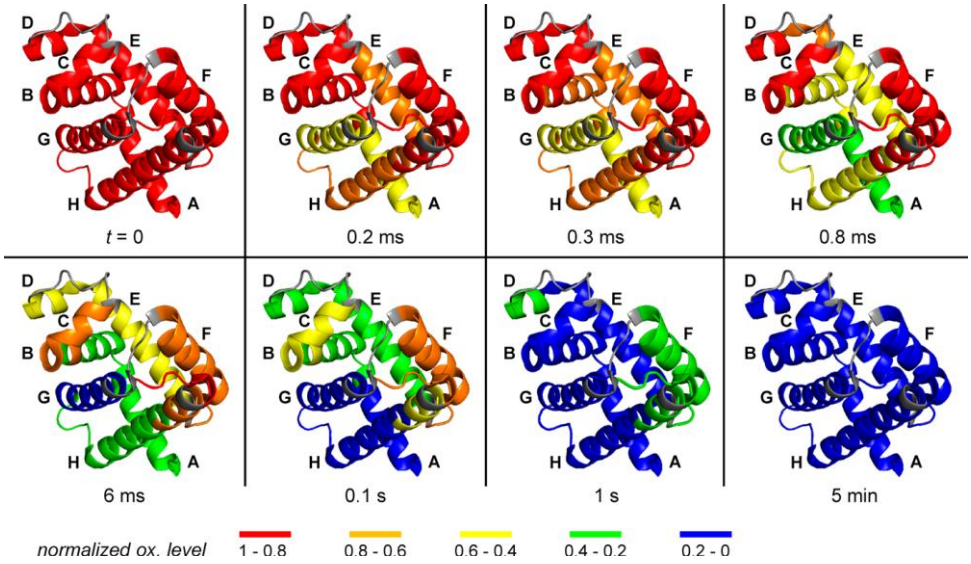

Fig. 8: Structural changes of myoglobin folding measured by fast photochemical oxidation of proteins. Level of myoglobin oxidation was visualized onto the protein crystal structure using a five colour code. Red corresponds to unfolded structure whereas blue represents segments with native structure [Konermann 2014].

1.3.4 Chemical cross-linking

Another method which is based on the covalent modification of proteins and is combined with mass spectrometry is chemical cross-linking. The principle of chemical cross-linking is the formation of a covalent linkage between two amino acids which are located close together in the spatial assembly within one or two molecules [Sinz 2005, Young 2000]. This technique allows determining the intra- and inter-molecular distances and plays an important role in refining the already proposed structural models [Lasker 2012, Rozbesky 2012] The conversion of distance constraint information into molecular structures is made possible due to a mathematical technique called distance geometry. Distance geometry, which was introduced for structural purposes by Crippen and Havel remains an important method for deriving structures from NMR studies in solution and for homology modelling [Havel 1979, Crippen 1988]. However, alternatives such as constrained molecular dynamics can also be utilized.

In general, chemical cross-linking reaction is a process forming a covalent bond between functional groups of amino acids using a cross-linking agent. Cross-links (forming bonds) are created only if the distance between modified amino acids approximately corresponds to the length of the cross-linking agent. It is possible to get information about the distances from all areas of studied molecule via appropriately selected cross-linking agents with different length and functional specificity. Cross-linking experiments have to be thoroughly planned to avoid unwanted side reactions, agent hydrolysis or change of native structure and to achieve a maximum yield of the anticipated cross- linked products. Therefore, the optimization of reaction conditions (molar excess of agent over protein, concentration of protein and agent, buffer, pH, incubation time) is always a necessary and crucial step [Sinz 2005]. In combination with mass spectrometry, chemical cross-linking represents an established and powerful tool for elucidation of three-dimensional structure of biomacromolecules, their complexes and interaction partners. Chemical cross-linking is a fast procedure with low material consumption that represents a low resolution alternative to X-Ray crystallography and NMR: In addition, the reaction occurs under physiological conditions in solution and there is not any limitation for the size of the studied molecule.

Cross-linking agents

Hundreds of cross-linking agents have already been described in the literature and most used agents are also offered commercially. However most of them utilize common organic chemical principles that can be reduced to a few primary reactions. Reactions of the most common cross-linking agents with functional groups are shown in the Fig. 9.

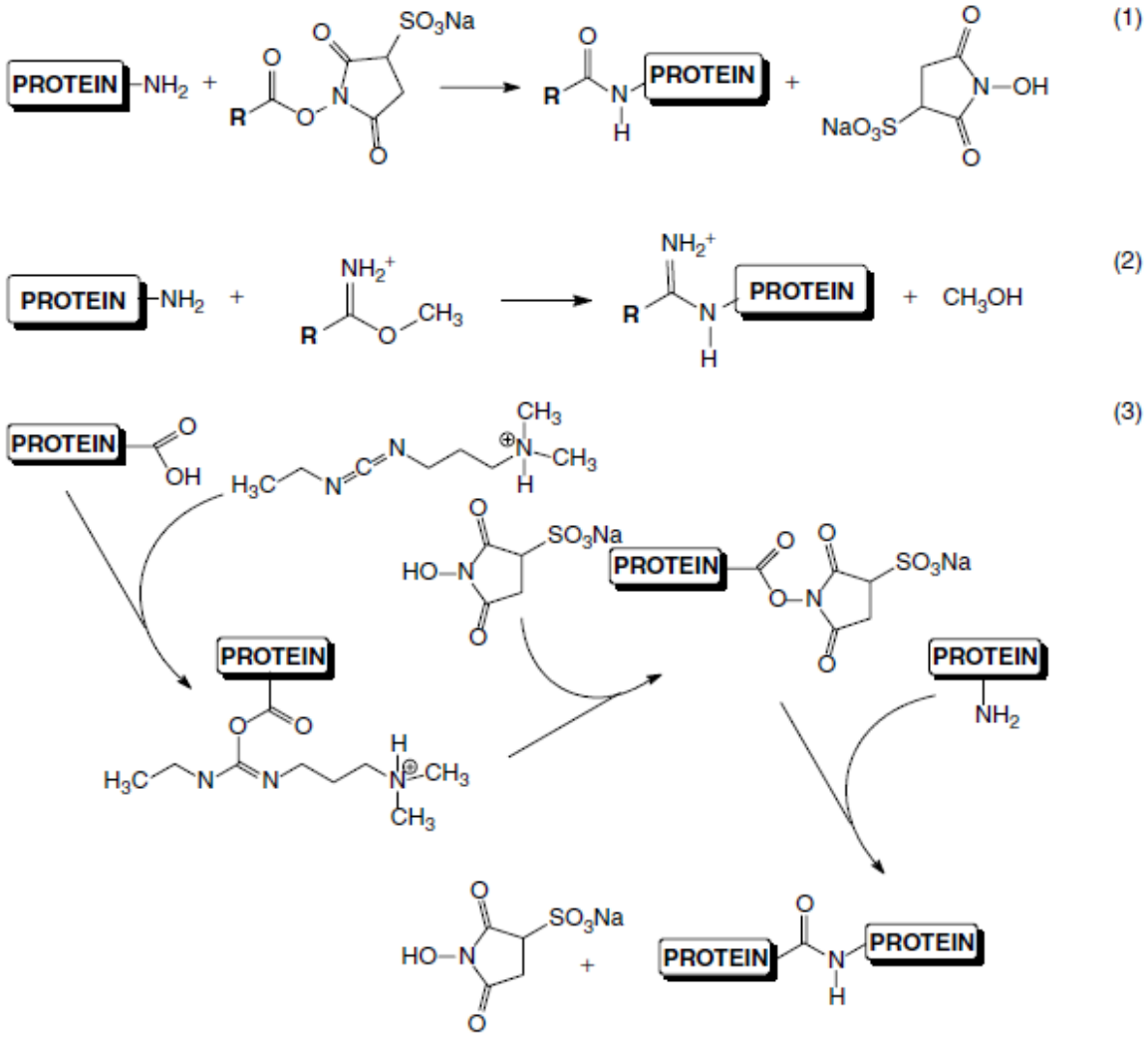

Fig. 9: Reactions of some of the most common functional groups in cross-linking reagents. (1) N-hydroxysuccinimide (NHS) esters, (2) imidoesters and (3) carbodiimides [Sinz 2003].

Cross-linking agents can be divided according to the number of reactive groups into bi- or polyfunctional agents. The two reactive groups of bifunctional reagents can be chemically inducible, photoactivatable or both. If the functional groups of the cross-linking agent are different then the gents are called heterobifunctional whereas if the reactive

groups are identical, we speak about homobifunctional reagents. Polyfunctional cross-linking agents are a relatively new group of agents, possessing more than two reactive groups. The polyfunctional cross-linker approach comes from the concept of the heterobifunctional cross-linkers with the an additional third functional group that is able to link specifically to a protein or be used for affinity purification of the cross-linking products in case the affinity moiety is incorporate. Generally, the design of cross-linking agents is very similar. Bi- and polyfunctional agents consist of a minimum of two reactive groups that react with functional side chain groups of amino acids and that are connected with a carbon chain spacer (arm, linker) whose length indirectly determines the maximum distance between modified residues. It is possible to predict the maximum distance Cα-Cα restrains by summing the length of the agent spacer a double length of connected residues. An exception is represented by zero-length cross-linkers which does not contain any carbon spacer and directly connect two side chains without any additional atoms.

Cross-linking agents can be further divided into two groups. The first group consists of agents whose reactivity is modulated by the presence of functional groups in the molecule. Reactive functional groups include for example primary amines, carboxylic acids or aldehyde groups. Representatives of this group are also NHS (N-hydroxysuccinimide) esters which were used in this thesis and will therefore be described in more detail later. The second class of agents includes the so-called photoactivatable agents whose reactivity can be induced by ultraviolet irradiation pulse. The most popular types of photosensitive agents are aryl azides [Sinz 2003].

Many improvements of chemical cross-linking strategy have been introduced in last decade. For example, to simplify identification of cross-linking reaction products, new types of agents were developed such as isotopically labelled agents which result in specific peak patterns [Fisher 2013]or CID cleavable cross-linkers which can generate easily recognizable peak patterns as well. Other new agents include cross-linkers with affinity tags that enable the enrichment of cross-linker-containing digestion products [Lutz 2012].

A very promising alternative is cross-linking using photoactivatable amino acids (photo-Ile, photo-Leu, photo-Met) [Haladova 2012, Ptackova 2014]. Due to their structural similarity to natural amino acids, photoactivatable analogues may be incorporated directly into the structure of the protein during recombinant expression. In terms of reaction mechanism the analogues behave as a photo-reactive zero length cross-linkers. After

irradiation with UV light the diazirine groups is converted to form a highly reactive carbene radical which covalently bonds to any amino acid residue in its vicinity.

Another really challenging approach is the application of cross-linking studies *in vivo* in which experiments are performed directly within cells [Bruce 2012]. The primary advantage of *in vivo* technology that distinguishes it from other available methods is the capability of concurrently mapping protein-protein interactions and their binding interfaces in native biological systems. An obvious challenge with such cross-linking studies is that the bifunctional reagents have to be able to penetrate into subcellular compartments without causing major physiological perturbations. So-called PIR (Protein Interaction Reporter) cross-linking agents were developed for this purpose. The most commonly used PIR cross-linker is BDP-NHP (Biotin Aspartate Prolin-PIR-N-hydroxyphthalimide) [Bruce 2012, Chavez 2013].

NHS esters

N-hydroxysuccinimide (NHS) esters belong into the group of the most popular agents and therefore were also used for experiments presented in this thesis. Generally, NHS esters react with primary amines; hence thus they interact with the ε-amino group of lysine or the N-terminus in the protein structure. Unfortunately, their selectivity is not high. Depending on the reaction pH of these agents can also react with hydroxyl groups of tyrosine, serine and threonine. NHS esters are soluble in an aqueous environment where they rapidly hydrolyse to form carboxylic acids which are not reactive. pH optimum for the modification of primary amines by these agents is from 7 to 9. Because of the reaction principle it is necessary to use pH buffers that do not contain any primary amines. A typical representative of NHS esters is disuccinimidyl glutarate (Fig. 10) that allows the connection of primary amines in the range from 3.1 to 7.7 Å. Another frequently used crosslinking agent is disuccinimidyl suberate, which enables covalent linkage of a primary amine in the range from 5.6 to 11.4 Å. Water-soluble analogue of the above mentioned agents are formed by modification with sulfate groups on imidyl rings.

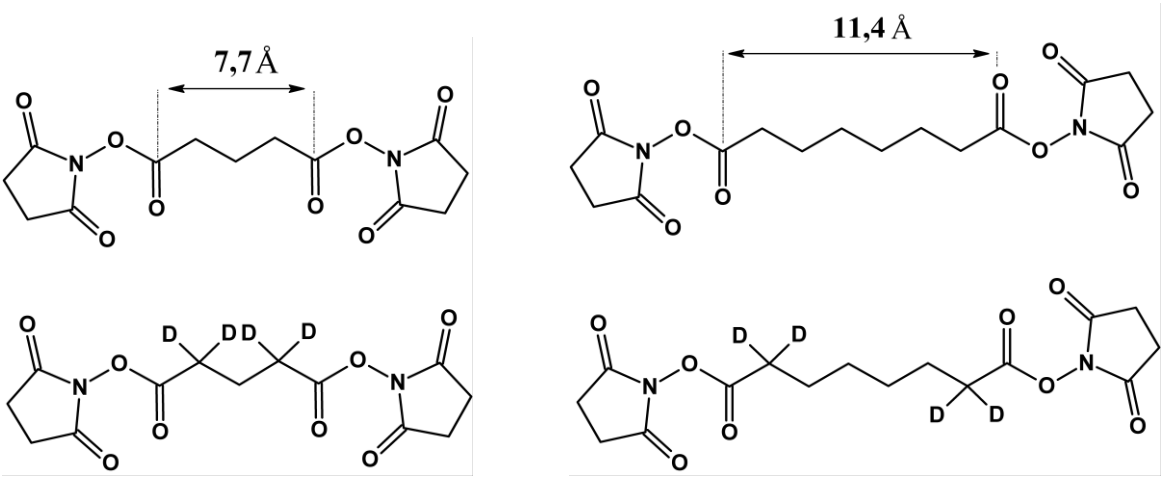

Fig. 10: Formulas of amine-reactive NHS esters disuccinimidyl glutarate and disuccinimidyl suberate and their deuterated forms.

Digestion and products of cross-linking reaction

After the cross-linking reaction, the resulting mixture is mostly digested by specific proteases and further processed via a bottom-up approach. The application of mass analysers with extremely high resolution and mass accuracy is highly beneficial in this context. By analysing the acquired spectra, the products of cross-linking reaction are identified and information about the structure is gained. During a cross-linking study of protein-protein interaction, four different types of products could be generated. (i) Dead-end cross-link (also called monolink) is formed when the cross-linking agent reacts with only one of its reactive groups. (ii) Intrapeptide cross-link (also called looplink) originates from the reaction of the cross-linking agent with side chains of the same peptide. (iii) Intramolecular cross-links represent linkage of two peptides of the same protein. (iv) Intermolecular cross-link connections originate when the cross-linker reacts with two peptides from different proteins. Only the intermolecular cross-link carries valuable information about the interaction site of the studied protein complex (Fig. 11) [Sinz 2003].

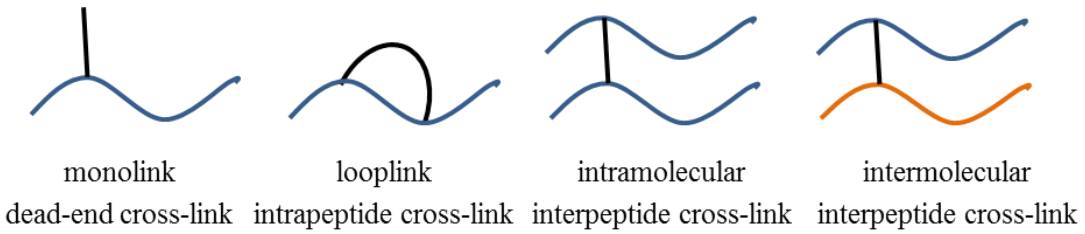

Fig. 11: Possible products of cross-linking reaction.

2 AIMS OF THE THESIS

1) To develop the novel mass spectrometric approach for monitoring of conformational changes in proteins using isotope-labelled cross-linking agent
   a) To apply the novel approach on calmodulin model system.
   b) To optimize the conditions for enzymatic proteolysis of cross-linking reaction products

2) To characterize structure of neutral trehalase Nth1 in complex with Bmh1 using chemical cross-linking and hydrogen/deuterium exchange combined with high resolution mass spectrometry
   a) To identify structural changes occuring upon the complex formation
   b) To elucidate the role of the EF-hand –like motif in the 14-3-3 protein-mediated activation of yeast neutral trehalase Nth1

3 METHODS

The publications in this thesis describe each the used methods in detail, including all the technical detail necessary for their reproducibility. Therefore, this chapter presents only a list of research methods that were used in this thesis.

List of research methods:

Analytical ultracentrifugation

Circular dichroism spectroscopy

Differential scanning fluorimetry

Enzyme activity measurements

Chemical cross-linking in combination with mass spectrometry

Hydrogen/deuterium exchange in combination with mass spectrometry

Homology modelling of proteins

Protein expression and purification

4 RESULTS AND DISCUSSION

4.1 Paper 1

Chemical cross-linking combined with high resolution mass spectrometry is an established and powerful tool for determination of three-dimensional protein structure. Unfortunately, proteins are not static objects and molecules are continuously structural changed in solution. Here we demonstrate the utilization of isotopically labelled chemical cross-linking agents to monitor and quantify these protein conformation changes. The results of this study are described in detail in attached publication (appendices 1):

Kukacka Z., Rosulek M., Strohalm M., Kavan D and Novak P.: Mapping protein structural changes by quantitative cross-linking. *Methods.* (accepted)

The novel mass spectrometric approach was demostrated on the protein calmodulin whose structure was well characterized by X-ray and NMR. Two conformational states (with and without calcium ions) of calmodulin were conducted with the amine-reactive reagents DSGd0/d4 and DSSd0/d4. The setup of a cross-linking experiment for the quantification of conformational changes was different from usual cross-linking experiments because non-deuterated and deuterated forms of the agents were used separately. One form was added to the protein with cofactor, while the second form was added to the protein without cofactor. After quenching both reactions were mixed. Detailed scheme of the experiment is given in Fig 12.

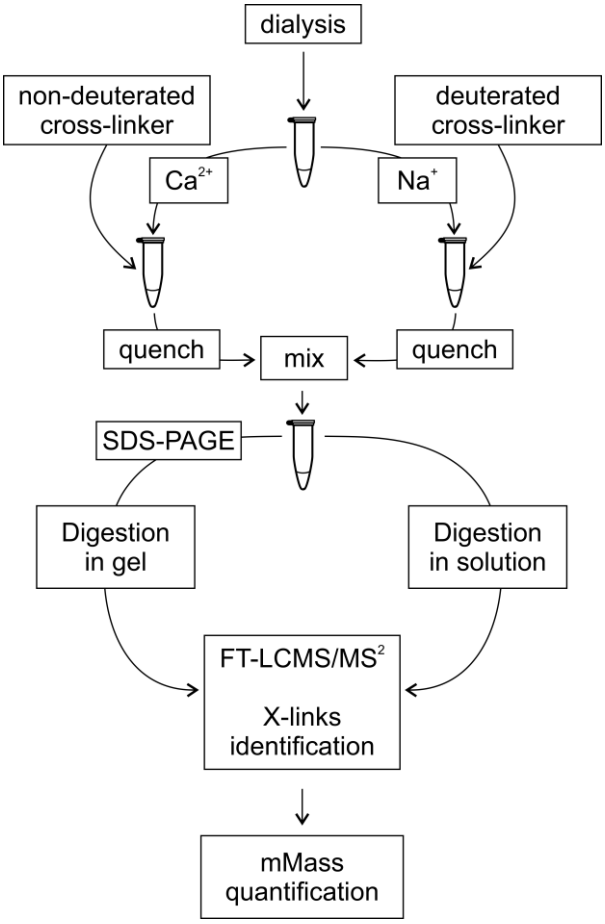

Fig. 12: Workflow of cross-linking experiment for quantification of protein conformational changes.

Products of cross-linking reaction were monitored by SDS-PAGE electrophoresis where several forms of cross-linked ~17kDa protein monomer were observed. The gel clearly shows that protein bands obtained by cross-linking calcium-free calmodulin (Fig. 13, lane 3 and 4) differ significantly from the bands which represented cross-linked calcium-containing state. (Fig. 13, lane 7 and 8). Electrophoresis also showed the patterns in lane 5 and 6 containing a mixture of calcium-free and calcium-containing calmodulin are not identical. This phenomenon prevents quantitation analysis of individual distinguished bands and therefore the whole region containing cross-linked protein was analysed by MS. Unfortunately, results revealed only a few cross-links indicating the electrophoretic separation hampers the comparison of two conformers and thus it is not suitable for quantitative cross-linking experiments.

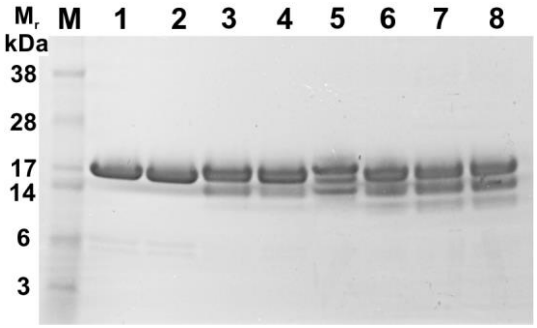

Fig. 13: SDS electrophoresis of chemical cross-linking products

M: protein marker, Lanes 1 and 2: calmodulin control sample without cross-linker, Lanes 3 and 4: calmodulin cross-linked with 10/30 molar excess of mixture DSGd0/d4 (1:1) in calcium-free state, Lanes 5 and 6: mixture of calmodulin cross-linked by DSGd0 in calcium-containing state and calmodulin cross-linked by DSGd4 in calcium-free state (10 and 30 molar excess), Lanes 7 and 8: calmodulin cross-linked with 10/30 molar excess mixture DSGd0/d4 (1:1) in calcium-containing state.

However the absence of aggregates or multimeric forms of calmodulin allows digestion in solution. Since we observed a large amount of uncleaved protein in the calcium-containing samples (Fig. 14B) after digestion we optimized conditions for enzymatic proteolysis. When two shots of trypsin were used and temperature was increased from 37°C to 55 °C we achieved the almost complete tryptic proteolysis with similar total spectral intensity for the calcium-free and calcium-containing states (Fig. 14D). However, this behaviour lead us to conclusion the utilization of proteases with cleavage specificities different from cross-linking agents, non-specific proteases or middle down approach in combination with chemical proteolysis would probably be beneficial. Using subsequent LC-MS and LC-MS/MS analysis of peptide mixture, which was not different from classical cross-linking workflow, ten cross-links were identified.

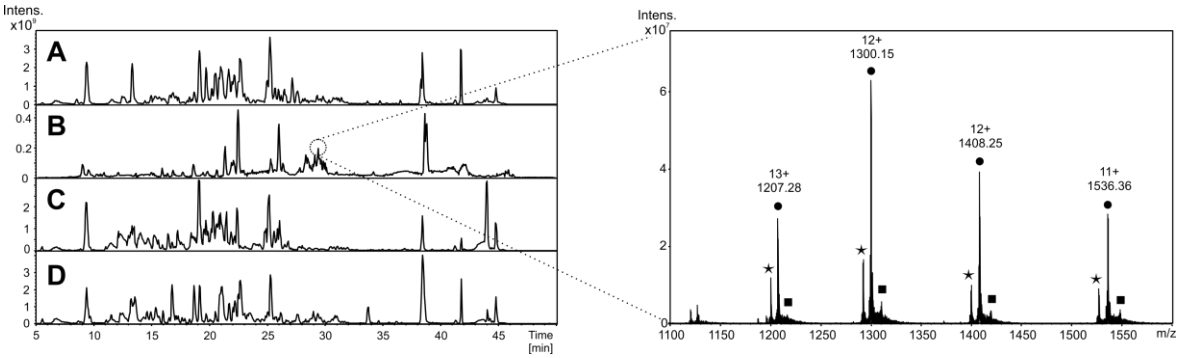

Fig. 14: Comparison of LC-MS chromatograms (A) Chromatogram of calmodulin in the calcium-free state after digestion at 55°C trypsin: protein ratio 1:10. (B) Chromatogram of calmodulin in the calcium-containing state after digestion at 37°C trypsin: protein ratio 1:20. (C) at 37°C trypsin: protein ratio 1:10. (D) at 55°C trypsin: protein ratio 1:10. Zoom of the selected region corresponding to uncleaved calmodulin. Signals originating from unmodified protein (star), protein with one cross-linker (filled circle), and protein with two cross-linkers (square) are indicated.

In order to quantify the structural changes in calmodulin the ratio of non-deuterated to deuterated forms of the reagents (i.e., the "quantifying ratio") was determined for each cross-link by using the open source software, mMass. Special function envelope fit calculates the quantifying ratio on the basis of comparison of acquired centroid spectra with in-silico simulation.

Table 3: Summary of identified cross-links as well as their quantifying ratios.

Peptide	Modified AA	DSG Ca^{2+}:Na^{+}	DSS Ca^{2+}:Na^{+}
91-106x76-86	K94-K77	11:89 ± 0	9:91 ± 1
91-106x75-77	K94-K75	88:12 ± 0	76:24 ± 0
91-106x22-37	K94-K30	16:84 ± 1	21:79 ± 0
91-106x14-30	K94-K21	37:63 ± 1	71:29 ± 1
75-77x22-37	K75-K30	87:13 ± 0	51:49 ± 2
75-77x14-30	K75-K21	87:13 ± 0	76:24 ± 0
75-77x1-21	K75-K13	34:56 ± 1	4:96 ± 1
75-90	K77-K75	81:19 ± 1	76:24 ± 0
75-86	K77-K75	60:40 ± 2	71:29 ± 0
14-37	K21-K30	52:48 ± 1	48:52 ± 1

A comparison of isotopic envelopes for cross-linked peptides from control samples corresponded to the expected isotopic pattern (i.e., the ratio of the envelopes is 52:48 for DSGd0/d4 and 56:44 for DSSd0/d4). This nearly 1:1 ratio confirmed that the measurement and subsequent quantification of cross-linked proteins should be possible. In addition, data show really good quantification accuracy and precision. The results from model calmodulin analysis further revealed the quantifying ratio of cross-linked peptide nicely correspond to accessibility of cross-linked residues in that conformation state. In the case, the residues were equally accessible in both conformational states, the quantifying ratio was close to 50:50 (i.e. cross-link K21-K30) whereas when the cross-link was preferentially formed in calcium-containing state the quantifying ratio was significantly higher (i.e. cross-link 94-75) (Table 3 and Fig. 15). Similar or opposite behaviour was observed for all cross-links, indicating that they were state-specific (Table 3 and Fig. 15).

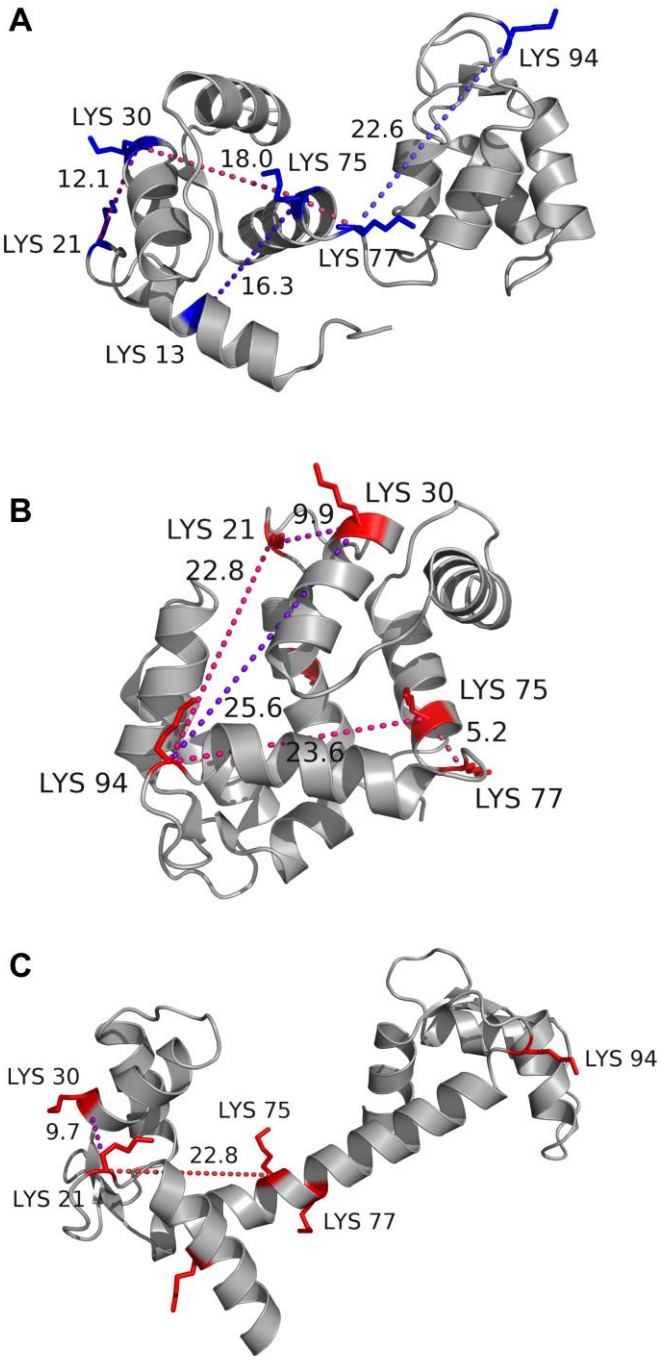

Fig. 15. Structures of calmodulin with identified cross-links. (A) NMR structure of calcium-free state (1DMO/4). (B) X-Ray structure of calcium-containing state (1PRW). (C) X-Ray structure of calcium-containing state (3CLN). Side chains of modified lysines are visualized. Lines indicate distances between Cα atoms. The color of the lines correspond to quantifying ratio (blue=ratio 0-30, violet=ratio 30-70 and red=ratio 70-100).

4.2 Paper 2

Trehalases are glycoside hydrolyses which catalyze the convertion of trehalose to glucose in a wide range of organisms. The activity of yeast neutral trehalase Nth1 is regulated using a 14-3-3 proteins and calcium ions. The Bmh1 protein (the yeast 14-3-3 isoform) enhances the enzymatic activity of phosphorylated Nth1 through an unknown mechanism. In order to elucidate the mechanism of the 14-3-3-dependent activation of pNth1as well as process of Nth1 activity regulation, we performed a structural study of the Bmh1-pNth1 complex using CD, H/D exchange and chemical cross-linking combined with high-resolution mass spectrometry. Results of this study are described in detail in attached publication (appendices 2):

Macakova E., Kopecka M., Kukacka Z., Veisova D., Novak P., Man P., Obsil T., Obsilová V.: Structural basis of the 14-3-3 protein-dependent activation of yeast neutral trehalase Nth1. *Biochim Biophys Acta.* 1830, 4491-9 (2013)

Studied proteins were prepared using heterologous expression in *E. coli* according previously described protocols. Purity of samples was monitored using SDS-PAGE and amino acids sequence and phosphorylation sites were checked by mass spectrometry analysis.

Solvent accessibility of free Nth1 and Bmh1 as well as conformational changes and interaction sites of Bmh1-pNth1 complex were studied using H/D exchange. H/D data of Nth1 revealed many regions around the whole molecule (2–110 111–151 156–262, 276–303, 412–465, 607–636, 665–712 and 738–751) whose deuteration kinetic is relatively fast. This phenomenon suggests that these regions are solvent exposed or characterized by high flexibility. Similarly, regions with fast deuteration kinetics (helix H6, loops between helices H2 and H3, H3 and H4, H4 and H5, H8–H9, and the C-terminal tail) were determined for Bmh1 protein.

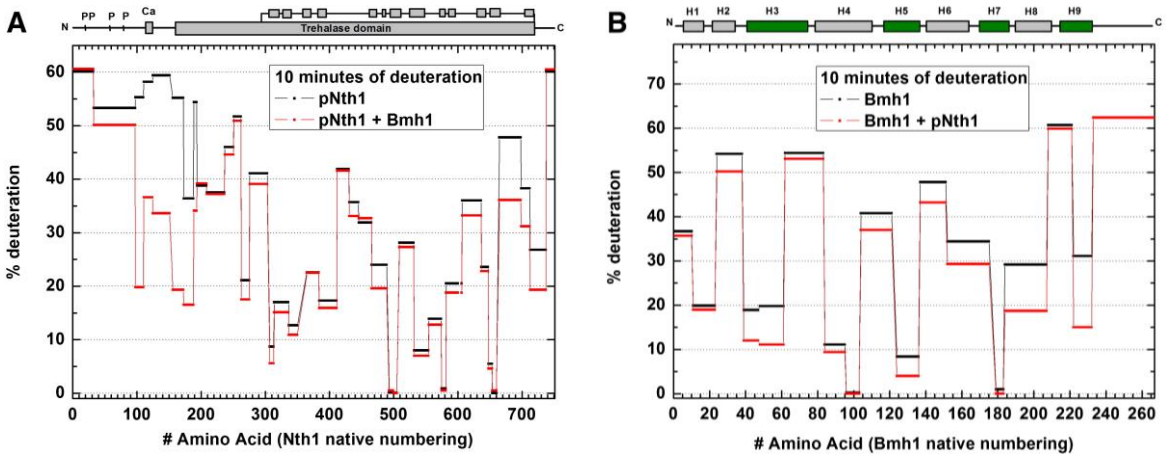

Fig. 16: A) Protection plot showing deuteration level of pNth1 in the presence/absence of Bmh1. B) Protection plot showing deuteration level of Bmh1 in the presence/absence of pNth1

Comparison of results from H/D measurement of free proteins and results from H/D measurement of complex showed significant differences in deuteration on both studied molecule. The segments with most apparent decrease in deuteratium were 98-198, 263–275, 307–313, 431–445, 466–489, 607–636 and 665–737 for Nth1 (Fig. 16A and Fig. 17) and 39–47, 48–61, 137–151, 152–175,184–207, 222–232 for Bmh1 (Fig. 16B and Fig. 18). The decrease in deuterium incorporation can be interpreted as lower solvent exposure or the change in hydrogen bonding during the complex formation, thus strongly suggesting that these segments form the interaction surface of pNth1 and/or undergo a structural rearrangement upon Bmh1 binding. Most of these regions are around the active site. However, some regions with significant decrease in deuteration are even involved in enzymatic catalysis. This behaviour confirmed the previous published studies which predict that Bmh1 binding is necessary for trehalase activation. Since active site on trehalases is not solvent exposed, it is reasonable to speculate that the activation of Nth1 requires a conformational change that opens the active site and allows a better substrate and product entry and departure, respectively.

Representation of regular secondary structures in molecules and structural changes of Bmh1 and Nth1 upon the complex formation were verified by circular dichroism spectroscopy. Circular dichroism measurements in far- and near UV spectra region were performed with reconstituted complex Bmh1:pNth1 (molar stoichiometry 2:1)

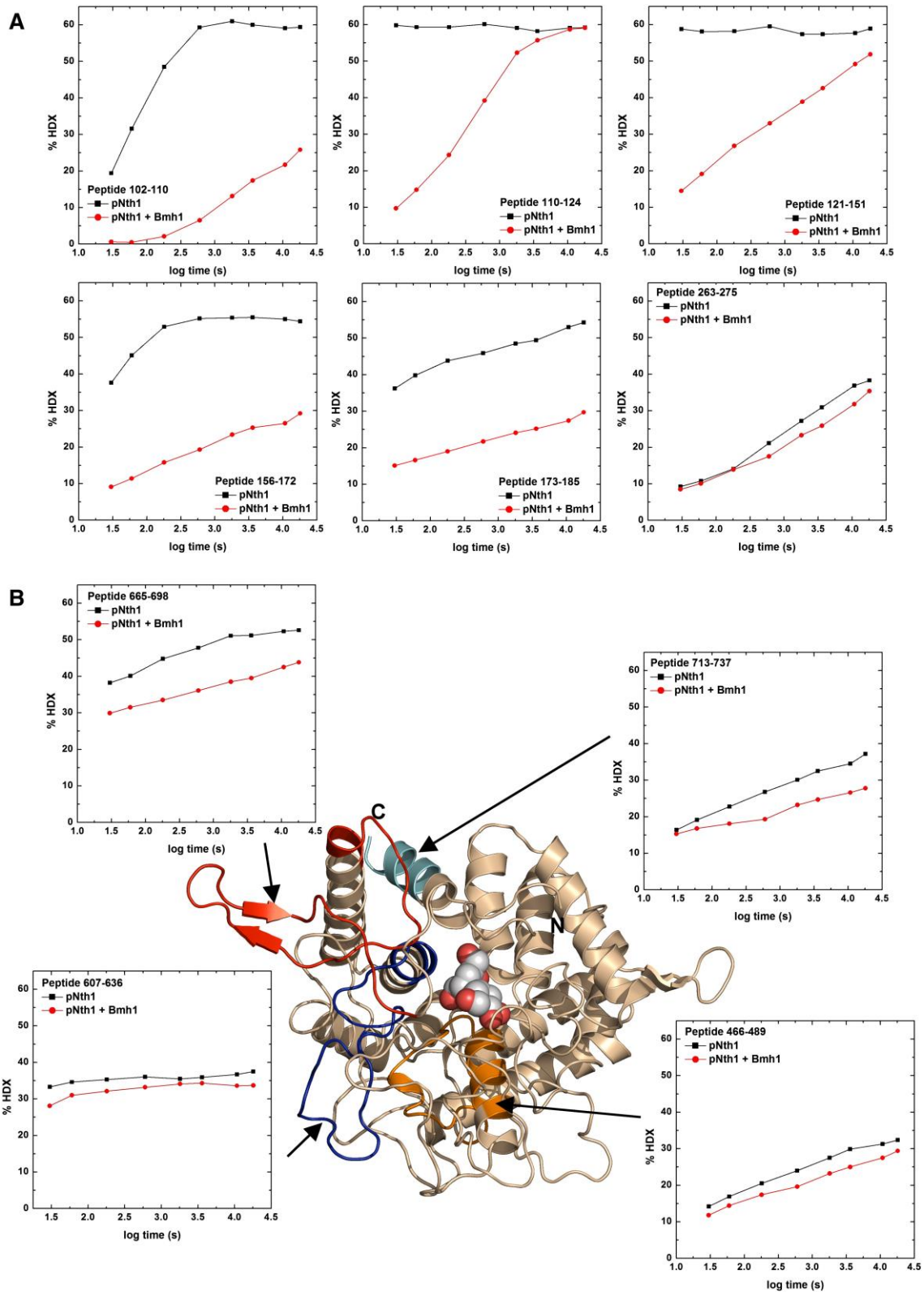

Fig. 17: HDX-MS reveals the binding surface of pNth1. (A) HDX kinetics for Bmh1 regions that show slower deuterium exchange kinetics upon pNth1 binding mapped on the structural model of Bmh1. Peptides forming the binding groove are labelled by asterisks.

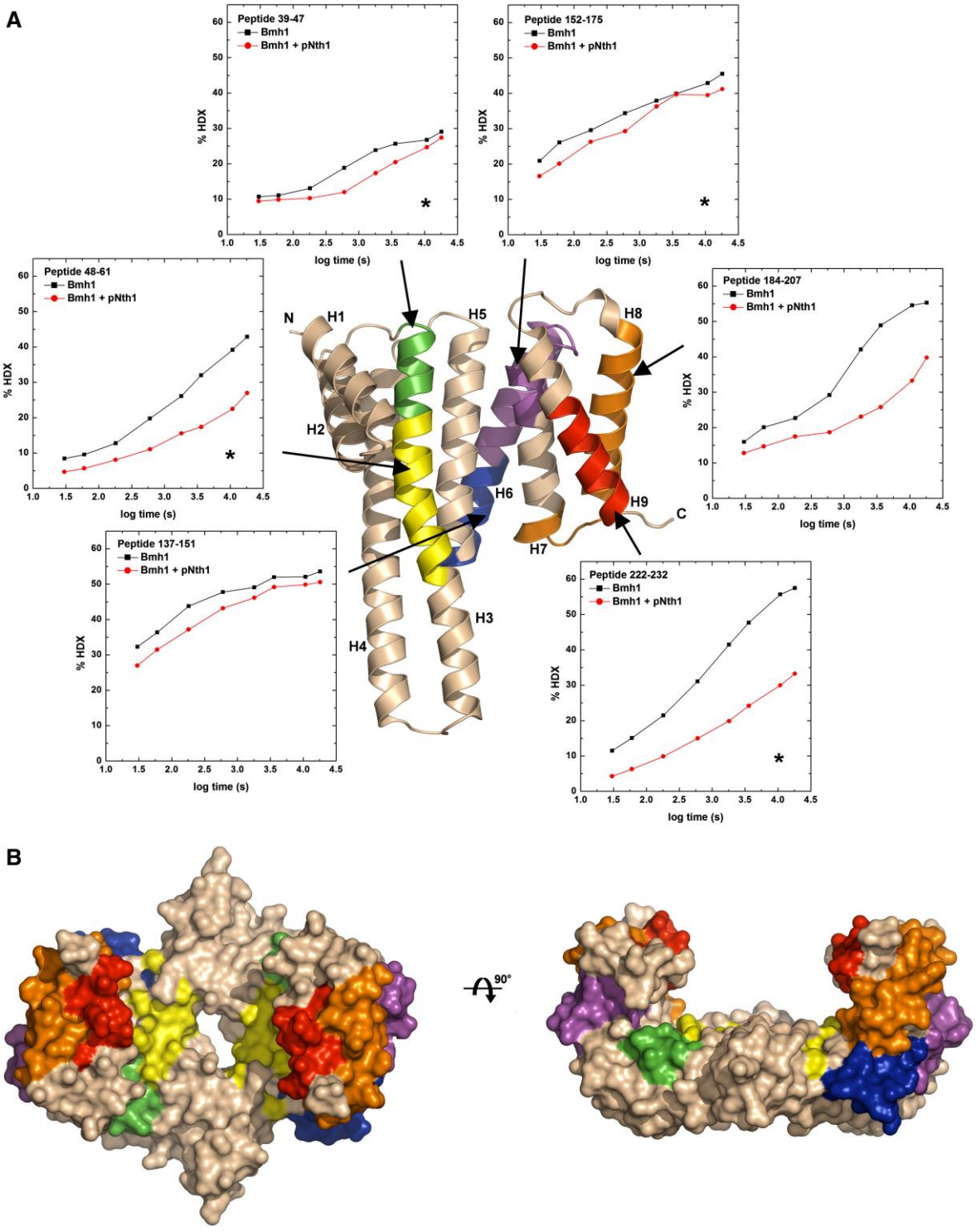

Fig. 18: HDX–MS reveals the binding surface of Bmh1. A. HDX kinetics for Bmh1 regions that show slower deuterium exchange kinetics upon pNth1 binding mapped on the structural model of Bmh1. Peptides forming the ligand binding groove are labelled by asterisks. B. Regions that show slower deuterium exchange upon pNth1 binding mapped on the surface representation of the Bmh1 dimer.

and with individual proteins (Bmh1, pNth1 and Nth1). From the measured far-UV spectra was revealed that Bmh1 molecule contains ~84% of α-helix and ~16% of random coil regions, pNth1 contains ~31% of α-helix, ~17% of β-sheet and ~52% of random coil regions and unphosphorylated molecule of Nth1 contains ~26% of α-helix, ~24% of β-sheet and ~50% of random coil regions. The comparison of far-UV CD spectra acquired for complex and sum of spectra acquired for individual proteins did not reveal significant difference in the secondary structure composition. However, comparison of near-UV spectra suggests changes in tertiary structures. This phenomenon is in good agreement with above described data from H/D exchange.

On the basis of data from circular dichroism and sequence alignment with known crystal structures of proteins from same families, the homology models of Bmh1 and Nth1 were generated. For modelling were used the DeepView, SWIS-MODEL and PROCHECK programs. In order to validate the homology models of individual protein, the chemical cross-linking experiments with amine-reactive homobifunctional agents DSG (disuccinimidyl glutarate) and DSS (disuccinimidyl suberate) were done. The results from cross-linking experiments show that all distance constraints of modified residues are in length range that used cross-linking agents allow. Thus, the generated models were experimentally validated. In addition, the homology models really well correspond to H/D exchange results. Nth1 regions with slower exchange kinetics (307–350, 384–411, 493–505, 532–581, and 648– 660) are according the model buried in structure or involve in regular secondary structural elements. These results imply that novel homology models reflect real structure of proteins well.

4.3 Paper 3

Trehalases are important highly conserved enzymes which are responsible for hydrolysis the trehalose that serve as a universal protectant and storage carbohydrate. N-terminal extensions of some yeast neutral trehalases contain protein kinase A phosphorylation sites and the EF-hand like motif that are involved in the regulation of their activities. Recently, it has been shown that the activity of neutral trehalase Nth1 from Saccharomyces cerevisiae is mediated by 14-3-3 protein that affects the conformation of the catalytic domain as well as the EF-hand-like motif. This suggested that this motif plays an important, although unclear, role in the regulation of Nth1. In this work, the importance of this EF-hand-like motif located between residues 114 and 125 in the activation of Nth1 as well as structure pNth1 was investigated using site-directed mutagenesis, circular dichroism, small angle X-ray scattering, hydrogen/deuterium exchange coupled to mass spectrometry and chemical cross-linking. Results of this study are described in detail in attached publication (appendices 3):

Kopecka M, Kosek D, Kukacka Z, Rezabkova L, Man P, Novak P, Obsil T, Obsilova V. Role of the EF-hand-like Motif in the 14-3-3 Protein-mediated Activation of Yeast Nth1.*J Biol Chem.* 289, 13948-61 (2014)

The main goal of this work was to investigate the role of the putative EF-hand like motif in the regulation of *S. cerevisiae* Nth1. Since was recently described that the Ca^{2+}-dependent activation of Nth1 from *Schizosaccharomyces pombe* is mediated by a conserved Ca^{2+}-binding EF-hand like motif (sequence D^{114}TDKNYQITIED^{125}) which is also present in sequence of Nth1 from *S. cerevisiae* we performed site-directed mutagenesis of several important residues that correspond to both conserved and not-conserved positions from EF-hand motifs of Ca^{2+}-binding proteins. The stability and binding of mutants to Bmh1 was monitor by using differential scanning fluorimetry (DSF) and analytical ultracentrifugation respectively. Results from these two methods revealed no significant changes compared to wild type pNth1. No differences between mutant and pNth1 wild were also observed from CD spectra from near-UV region. It seems that mutants behave similar to wild type.

In previous publication, we described the Bmh1-mediated conformational changes of pNth1 and Bmh1 binding affects the structure of both the N-terminal EF-hand like motif

and the catalytic trehalase domain. However, many proteins containing the EF-hand motif change their structure upon the Ca^{2+} binding, therefore the hydrogen/deuterium exchange and quantitative chemical cross-linking experiments were used to determine structural changes of pNth1 that can be mediated by Ca^{2+}. pNth1 alone and the pNth1:Bmh1 complex were analysed by both techniques in the presence and absence Ca^{2+}. The comparison of HDX-MS data for pNth1 in the presence Ca^{2+}, Bmh1 and Bmh1+Ca^{2+} show big differences in the deuteration for several peptides from the N-terminal region containing the EF-hand like domain as well as from catalytic trehalase domain. HDX-MS data suggest that observed Ca^{2+}-dependent change in pNth1 activity (Fig. 2A) reflect different conformational state of the EF-hand-like motif-containing region and/or different relative position of the N-terminal region and the catalytic domain.

We also investigated whether the presence of Ca^{2+} affects the deuterium exchange kinetics of Bmh1 peptides. These experiments revealed significant decrease in the deuteration level in the presence of Ca^{2+} for several peptides, with the strongest effect being observed for helices H3 (peptides 39-47 and 48-61), H8 (peptide 184-207), and H9 (peptide 227-232) (Fig. 19 and Fig. 20). Only two peptides (184-207 and 222-232 from helices H8 and H9, respectively) showed significantly decreased exchange kinetics when comparing peptides from the pNth1:Bmh1 complex with or without Ca^{2+} (Fig. 21).

The cross-linking experiments with pNth1 revealed 33 cross-links (Table 4). However quantification ratio between non-deuterated and deuterated cross-links is for most cross-link close to 50:50. Exceptions was the peptide from the region containing the EF-hand like motif whose lysines 132 and 142 were cross-linked only in the presence of Ca^{2+} (DSG and DSS cross-links are ~78 % and ~90 %, respectively). This seems that in the presence of Ca^{2+} these two lysines are close enough to form a cross-link whereas in the absence of Ca^{2+} this region possesses different conformation and/or flexibility and the distance between these two residues is too large to form a cross-link.

The cross-linking experiments with pNth1:Bmh1 complex revealed 17 cross-links (Table 5). In this case the presence of Ca^{2+} changed the abundances of significantly more cross-links compared to pNth1 alone. This confirms that pNth1 (complexed with Bmh1) significantly changes its structure in the presence of Ca^{2+}. The most interesting is the presence of the cross-link Lys214−Lys563, which was not observed for analysis of pNth1 alone. These facts lead to conclusion that the N-terminal part (containing Lys214) and the

catalytic domain (containing Lys563) of pNth1 are much closer to one another in the Bmh1-bound form.

All results from above noted methods suggested that for pNth1 activation, the structural integrity and the conformational change of the region containing the EF-hand-like motif are essential. This suggests that this region is adjacent to the catalytic domain and its conformational changes affect the structure of the active site and hence enable the activation.

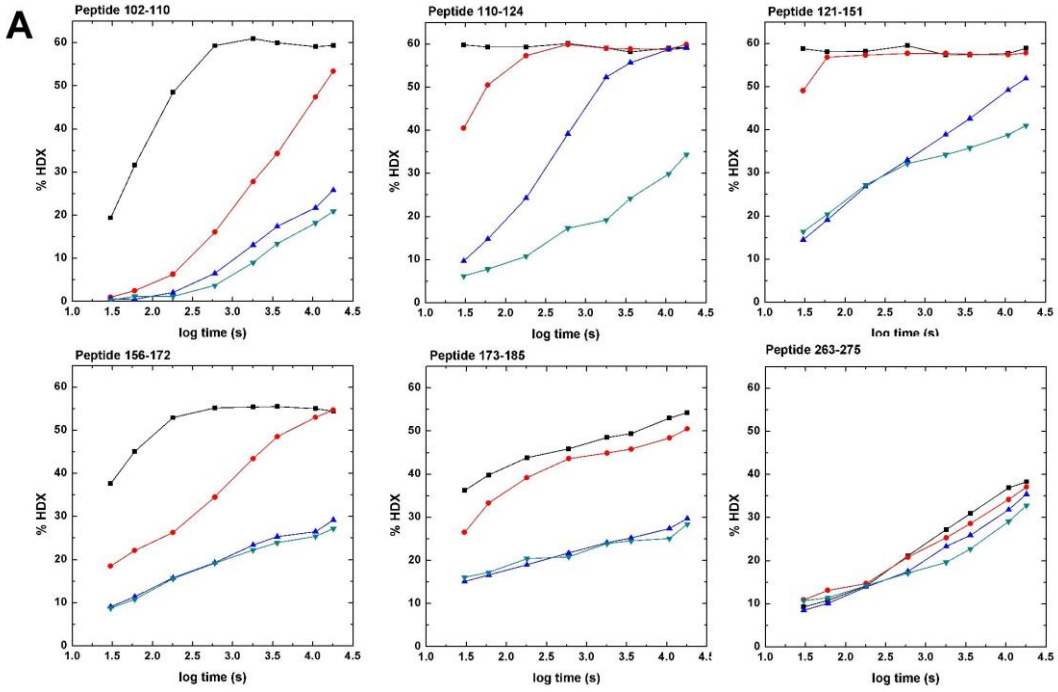

Fig. 19: HDX-MS reveals regions of pNth1 that are affected by Ca^{2+} and Bmh1 binding. (A) Graphs represent HDX kinetics for selected pNth1 regions that show slower deuterium exchange kinetics upon the Bmh1 binding.

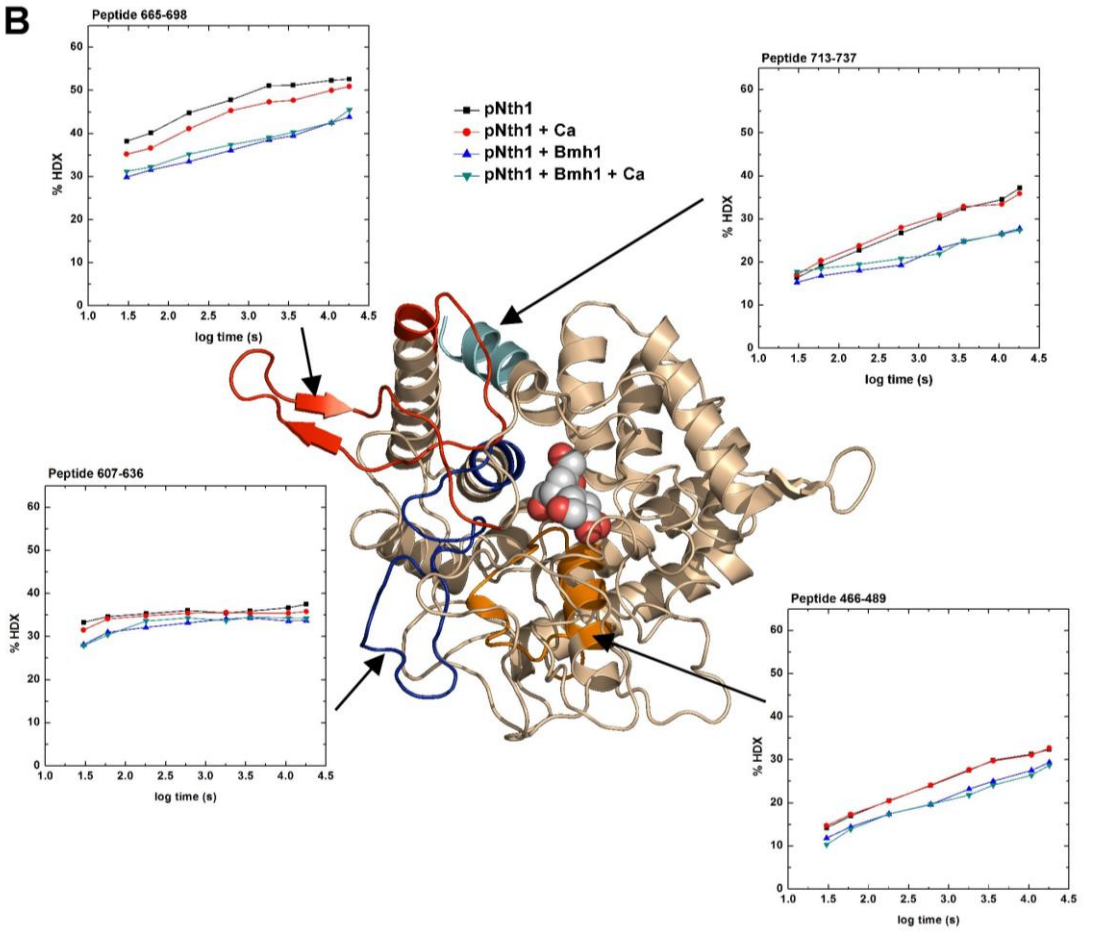

Fig. 20: HDX-MS reveals regions of pNth1 that are affected by Ca^{2+} and Bmh1 binding. (B)Peptides from the catalytic trehalase domain (shown in red, blue, cyan and orange) are mapped on its homology structural model sequence 295-721. Deuterium exchange is expressed as percentages relative to the maximum theoretical deuteration level for pNth1 alone (black squares), pNth1 in the presence of Ca^{2+} (red circles), pNth1 in the presence of Bmh1 (blue triangles) and pNth1 in the presence of Bmh1 and Ca^{2+} (green triangles). Time units are in seconds.

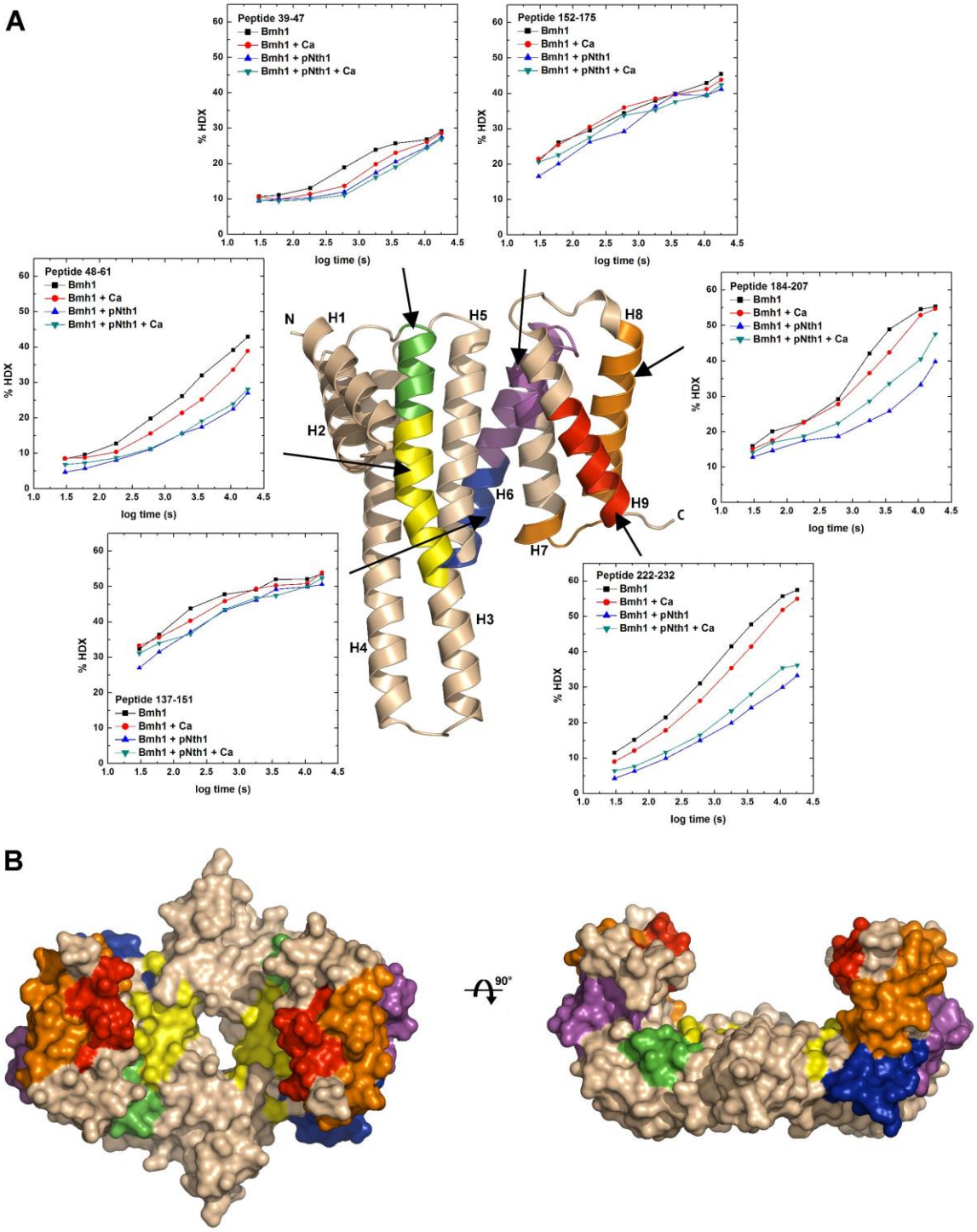

Fig. 21: HDX-MS reveals regions of Bmh1 that are affected by Ca^{2+} and pNth1 binding. (A) HDX kinetics for Bmh1 regions that show slower deuterium exchange kinetics upon pNth1 binding mapped on the structural model of Bmh1 (shown in various color). Bmh1 in the presence of Ca^{2+} (red circles), Bmh1 in the presence of pNth1 (green triangles) and Bmh1 in the presence of pNth1 and Ca^{2+} (blue triangles). (B) Regions that show slower deuterium exchange upon pNth1 and/or Ca^{2+} mapped on the surface representation of the Bmh1 dimer.

Table 4: Distance constraints of Nth1 derived from the cross-linking experiments in the presence and the absence of Ca^{2+} and their comparison with distance constraints derived from the homology model of the catalytic domain of Nth1.

Cross-linker	Cross-linked residues[a]	Cα-Cα distance from the homology model	Cα-Cα distance constraint from the cross-linking experiments[b,c]	Nth1 DSS(G)/DSS(G)D4[d]	
				DSS(G)	DSS(G)D4
		Å	*Å*	*%*	*%*
DSG/DSGD4	K49-K584, inter	-	≤20	49.8	50.2
DSG/DSGD4	K49-K69, inter	-	≤20	55.7	44.3
DSS/DSSD4	K52-K104, inter	-	≤24	42.2	57.8
DSS/DSSD4	K52-K584, inter	-	≤24	48.4	51.6
DSG/DSGD4	K70-K75, intra	-	≤20	45.1	54.9
DSS/DSSD4	K70-K75, intra	-	≤24	53.4	46.6
DSG/DSGD4	K132-K142, intra	-	≤20	77.6	22.4
DSS/DSSD4	K132-K142, intra	-	≤24	89.8	10.2
DSG/DSGD4	K210-K213, intra	-	≤20	51	49
DSS/DSSD4	K210-K213, intra	-	≤24	45.4	54.6
DSG/DSGD4	K257-K258, intra	-	≤20	47	53
DSS/DSSD4	K257-K258, intra	-	≤24	50.3	49.7
DSG/DSGD4	K258-K343, inter	-	≤20	47.8	52.2
DSS/DSSD4	K258-K343, inter	-	≤24	55.6	44.4
DSG/DSGD4	K258-K393, inter	-	≤20	51	49
DSS/DSSD4	K258-K393, inter	-	≤24	51.3	48.7
DSG/DSGD4	K370-K371, intra	3.9	≤20	49.7	50.3
DSS/DSSD4	K370-K371, intra	3.9	≤24	45.4	54.6
DSG/DSGD4	K371-K718, inter	17.7	≤20	50.1	49.9
DSS/DSSD4	K371-K718, inter	17.7	≤24	48.9	51.1
DSG/DSGD4	K385-K517, inter	17.5	≤20	48.8	51.2
DSS/DSSD4	K385-K517, inter	17.5	≤24	45.5	54.5
DSG/DSGD4	K456-K458, intra	6.5	≤20	46.4	53.6
DSS/DSSD4	K456-K458, intra	6.5	≤24	51.4	48.6
DSS/DSSD4	K458-K461, intra	7.6	≤24	41.3	58.7
DSG/DSGD4	K461-K561, inter	16.4	≤20	48.1	51.9
DSS/DSSD4	K461-K561, inter	16.4	≤24	48.8	51.2
DSS/DSSD4	K537-K584, inter	16.4	≤24	44.9	55.1
DSG/DSGD4	K561-K563, intra	5.6	≤20	52.4	47.6
DSG/DSGD4	K589-K593, intra	6.1	≤20	46.2	53.8
DSS/DSSD4	K589-K593, intra	6.1	≤24	46.9	53.1
DSG/DSGD4	K593-K597, intra	6.3	≤20	46.9	53.1
DSS/DSSD4	K593-K597, intra	6.3	≤24	47.7	52.3

Table 5: Distance constraints of pNth1 bound to Bmh1 derived from the cross-experiments in the presence and the absence of Ca^{2+} and their comparison with distance constraints derived from the homology model of the catalytic domain of Nth1.

Cross-linker	Cross-linked residues[a]	Cα-Cα distance from the homology model	Cα-Cα distance constraint from the cross-linking experiments[b,c]	Nth1 DSS(G)/DSS(G)D4[d]	
				DSS(G)	DSS(G)D4
		Å	*Å*	*%*	*%*
DSG/DSGD4	K70-K75, intra	-	≤20	55.5	44.5
DSS/DSSD4	K70-K75, intra	-	≤24	49.0	51.0
DSG/DSGD4	K132-K142, intra	-	≤20	56.8	43.2
DSS/DSSD4	K132-K142, intra	-	≤24	52.9	47.1
DSG/DSGD4	K210-K213, intra	-	≤20	65.3	34.7
DSS/DSSD4	K210-K213, intra	-	≤24	58.8	41.2
DSG/DSGD4	K214-K563, inter	-	≤20	80.0	20
DSS/DSSD4	K214-K563, inter	-	≤24	60.1	39.9
DSG/DSGD4	K257-K258, intra	-	≤20	66.7	33.3
DSS/DSSD4	K257-K258, intra	-	≤24	59.3	40.7
DSG/DSGD4	K258-K393, inter	-	≤20	68.3	31.7
DSS/DSSD4	K258-K393, inter	-	≤24	71.2	28.8
DSG/DSGD4	K370-K371, intra	3.9	≤20	54.9	45.1
DSS/DSSD4	K370-K371, intra	3.9	≤24	47.9	52.1
DSG/DSGD4	K385-K517, inter	17.5	≤20	70.2	29.8
DSS/DSSD4	K385-K517, inter	17.5	≤24	50.8	49.2
DSG/DSGD4	K393-K396, intra	5.1	≤20	51.1	48.9
DSS/DSSD4	K393-K396, intra	5.1	≤24	49.5	50.5
DSG/DSGD4	K456-K458, intra	6.5	≤20	68.8	31.2
DSS/DSSD4	K456-K458, intra	6.5	≤24	63.7	36.3
DSS/DSSD4	K458-K460, intra	7.6	≤24	50.2	49.8
DSS/DSSD4	K537-K584, inter	16.4	≤24	51.1	48.9
DSG/DSGD4	K589-K593, intra	6.1	≤20	71.1	28.9
DSS/DSSD4	K589-K593, intra	6.1	≤24	55.1	44.9

[a] Intra denotes cross-link between residues from the same peptide, inter denotes cross-link between residues from two different peptides.

[b,c] The Cα-Cα inter-residue distances constraints used were based on the length of the spacer arm which is 7.7 Å for DSG and 11.4 Å for DSS. Concerning the flexibility of the lysine side chains the following cutoffs are generally used: 20 Å for α-carbons of lysine cross-linked with DSG, and 24 Å for α-carbons of lysine cross-linked with DSS (31).

[d] Representation (%) of individual cross-link isoform.

SUMMARY

1) Using isotope-labelled cross-linking agent it was developed the novel mass spectrometric approach for monitoring of conformational changes in proteins.
2) The novel approach was successfully applied on calmodulin system.
3) The conditions for enzymatic proteolysis of cross-linking reaction products were optimized.
4) Using hydrogen/deuterium exchange and chemical cross-linking experiments the structural changes of complex pNth1 with Bmh1were identified.
5) The role of EF-hand-like motif was elucidate in in the 14-3-3 protein-mediated activation of yeast neutral trehalase Nth1

LIST OF PUBLICATIONS

Kukačka Z., Rosůlek M., Strohalm M., Kavan D. and Novak P.
Mapping Protein Structural Changes by Quantitative Cross-linking
Methods (*accepted*)

Řeha D, Harish B, Sinha D, **Kukačka Z**, Ettrichová O, Novák P, Carey J, Ettrich R.
Molecular dynamics comparison of E. coli WrbA apoprotein and holoprotein.
J Mol Model. 20, 2400 (2014)

Kopecká M, Košek D, **Kukačka Z**, Řežábková L, Man P, Novák P, Obšil T, Obšilová V.
Role of the EF-hand-like Motif in the 14-3-3 Protein-mediated Activation of Yeast Nth1.
J Biol Chem. 289, 13948-61 (2014)

Macaková E., Kopecká M., **Kukačka Z.**, Veisová D., Novák P., Man P., Obšil T., Obšilová V.
Structural basis of the 14-3-3 protein-dependent activation of yeast neutral trehalase Nth1.
Biochim Biophys Acta. 1830, 4491-9 (2013)

Kishko I., Carey J., Řeha D., Brynda J., Winkler R., Harish B., Guerra R., Ettrichová O., **Kukačka Z.,** Novák P., Kutý M., Kutá Smatanová I., Ettrich R., Lapkouski M.
1.2Å resolution crystal structure of Escherichia coli WrbA holoprotein.
Acta Crystallogr D Biol Crystallogr. 69, 1748-57 (2013)

Ryšlavá H., Kalendová A., Doubnerová V., Skočdopol P., Kumar V., **Kukačka Z.,** Pompach P., Slámová K., Bojarová P., Kulik, N., Ettrich R., Křen V., Bezouška K.
Enzymatic characterization and molecular modeling of an evolutionarily interesting fungal of β-*N*-acetylhexosaminidase.
FEBS J. 278, 2469-83 (2011)

Vaněk O., Brynda J., Hofbauerová K., **Kukačka Z.,** Pachl P., Bezouška K., Řezáčová P.
Crystallization and diffraction analysis of β-*N*-acetylhexosaminidase from *Aspergillus oryzae*. ***Acta Cryst F.*** 67, 498-503 (2011)

REFERENCES

Aebersold, R.; Mann, M.: Nature 422, 198-207 (2003).

Bai, Y.1.; Milne, J.S.; Mayne, L.; Englander, S.W.:17, 75-86 (1993).

Barth, A.: Biochim. Biophys. Acta 1767, 1073-101 (2007).

Berg, J. M.; Tymoczko, J. L.; Stryer, L.: *Biochemistry* (5th ed.), W.H. Freeman (2002).

Bohrer, B. C.; Merenbloom, S. I.; Koeniger, S. L.; Hilderbrand, A. E.; Clemmer, D. E.: Annu. Rev. Anal. Chem. 1, 293−327 (2008).

Bonfils, C.; Balny, C.; Maurel, P.: J Biol Chem. 256, 9457–9465 (1981).

Bruce, J. E.: Proteomics 12, 1565−1575 (2012).

Comisarow, M. B.; Marshall, A. G.: Chem. Phys. Lett. 25, 282 –283 (1974).

Coon, J.: J. Anal. Chem. 81, 3208−3215 (2009).

Crippen, G.M.; Havel, T.F.: Research Studies, John Wiley and Sons (1988).

Dass, Ch.: Fundamentals of contemporary mass spectrometry, John Wiley and Sons, (2007).

Demartini, D.R.: Tandem Mass Spectrometry - Molecular Characterization, Intech (2013).

Dreisewerd, K.: Chem. Rev. 103, 395 – 425 (2003).

Fabris, D.; Kellersberger, K. A.; Wilhide, J. A.: Int. J. Mass Spectrom.. 312, 155−162 (2012).

Fenn, J. B.; Mann, M.; Meng, C. K.; Wong, S. F.; Whitehouse, C. M.: Science 246 (4926), 64-71 (1989).

Fischer, L.; Chen, Z.A.; Rappsilber, J.: J. Proteomics. 88, 120–128 (2013).

Glatter, O.; Kratky, O.: *Small Angle X-ray Scattering*. Academic Press. (1982).

Haladová, K.; Mrázek, H.; Ječmen, T.; Halada, P.; Man, P.; Novak, P.; Chmelík, J.; Obšil, T.; Šulc, M.: J. Struc. Biol. 179, 10-17 (2012).

Havel, T.F.; Crippen, G.M.; Kuntz, I.D.: Biopolymers 18, 73–81 (1979).

Heeren, R. M. A.; Keinnijenhuis, A. J. ; McDonnell, L. A. ; Mize, T . H.: Anal. Bioanal. Chem. 378, 1048-1058 (2004).

Hirsch, J.; Hansen, K.C.; Burlingame, A.L.; Matthay M.A.: Am. J. Physiol. Lung Cell. Mol. Physiol. 287, 1–23, (2004).

Holčapek, M.; Jirásko, R.; Lísa, M.: J. Cromatogr. A. 1259, 3-15 (2012).

Hyung, S.-J.; Robinson, C.V.; Ruotolo, B. T.: Chem. Biol. 16, 382–390 (2009).

Chaurand, P.: J. Proteomics 75, 4883−4892 (2012).

Chavez, J. D.; Weisbrod, C. R.; Zheng, C. X.; Eng, J. K.; Bruce, J. E.: Mol. Cell. Proteomics 12, 1451−1467 (2013).

Chen, J.; Rempel, D. L.; Gau, B.; Gross, M. L. J. Am. Chem. Soc., 134, 18724−18731 (2012).

Iacob, R. E.; Engen, J. R.: J. Am. Soc. Mass Spectrom., 23, 1003−1010. (2012)

Illari, A., Savino, C.:, Methods Mol Biol 452, 63-87 (2008).

Inutan, E. D.; Wager-Miller, J.; Mackie, K.; Trimpin, S.: Anal. Chem. 84, 9079−9084 (2012).

Jerabek-Willemsen, M, Wienken, C.J.; Braun, D., Baaske, P., Duhr, S.: Assay Drug Dev Technol. 9, 342-53 (2011).

Johnson, C.; Crowther, S.; Stafford, M. J.; Campbell, D. G.; Toth, R.; Mackintosh, C.: Biochem. J. 427,

Kaltashov, I. A.; Bobst, C. E.; Abzalimov, R. R.: Protein Sci. 22, 530−544 (2013).

Karas, M.; Hillenkamp, F.: Anal. Chem. 60 (20), 2299-301 (1988).

Karas, M.; KrIger, R.: Chem. Rev. 103, 427 – 439 (2003).

Kiselar, J.G.; Chance, M.R.: J. Mass Spectrom. 45, 1373–1382 (2010).

Knochenmuss, R.; Zenobi, R.: Chem. Rev. 103,441 –452 (2003).

Konermann, L.; Pan, J.; Liu, Y. Chem. Soc. Rev. 40, 1224−1234 (2011).

Konermann, L.; Stocks, B. B.; Pan, Y.; Tong, X.: Mass Spectrom. Rev. 29, 651–667 (2010).

Konermann, L.; Vahidi, S.; Sowole, M. A.: Anal. Chem. 86, 213-232 (2014).

Konijnenberg, A.; Butterer, A.; Sobott, F.: Biochim. Biophys. Acta 1834, 1239–1256 (2013).

Lasker, K.; Forster, F.; Bohn, S.; Walzthoeni,T.; Villa, E.; Unverdorben, P. et al.: Proc. Natl. Acad. Sci. 109, 1380–1387 (2012).

Little, D. P.; Speir, J. P.; Senko, M. W.; O'Connor, P. B.; McLafferty, F. W.: Anal. Chem. 66, 2809 –2815 (1994).

Marion, D.: Mol Cell Proteomics 12, 3006–3025 (2013).

Markwick, P.R.; Malliavin, T.; Nilges, M.:Plos Compu Biol. 26, (2008).

Marshall, A. G.; Hendrickson, C. L.; Jackson, G. S.: Mass Spectrom. Rev. 17, 1–35 (1998).

Marshall, A. G.: Int. J. Mass Spectrom. 200, 331 –356 (2000).

Marshall, A. G.; Hendrickson, C. L.: Int. J. Mass Spectrom. 215, 59–75 (2002).

McLuckey, S. A.: J. Am. Soc. Mass Spectrom. 3, 599–614 (1992).

McPherson, A.: Eur J Biochem.;189,1-23 (1990).

Milne, J. L. S.; Borgnia, M. J.; Bartesaghi, A.; Tran, E. E. H.; Earl, L. A.; Schauder, D. M.; Lengyel, J.; Pierson, J.; Patwardhan, A.; Subramaniam, S.: FEBS J. 280, 28−45 (2013).

Mittermaier, A.; Kay, L. E.: Science 312, 224−228 (2006).

Obsil, T.; Obsilova, V.: Semin Cell Dev Biol 22, 663-672 (2011).

Paizs, B.; Suhai, S.: Mass Spectrom. Rev. 24, 508−548 (2005).

Parker, J.: Microbiol. Rev. 53, 273-289 (1989).

Parker, M. W.: J. Biol. Phys., 29, 341−362 (2003).

Petrotchenko, E.V.; Borchers, C.H.: Mass Spectrom. Rev. 29, 862–876 (2010).

Ptáčková, R.; Ječmen, T.; Novák, P.; Hudeček, J.; Stiborová, M.; Šulc, M.: Int. J. Mol. Sci. 15, 9224–9241 (2014).

Robinson, C. V.; Sali, A.; Baumeister,W.: Nature 450, 973–982 (2007).

Robinson, C. V.: FEBS J. 279, 663–677 (2012).

Rozbeský, D.; Man, P.; Kavan, D.; Chmelík, J.; Černý, J.; Bezouška, K.; Novák, P.: Anal. Chem. 84, 867–870 (2012).

Schuck P.:Anal Biochem. 320, 104-24 (2003).

Schuck, P.:Annu Rev Biophys Biomol Struct. 26, 541-66 (1997).

Schmidt, C.; Robinson, C.V.: FEBS J. 281, 1950–1964 (2014).

Schumacher, B.; Mondry, J.; Thiel, P.; Weyand, M.; Ottmann, C.: FEBS Lett. 584 (8), 1443-8 (2010).

Sinz, A.: J. Mass Spectrom. 38, 1225–1237 (2003).

Sinz, A.: Mass Spectrom. Rev. 25, 663–682 (2006).

Sinz, A.: Chem. Med. Chem. 2, 425–431 (2007).

Schorzman, A. N.; Perera, L.; Cutalo-Patterson, J. M.;Pedersen, L. C.; Pedersen, L. G.; Kunkel, T. A.; Tomer, K. B. DNA Repair , 10, 454−465 (2011).

Skinner, O. S.; McLafferty, F. W.; Breuker, K.: J. Am. Soc. Mass Spectrom. 23, 1011−1014 (2012).

Sobott, F.; McCammon, M. G.; Robinson, C. V.: Int. J. Mass Spectrom. 230, 193–200 (2003).

Takamoto, K.; Chance, M. R.: Annu. Rev. Biophys. Biomol. Struct. 35, 251–276 (2006).

Veisova, D.; Rezabkova, L.; Stepanek, M.; Novotna, P.; Herman, P.; Vecer, J.; Obsil, T.; Obsilova, V.: Biochemistry 49, 3853-3861(2010)

Voet D.; Voet, D.J.: Biochemistry (4th ed.), John Wiley and Sons (2011).

Wang, L.; Chance, M.R.: Anal. Chem. 83, 7234–7241 (2011).

Whitford, D.: Proteins – structure and function, John Wiley and Sons (2005).

Wilm, M.; Mann, M.: Int. J. Mass Spectrom. Ion Processes 136, 167–180 (1994).

Wilm, M.; Mann, M: Anal. Chem. 68, 1– 8 (1996).

Wyttenbach, T.; Bowers, M. T. J.: Phys. Chem. B 115, 12266−12275 (2011).

Young, M. M.; Tang, N.; Hempel, J. C.; Oshiro, C. M.; Taylor, E. W.; Kuntz, I. D.; Gibson, B. W.; Dollinger, D.: Proc. Natl. Acad. Sci. USA 97, 5802–5806 (2000).

Zubarev, R. A.; Zubarev, A. R.; Savitski, M. M.: J. Am. Soc. Mass Spectrom. 19, 753−761 (2008).

APPENDICES

Paper 1

Kukacka Z., Rosulek M., Strohalm M., Kavan D. and Novak P.

Mapping Protein Structural Changes by Quantitative Cross-linking

Methods. X, X-X (2015) accepted

My contribution to the publication: *Characterization of calmodulin using ESI-FTICR-MS, some of chemical cross-linking experiments, enzymatic digestion in Barrocyler, LC-MS and LC-MS/MS analysis, data interpretation, manuscript writing*

Mapping Protein Structural Changes by Quantitative Cross-linking

Authors: Zdenek Kukacka[1,2], Michal Rosulek[1,2], Martin Strohalm[1], Daniel Kavan[1,2] and Petr Novak[1,2*]

Affiliations:

[1]Laboratory of Structural Biology and Cell Signaling, Institute of Microbiology, Academy of Sciences of the Czech Republic, Prague, Czech Republic

[2]Department of Biochemistry, Faculty of Science, Charles University, Prague, Czech Republic

*To whom correspondence should be addressed: Dr. P Novak, Laboratory of Structure Biology and Cell Signaling, Institute of Microbiology ASCR, Videnska 1083, Prague 14220, Czech Republic. E-mail: pnovak@biomed.cas.cz

Keywords: chemical cross-linking, proteolysis, mass spectrometry, quantification, protein structure design

Abstract

Chemical cross-linking is a promising technology for protein tertiary structure determination. Though the data has low spatial resolution, it is possible to obtain it at physiological conditions on proteins that are not amenable to standard high resolution techniques such as X-ray, NMR analysis and cryo-EM. Here we demonstrate the utilization of isotopically labeled chemical cross-linking to visualize protein conformation rearrangements. Since calmodulin exists in two distinct conformations (calcium-free and calcium-containing forms), we selected this protein for testing the potential and the limits of a new technique. After cross-linking of both calmodulin forms, the calcium-free and calcium-containing forms were mixed together and digested under different conditions and the products of proteolysis were monitored using high resolution mass spectrometry. Finally, the ratios of heavy/light cross-links were calculated by mMass open source platform.

1. Introduction

Chemical cross-linking in combination with mass spectrometry (XL-MS) is an established and powerful tool for the elucidation of three-dimensional protein structures which also provides valuable information about protein-protein and protein-nucleic acid interactions[1–5]. Current cross-linking strategies do not significantly differ from early experiments in which the analysis of products was limited to photometric and electrophoretic methods[6]. The methodology has, however, been significantly improved by the introduction of soft ionization techniques, which enabled the analysis of cross-linked biomolecules by mass spectrometry[7,8].

Current XL-MS includes chemical and photo-crosslinking whose aim is to determine distances in proteins or protein complexes[9–11]. Modified proteins with amino acids connected by cross-linkers are enzymatically digested and the resulting peptide mixture is separated by liquid chromatography and analyzed by mass spectrometer coupled on-line. The initial structural information includes the length of cross-linker spacer and the position of cross-linked amino acids in protein sequence. The cross-links formed provide distance constraints which form a basis for generating three dimensional models[12–15], mapping protein interaction interface[16–19] or refinement of earlier resolved structures[20–23].

Analysis of conformational changes in proteins represents a very challenging task because proteins are not static objects and their structural dynamics has crucial effect on the behavior of biological systems. Until recently XL-MS was used for studying the dynamics of proteins or protein complexes in a qualitative manner by identifying cross-links that are specifically formed only in one conformation or state[24,25]. However, recent publications show that XL-MS analysis using isotope-labelled cross-linkers allows quantification of structural changes and protein interaction dynamics[26,27]. While quantitative proteomics is a well-established tool, quantitative determination of dimension in protein structural analysis by XL-MS is still challenging. Quantification based on the proportional relationship between the sample concentration and the measured intensities of signal is a commonly used method in differential proteomics[28–31]. Isotope labeling for XL-MS quantification was introduced eight years ago, and included only 180-labeling of cross-linked peptides[32].

Isotope-labelled cross-linkers were introduced at the beginning of the millennium and immediately became a valuable tool for the identification of modified peptides. Only peptides containing the cross-linker will be represented by a specific doublet (light and heavy form) isotopic pattern in a mass spectrum [33–35]. This distinguishing feature is advantage of quantification by isotope-labelled cross-linker over other general differential labeling methods such as iTRAQ[36,37] or TMT[38]. The use of the isotope-labelled cross-linkers is also an alternative technique to SILAC[39] and does not require preparation of labeled proteins.

In the present work, we used isotope-labeled cross-linkers for quantification of two different conformational states of the model protein, the 17kDa large calmodulin. The sequence of this protein is highly conserved across many organisms. It is known that calmodulin exists in two structurally different conformations – calcium containing and calcium free forms[40]. Using this simple system we describe the feasibility and limitation of the cross-linking strategy.

The structures of calmodulin forms with and without calcium ions are completely different[40]. Both conformational states have been well characterized by X-Ray and NMR spectroscopy[41–43] and calmodulin has been often used for developing and improving cross-linking approaches[44–46]. Different software tools for quantification of the acquired spectra have also been described [26,47]. In this study, we introduce another method to determine the ratios of light and heavy cross-linker in modified peptides -- mMass 5.5 software[48–50].

2. Material and methods

2.1 *Material*

Calmodulin from bovine brain was obtained from Calbiochem (Germany). Cross-linkers disuccinimidyl glutarate (DSGd0/DSGd4) and disuccinimidyl suberate (DSSd0/DSSd4) were purchased from Proteochem (USA). Sequencing grade modified trypsin was obtained from Promega (USA). Water and HPLC solvents were LC/MS grade purity and were obtained from Thermo Scientific (USA). Other chemicals at the highest available purity were purchased from Sigma-Aldrich (USA).

2.2 *Sample preparation*

Calmodulin was dissolved in 1mM EGTA to 1 mg/ml concentration and transferred to 10mM HEPES buffer (pH 7.5) containing 100mM NaCl and 1mM EGTA using Micro Bio-Spin^{TM} 6 columns (cut off 6 kDa BioRad, USA). Calmodulin concentration after chromatography was monitored by Bradford assay[51].

2.3 *Calmodulin characterization using ESI-FTICR-MS*

One microgram of calmodulin was desalted on protein micro trap column (C4 phase, Michrom Bioresources, USA) according manufacturer instruction, and eluted in 100 µl of 80% acetonitrile/1% acetic acid. Protein was electrosprayed to solariX XR FT-ICR mass spectrometer (Bruker Daltonics, Germany) equipped with 12 T superconducting magnet. The instrument was internally calibrated using Agilent tuning mix (Agilent Technologies, USA). Mass spectra were acquired in the positive mode over the m/z range 245 to 2500 with 1 M data points transient and 0.4 s ion accumulation, 8 scans were accumulated per spectrum. Data acquisition was performed using solariXControl and interpreted by DataAnalysis 4.1.

2.4 *Chemical cross-linking reaction*

Calmodulin aliquots in 10mM HEPES buffer (pH 7.5) containing 100mM NaCl and 1mM EGTA for the induction of calcium conformational structural changes were spiked with calcium ions ($CaCl_2$) to produce a 12mM final concentration of Ca^{2+}. Aliquots intended to represent the calcium-free state were mixed with sodium ions (NaCl) to balance ionic strength to achieve a 136mM final concentration of Na^{+}. After 30 min incubation at room temperature, aliquots were mixed with the cross-linking reagents. Calmodulin samples representing the calcium-containing state were mixed only with non-deuterated cross-linker (DSGd0 or DSSd0) while calcium-free samples were mixed with deuterated cross-linker (DSGd4 or DSSd4). A ten and thirty-fold molar excess of cross-linker (dissolved in DMSO to 15 mM concentration, final content of DMSO in reaction mixture was 1.3 %) compared to the protein was used. Thus the final concentration of calmodulin was 20µM and concentrations of cross-linking agents were 200µM/600µM. The cross-linking reactions were quenched after two hours of incubation at room temperature by adding ethanolamine to a final concentration of 0.4/1.2 mM. Calcium-containing samples and identical calcium-free samples were mixed in 1:1 ratio. Control samples without cross-linkers, and samples cross-linked

with 1:1 mixture DSGd0/DSGd4 or DSSd0/DSSd4 were prepared at the same time, in order to obtain the chemical activities of each cross-linker which could have changed during synthesis, transport, storage and/or preparation of cross-linking agents. Reaction mixtures were split into two identical aliquots. One half of each cross-linked protein sample was analyzed using SDS-PAGE and the other was taken for high-resolution mass spectrometric characterization. Three sets of replicates were prepared and measured.

2.5 *Protein electrophoresis*

The cross-linking reaction mixture (approximately 10 µg of calmodulin in 30 µl) was mixed with 4x-concentrated LDS sample buffer (Invitrogen) containing 100 mM dithiothreitol as the reducing agent in a 3:1 (v:v) ratio. Samples were incubated for 5 min at 90°C and then loaded onto a NuPage 4-12% Bis-Tris gel (80.0×80.0×1.0 mm, 10 wells). Separation was performed in MES running buffer for 35 min at 200V. After separation, the gels were stained by Coomassie Brilliant Blue R250 and destained by solution containing ethanol, water, and acetic acid in the ratio 55:35:10[52].

2.6 *Enzymatic digestion*

For *in-gel* digestion, the calmodulin bands were excised and destained. The gel pieces were covered with trypsin solution (trypsin in 100 mM ethylmorpholine buffer, pH 8.5 with 10% AcN, enzyme:protein ratio 1:20) and incubated at 37°C overnight.

For *in solution* digestion, the cross-linked protein was digested with trypsin in five different ways:

A) The cross-linking reaction mixture was diluted 1:1 (protein;buffer) with 100 mM ethylmorpholine buffer (pH 8.5) with 10% AcN, while the pH of the mixture was monitored. Trypsin in 100 mM ethylmorpholine buffer (pH 8.5) with 10% was added to give a final concentration 1:20 (w/w) trypsin to protein and digestion was carried out at 37°C overnight.

B) The cross-linking reaction mixture was diluted 1:1 (protein;buffer) with 100 mM ethylmorpholine buffer (pH 8.5) with 20% AcN. Trypsin in 100 mM ethylmorpholine buffer (pH 8.5) with 10% was added to give a final concentration of 1:20 (w/w) trypsin to protein and digestion was carried out at 37 or 55°C. After a 6-

hour incubation, trypsin was added to give a final concentration of 1:10, and digestion was allowed to proceed at 37 or 55°C overnight.

C) Guanidine was added to the cross-linking reaction mixture to give a final concentration of 6 M and the reactions were carried out for 2 min at 90°C. After incubation, the guanidine was diluted by 100 mM ethylmorpholine buffer (pH 8.5) with 20% AcN to give a final concentration of 2 M. Trypsin in 100 mM ethylmorpholine buffer (pH 8.5) with 10% was added to give a final concentration of 1:20 (w/w) trypsin:protein, and digestion was carried out at 37 or 55°C. After a 6-hour incubation, trypsin was added to give a final concentration of 1:10, and digestion was allowed to proceed at 37°C overnight.

D) Guanidine and RapiGest (Waters, USA) were added to the cross-linking reaction mixture. Final concentrations were 6 M for guanidine and 0.05% (v/v) for RapiGest. After a 1-hour incubation at 60°C, guanidine was diluted by 50 mM ammonium bicarbonate buffer (pH 8.0) with 20% AcN to give a final concentration of 2 M. Trypsin in 100 mM ethylmorpholine buffer (pH 8.5) with 10%was added to the final concentration 1:20 (w/w) trypsin:protein and digestion was carried out at 37°C. After 6 hours incubation trypsin in 100 mM ethylmorpholine buffer (pH 8.5) with 10% was added to give a final concentration of 1:10 trypsin: protein and digestion was allowed to proceed at 37°C overnight.

E) Trypsin in 100 mM ethylmorpholine buffer (pH 8.5) with 10% was added to give a final concentration of 1:20 (w/w) trypsin: protein. Trypsin digestion was carried out at 37 or 55°C in Barocycler Nep2320 (Pressure BioSciences, USA) for 1 hour (36 cycles; 1 cycle corresponds to 100 second, 95 s at 24 psi and 5 s at atmospheric pressure) at pressure 24 psi.

2.7 *Nano-UHPLC/Nano-ESI-FTICR mass spectrometry*

The resulting peptides were desalted by peptide micro trap column (C8 phase, Michrom Bioresources, USA) according manufacturer instruction. Samples were dried by SpeedVac and re-suspended in 100 µl of solvent A (0.1% formic acid in 2% ACN) for further processing. A 1 µl of each peptide mixture was injected onto a reversed-phase trap column (Acclaim PepMap™ 100, C18, 0.1 x 20mm, 5µm, Thermo Scientific, USA) heated to 60°C. Eluting peptides were subsequently separated on a 60°C-heated reversed-phase analytical column (Acclaim PepMap™ 100, C18, 0.075 x 150mm, 3µm, Thermo

Scientific,USA) using UltiMate 3000 RSLCnano System (Dionex , USA) at a flow rate of 0.5 µl/min under the following gradient conditions: 2-45% solvent B (0.1% formic acid) in 43 min, 45-95% B in 3 min, 3 min in 95% B, 95-2% B in 1 min and 10 min in 2% B. The nano-UHPLC system was coupled to CaptiveSpray which directly introduces ions into a solariX XR FT-ICR mass spectrometer (Bruker Daltonics, Germany) equipped with 12 T superconducting magnet. The instrument was calibrated on-line by using The Agilent tuning mix (Agilent Technologies, USA). Mass spectral data was acquired in positive broadband mode over the m/z range 245 to 2000, with 1 M data points transient and 0.4 second ion accumulation and 4 scans were accumulated per spectrum. Data acquisition was performed using solariXControl.

2.8 *Data interpretation*

For cross-link identification, we used the Links algorithm, previously described as ASAP (Automated Spectrum Assignment Program)[3,53]. Because it requires input in the format of tab separated m/z and intensity values, it was necessary to program a data output script using the internal scripting language (Visual Basic) in DataAnalysis 4.1 software suite (Bruker Daltonics, Germany) This script uses DataAnalysis implementation of the SNAP 2.0 algorithm to generate deconvoluted spectra and then exports a file containing the sorted monoisotopic masses and corresponding intensities (and other related data).

2.9 *Identification of cross-links*

Cross-links were identified using our self-written software that also uses the Links algorithm [3,53]. This algorithm identifies cross-linked peptides by matching experimental data to a theoretical library generated based on the protein sequence, protease specificity, cross-linker reactivity and composition, and protein chemical modification. The parameters for the search were defined as follows: enzyme – trypsin (specificity – cleavage after lysine and arginine, not cleaved after modification, 3 missed cleavages); variable modification – oxidation on methionine, dead-end cross-link (hanging DSGd0/DSGd4 or hanging DSSd0/DSSd4), dead-end cross-link with ethanolamine; cross-linker – DSGd0/DSGd4 or DSSd0/DSSd4 (specificity to lysine, tyrosine); mass error – 2 ppm. All cross-links identified by the Links algorithm were manually confirmed by examination of the raw data.

2.10 *Quantification of cross-links*

All spectra containing the appropriate isotopic pattern of manually validated cross-linked peptides were summed, reduced to centroid spectra, and exported from DataAnalysis 4.1 as an XY ASCII format (.xy) for further processing by mMass 5.5 (http://www.mmass.org/)[50,54]. Spectra in mMass 5.5 were swapped (transfer spectrum points to peak list data) and all unrelated peaks were manually removed. Ratios of light and heavy cross-linker were calculated using an envelope fit function which generates theoretical profiles of light and heavy cross-linked peptides and calculates the percentage of each form in the experimental data by linear combination and least-square fitting. These *in-silico* simulations were compared with and fitted to experimental data. mMass's advantage over other methods is its support of modern open formats that are used for spectrometric data. Moreover mMass can also run on different operating systems. Quantitative data from mMass were corrected by the quantifying ratio (ratio of non-deuterated and deuterated reagents form) for control calmodulin samples that was cross-linked with DSXd0/d4 (1:1). The quantifying ratio for control samples was calculated as the average of the quantifying ratios for all cross-links that were identified.

2.11 *LC-MS/MS analysis*

Cross-linked peptides were also evaluated by MS/MS analysis (qCID). The conditions for the separation of peptides resulting from enzymatic digestion were identical to those used for the LC-MS analysis. A solariX XR FT-ICR mass spectrometer (Bruker Daltonics, Germany) equipped with CaptiveSpray and 12 T superconducting magnet was coupled on-line with a nano UHPLC system. Data were acquired in auto MS/MS mode, with inclusion list of masses (window ±20 ppm) corresponding to the identified cross-links. Singly charged ions were excluded from fragmentation. MS boost was set to 2 seconds. The minimum threshold for fragmentation was defined as 5×10^6. Data analysis was performed using MS2links and GPMAW software packages [55,56].

3. Results and Discussion

3.1 *Calmodulin characterization*

The prerequisite for any protein structural analysis is a detailed characterization of the protein sequence, including post-translational modifications and splicing variants. Therefore, the exact mass of intact protein was measured by ESI-FTICR-MS. The acetylation at the N-terminus and trimethylation at position 115, noted by the supplier of calmodulin, was confirmed. The exact monoisotopic mass of calmodulin for base peak after spectral deconvolution was determined at m/z 16 781.862 (theoretical monoisotopic m/z 16 781.867, a difference of 0.005 mass units, 0.3 ppm). Data not shown.

3.2 *Chemical cross-linking SDS-electrophoresis, and in gel digestion.*

Cross-linking reactions were conducted with the amine-reactive reagents DSGd0/d4 and DSSd0/d4. Homobifunctional NHS esters (N-hydroxysuccinimide esters) were selected because they represent the most widely used group of isotope-labelled cross-linkers. In addition, amine-reactive reagents have also been used in previous calmodulin structural studies[34,46]. Two cross-linkers, differing only in spacer length, were used to get a better insight into the dynamics of the protein. Distance constraints acquired from an analysis with one reagent provides valuable information about the structure of the protein. However, two separate analyses -- each with a different cross-linker -- provide data that more accurately reflects the flexibility of molecule in solution by allowing a comparison of the distances obtained from the two experiments. The setup of a cross-linking experiment for the quantification of conformational changes differs from classical cross-linking because it uses non-deuterated (light) and deuterated (heavy) forms of the reagents separately. One form is added to the protein at a defined condition, while the second form is added to the protein under conditions that differ significantly from the first state. After quenching, both reactions are mixed. Detailed scheme of the experiment are shown in Fig. 1. After cross-linking experiments, half of each reaction mixture was separated by SDS-PAGE, the results of which are shown in Fig 2. Several forms of cross-linked ~17kDa protein monomer were observed. The gel clearly shows that protein bands obtained by cross-linking calcium-free calmodulin (lane 3 and 4) differ significantly from the bands obtained by cross-linking calcium-containing calmodulin (lane 7 and 8). Lanes 5 and 6 contain a mixture of calcium-free and calcium-containing calmodulin that were prepared for the quantification experiment. The observed protein bands are a superposition of both cross-linked

conformers. From Fig. 2, it is apparent the patterns in lane 5 and 6 are not identical. This is caused by the formation of different cross-linked products. This phenomenon prevents cross-linking product quantification by analyzing the two bands separately. Therefore the whole region containing cross-linked protein was excised for *in-gel* digestion and tryptic fragments were analyzed by LC-MS (Supplemental Table S1 and S2). Unfortunately, we observed only 3 cross-links for DSS and one more for DSG indicating the electrophoretic separation hampers the comparison of two conformers and thus it is not suitable for quantitative cross-linking experiments. Since no bands were visible in the higher mass region of the SDS gel, which confirms the absence of aggregates or multimeric forms of calmodulin and thus allows digestion in solution.

3.3 *Enzymatic digestion in solution*

Digestion of cross-linked protein is a critical step for this procedure. Cross-linking of two distinct protein conformers may lead to the formation of two different sets of cross-linked lysine residues so it is necessary to get a complete set of tryptic peptides from both states for successful quantification of any conformational changes. Tryptic digestion was performed in solution, and different conditions were tested to achieve complete tryptic proteolysis with similar total spectral intensity for the calcium-free and calcium-containing states. When this is done, LC-MS analysis revealed formation of the same peptides with different abundances. While the calcium-free state was easy to digest after cross-linking using trypsin (Fig. 3A), it was very difficult to cleave the cross-linked calcium-containing form. After tryptic digestion in solution at 37°C and with an enzyme:protein ratio of 1:20, we still observed a large amount of uncleaved protein in the calcium-containing samples (Fig. 3B). We therefore decided to double the trypsin concentration in digestion mixture by repeating the addition of protease 4 hours after the initial addition. The results showed that signals corresponding to the intact protein vanished (Fig. 3C). However, we still did not get the same abundances of unmodified peptides for the two conformations. To further improve the cleavage efficiency, we increased the temperature to 55°C (Fig. 3C). From the acquired chromatograms it was apparent that the intensities of the resulting peptides are almost identical (Fig. 3D). Although the differences between the intensities of unmodified peptides obtained from calcium-

free and calcium containing calmodulin digestion are less than 3% (Supplemental Fig. 1) -- and thus have extremely low influence on the quantification of conformers -- we tested many different digestion conditions (as described in the Methods section). However, we did not achieve any improvement in proteolysis. The guanidine and RapiGest conditions were worse, and the barocycles procedure gave results that were nearly identical to when the digestion was carried out at 55 °C and two shots of trypsin were added. Interestingly, in our previous study[27], where analysis of protein conformational changes by quantitative cross-linking was used, we did not observed this behavior. This lead us to conclude that this phenomenon occurs only for protein conformers whose structure becomes extremely compact after the cross-linking reaction. Since trypsin has R/K specificity and amine reactive cross-linking agents modifying lysines were used, we hypothesize that the utilization of proteases with different cleavage specificities or non-specific proteases may solve this problem. Also, middle down approach, in combination with chemical proteolysis, would probably be beneficial.

3.4 *Identification of cross-links by mass spectrometry*

After optimizing the enzymatic digestion conditions (55 °C and two shots of trypsin, condition 2.6B) we started analyzing mixtures of light and heavy conformers. The results of the cross-linking experiment with DSGd0/d4 a DSSd0/d4 for condition 2.6B are summarized in Table 1. Additional information on the cross-linked peptides identified is in Table S3 and Table S4. Using LC-MS analysis and Links software, three intra-peptide and seven inter-peptide cross-links of calmodulin were identified for both of the molecular rulers (DSG – spacer length 7.7 Å and DSS – spacer length 11.4 Å). In addition to the intra- and inter-peptide cross-links, we also observed a large number of dead-end cross-links and dead-end cross-links modified by ethanolamine which was used for termination of the cross-linking reaction (data are not shown). Although peptides with hydrolyzed cross-linker give information about the accessibility of amino acid side chains to the cross-linker they indirectly contribute to elucidation of conformational changes that are associated with changes of distances between amino acids.

3.5 *Identification of cross-links by MS/MS*

For unambiguous identification of cross-links, peptide mixtures resulting from enzymatic digestion were also analyzed by LC-MS/MS. To guarantee fragmentation of the cross-links, the analysis was performed with an inclusion list containing masses that corresponded to identified cross-linked peptides. An example of the product ion spectra is shown in Fig. 4. The y-ion series confirmed identity of cross-linked product. Next, the position of modified amino acids in the sequence was determined for all cross-links.

3.6 *Quantification by mMass*

The ratio of non-deuterated to deuterated forms of the reagents (i.e., the “quantifying ratio”) was determined by using the open source software, mMass. Input for this software was a list of masses with their abundances. As the source of this input file, we used mass spectrometric data that had to be summed and converted into centroid format. The quantifying ratio was determined using mMass *only* for identified and confirmed cross-links (an important prerequisite for calculation of this ratio is the correct peptide sequence). The generation of a theoretical isotopic envelope corresponding to peptides cross-linked with both non-deuterated and deuterated reagents was performed by using a special envelope-fit function and the quantifying ratio was calculated by comparison of this *in-silico* simulation with experimental data. The final quantification analysis data were adjusted by using the value of quantifying ratio for control calmodulin samples that were cross-linked with DSXd0/d4 (1:1). A comparison of isotopic envelopes for selected cross-linked peptides from control samples and from samples designed for quantification is shown in Fig. 6. The profile of cross-linked peptides from the control samples corresponds to the expected isotopic pattern (i.e., the ratio of the envelopes is 52:48 for DSGd0/d4 and 56:44 for DSSd0/d4). This nearly 1:1 ratio indicates that the measurement and subsequent quantification of cross-linked proteins should be possible and that this method should be applicable to different protein systems. This data also indicates good quantification accuracy and precision, based on ratio calculations considering all four cross-linkers signals. In addition, the exact sequence enables the simulation of the isotopic envelopes, including those with overlapping doublets (Fig. 5). The quantifying ratio was determined for all ten identified cross-links with different results, which are summarized in Table 1. The low values of standard deviation suggest that differences between measurements were minimal.

3.7 *Structure of calmodulin*

Due to the flexibility of calmodulin, many different structures (with and without calcium ions) have been obtained by NMR or X-Ray crystallography[41–43]. For visualization of our data in PyMOL we selected one calcium-free PDB structure determined by NMR analysis (1DMO, selected conformer 4 from 30) (Fig. 7A) and two calcium-containing PDB structures revealed by X-Ray crystallography (1PRW, 3CLN) (Fig. 7B and C). These PDB structures represent three different calmodulin conformations. Since our data shows only low calmodulin flexibility in the presence of calcium ions, we selected two calcium-containing structures. The distance between the alpha-carbon atoms of two cross-linked lysines can reach a maximum of 20-25Å for DSG (spacer length 7.7 Å) and 25-30 Å for DSS (spacer length 11.4 Å), considering the length and flexibility of lysine [26]. When we tried to visualize all of the identified cross-links on any unique calmodulin structure, some of the observed cross-links did not fall within these distances. On the other hand these cross-link uncovered conformation rearrangement among calmodulin structures which was further explained by quantifying ratio.

Quantification analysis revealed that the quantifying ratios of peptides cross-linked in the calcium-containing to peptides cross-linked in the calcium-free state is very high, indicating that the population of these cross-links is very low in the less-compact calcium-free structure – probably because the distances between the same alpha carbon atoms exceeds 30 Å (Table 1). An example of this is the inter-peptide cross-link 75-94, whose quantifying ratio is 76:24 for DSSd0/d4 and 88:12 for DSGd0/d4. This suggests that the cross-link is formed mainly in the calcium-containing state of calmodulin. Structures of calmodulin with visualized cross-links confirmed this, because lysine 75 and lysine 94 are very distant in the calcium-free structure (Fig. 7A), but much closer in the calcium-containing structure (Fig. 7B). Similar or opposite behavior was observed for most of the differentially observed cross-links, indicating that they were state-specific. One exception was the intra-peptide cross-link 21-30 that is equally accessible in both conformational states and therefore shows a quantifying ratio is 52:48 for DSGd0/d4 and 48:52 for DSSd0/d4 (Fig. 7). Interesting behavior was also observed for the inter-peptide cross-link 77-94. Although lysines 75 and 77 are almost adjacent in the calmodulin sequence cross-links 75-94 and 77-94

have opposite quantifying ratios. The explanation of this phenomenon is apparent from the calmodulin structure (Fig. 7). In the calcium-containing structures (Fig. 7B and 7C), cross-link 77-94 cannot be formed due to steric barriers; in the calcium-free state (Fig. 7A) no barriers are present. Differences between quantifying ratios for cross-linkers with different spacer lengths also provides useful information for studying protein dynamics, because it reflects protein flexibility. Regions of a protein with localized cross-links with minimal difference between cross-linkers represent parts of molecule with the same or very similar flexibility for both conformational states.

4. Conclusions

Chemical cross-linking in combination with mass spectrometry provides valuable information about the structures of proteins and protein complexes. Analysis using isotope-labeled cross-linkers can be used to monitor different protein conformational states. However, we have showed in this paper that this method has potential drawbacks due to limited enzymatic proteolysis. Moreover most research groups exploit gel electrophoresis for purification of desired the cross-linking product prior to proteolysis. Our data shows it is extremely important to be sure that the differentially labeled conformers are not separated into distinct protein bands. Also, successful quantification relies on the use of unlabeled and isotopically labeled cross-linkers. Since these chemical probes are difficult to synthetize, hydroscopic, and unstable, it is necessary to check and determine their chemical activities in a preliminary quantification experiment and use this correction factor in cases when regular and isotopic probes differ in their performance. Finally, some problems may arise from the general lack of software tools for quantification of cross-links. As an available solution, we described quantification of cross-linked peptides using the open-source multiplatform software, mMass 5.5. We believe that this technology will be of interest to laboratories trying to solving the three dimensional structure of proteins not amenable to standard high resolution techniques and research departments developing biosimilar recombinant therapeutics.

Acknowledgement

This work has been supported by the Institutional Research Concept of the Institute of Microbiology RVO61388971; and grants from the Ministry of Education Youth and Sports of the Czech Republic and

European Regional Development Funds (CZ.1.07/2.3.00/20.0055, CZ.1.07/2.3.00/30.0003 and CZ.1.05/1.1.00/02.0109); Charles University (project UNCE 204025/2012); Grant Agency of Charles University (800413) and the Czech Science Foundation (P207/10/1034). Access to instruments and other facilities was supported by the EU (Operational Program Prague – Competitiveness project CZ.2.16/3.1.00/24023).

References

[1] A. Sinz, Chemical cross-linking and mass spectrometry for mapping three-dimensional structures of proteins and protein complexes., J. Mass Spectrom. 38 (2003) 1225–1237.

[2] D. Fabris, E.T. Yu, Elucidating the higher-order structure of biopolymers by structural probing and mass spectrometry: MS3D., J. Mass Spectrom. 45 (2010) 841–60.

[3] M.M. Young, N. Tang, J.C. Hempel, C.M. Oshiro, E.W. Taylor, I.D. Kuntz, et al., High throughput protein fold identification by using experimental constraints derived from intramolecular cross-links and mass spectrometry., Proc. Natl. Acad. Sci. U. S. A. 97 (2000) 5802–5806.

[4] P. Novak, G.H. Kruppa, Intra-molecular cross-linking of acidic residues for protein structure studies, Eur. J. Mass Spectrom. (Chichester, Eng). 14 (2008) 355–65.

[5] G.H. Kruppa, J. Schoeniger, M.M. Young, A top down approach to protein structural studies using chemical cross-linking and Fourier transform mass spectrometry., Rapid Commun. Mass Spectrom. 17 (2003) 155–162.

[6] G.E. Davies, G.R. Stark, Use of dimethyl suberimidate, a cross-linking reagent, in studying the subunit structure of oligomeric proteins., Proc. Natl. Acad. Sci. U. S. A. 66 (1970) 651– 656.

[7] J.B. Fenn, Electrospray ionization mass spectrometry: How it all began., J. Biomol. Tech. 13 (2002) 101–18.

[8] M. Karas, F. Hillenkamp, Laser desorption ionization of proteins with molecular masses exceeding 10,000 daltons., Anal. Chem. 60 (1988) 2299–301.

[9] A. Sinz, The advancement of chemical cross-linking and mass spectrometry for structural proteomics: from single proteins to protein interaction networks., Expert Rev. Proteomics. 11 (2014) 733–43.
[10] C. Schmidt, C. V. Robinson, Dynamic protein ligand interactions - Insights from MS, FEBS J. 281 (2014) 1950–1964.
[11] E. V. Petrotchenko, C.H. Borchers, Crosslinking combined with mass spectrometry for structural proteomics, Mass Spectrom. Rev. 29 (2010) 862–876.
[12] S. Kalkhof, S. Haehn, M. Paulsson, N. Smyth, J. Meiler, A. Sinz, Computational modeling of laminin N-terminal domains using sparse distance constraints from disulfide bonds and chemical cross-linking, Proteins Struct. Funct. Bioinforma. 78 (2010) 3409–3427.
[13] Z.A. Chen, A. Jawhari, L. Fischer, C. Buchen, S. Tahir, T. Kamenski, et al., Architecture of the RNA polymerase II-TFIIF complex revealed by cross-linking and mass spectrometry., EMBO J. 29 (2010) 717–726.
[14] J.W. Back, L. de Jong, A.O. Muijsers, C.G. de Koster, Chemical cross-linking and mass spectrometry for protein structural modeling., J. Mol. Biol. 331 (2003) 303–13.
[15] R.B. Jacobsen, K.L. Sale, M.J. Ayson, P. Novak, J. Hong, P. Lane, et al., Structure and dynamics of dark-state bovine rhodopsin revealed by chemical cross-linking and highresolution mass spectrometry., Protein Sci. 15 (2006) 1303–1317.
[16] R. Ptáčková, T. Ječmen, P. Novák, J. Hudeček, M. Stiborová, M. Šulc, The application of an emerging technique for protein-protein interaction interface mapping: the combination of photo-initiated cross-linking protein nanoprobes with mass spectrometry., Int. J. Mol. Sci. 15 (2014) 9224–9241.
[17] K. Haladová, H. Mrázek, T. Ječmen, P. Halada, P. Man, P. Novák, et al., The combination of hydrogen/deuterium exchange or chemical cross-linking techniques with mass spectrometry: mapping of human 14-3-3ζ homodimer interface., J. Struct. Biol. 179 (2012) 10–7.
[18] A. Sinz, K. Wang, Mapping spatial proximities of sulfhydryl groups in proteins using a fluorogenic cross-linker and mass spectrometry, Anal. Biochem. 331 (2004) 27–32.

[19] K.L. Bennett, M. Kussmann, P. Björk, M. Godzwon, M. Mikkelsen, P. Sørensen, et al., Chemical cross-linking with thiol-cleavable reagents combined with differential mass spectrometric peptide mapping--a novel approach to assess intermolecular protein contacts., Protein Sci. 9 (2000) 1503–1518.
[20] D. Rozbesky, P. Man, D. Kavan, J. Chmelik, J. Cerny, K. Bezouska, et al., Chemical crosslinking and H/D exchange for fast refinement of protein crystal structure., Anal. Chem. 84 (2012) 867–870.
[21] K. Lasker, F. Forster, S. Bohn, T. Walzthoeni, E. Villa, P. Unverdorben, et al., Inaugural Article: Molecular architecture of the 26S proteasome holocomplex determined by an integrative approach, Proc. Natl. Acad. Sci. 109 (2012) 1380–1387.
[22] L. Peng, M.I. Rasmussen, A. Chailyan, G. Houen, P. Højrup, Probing the structure of human protein disulfide isomerase by chemical cross-linking combined with mass spectrometry, J. Proteomics. 108 (2014) 1–16.
[23] R.G. Walker, X. Deng, J.T. Melchior, J. Morris, P. Tso, M.K. Jones, et al., The structure of human apolipoprotein A-IV as revealed by stable isotope-assisted cross-linking, molecular dynamics, and small angle x-ray scattering., J. Biol. Chem. 289 (2014) 5596–608.
[24] S. Bhat, M.G. Sorci-Thomas, E.T. Alexander, M.P. Samuel, M.J. Thomas, Intermolecular contact between globular N-terminal fold and C-terminal domain of ApoA-I stabilizes its lipid-bound conformation: studies employing chemical cross-linking and mass spectrometry., J. Biol. Chem. 280 (2005) 33015–25.
[25] D. Rozbesky, Z. Sovova, J. Marcoux, P. Man, R. Ettrich, C. V Robinson, et al., Structural model of lymphocyte receptor NKR-P1C revealed by mass spectrometry and molecular modeling., Anal. Chem. 85 (2013) 1597–1604.
[26] L. Fischer, Z.A. Chen, J. Rappsilber, Quantitative cross-linking/mass spectrometry using isotope-labelled cross-linkers., J. Proteomics. 88 (2013) 120–128.
[27] M. Kopecka, D. Kosek, Z. Kukacka, L. Rezabkova, P. Man, P. Novak, et al., Role of the EFhand- like Motif in the 14-3-3 Protein-mediated Activation of Yeast Neutral Trehalase Nth1., J. Biol. Chem. 289 (2014) 13948–61.

[28] Y. Lu, P. Bottari, F. Turecek, R. Aebersold, M.H. Gelb, Absolute quantification of specific proteins in complex mixtures using visible isotope-coded affinity tags., Anal. Chem. 76 (2004) 4104–11.
[29] J. V Olsen, P.A. Nielsen, J.R. Andersen, M. Mann, J.R. Wiśniewski, Quantitative proteomic profiling of membrane proteins from the mouse brain cortex, hippocampus, and cerebellum using the HysTag reagent: mapping of neurotransmitter receptors and ion channels., Brain Res. 1134 (2007) 95–106.
[30] D.M. Walther, M. Mann, Accurate quantification of more than 4000 mouse tissue proteins reveals minimal proteome changes during aging., Mol. Cell. Proteomics. 10 (2011) M110.004523.
[31] S.P. Gygi, B. Rist, S.A. Gerber, F. Turecek, M.H. Gelb, R. Aebersold, Quantitative analysis of complex protein mixtures using isotope-coded affinity tags., Nat. Biotechnol. 17 (1999) 994–9.
[32] B.X. Huang, H.-Y. Kim, Interdomain conformational changes in Akt activation revealed by chemical cross-linking and tandem mass spectrometry., Mol. Cell. Proteomics. 5 (2006) 1045–53.
[33] D.R. Müller, P. Schindler, H. Towbin, U. Wirth, H. Voshol, S. Hoving, et al., Isotope-tagged cross-linking reagents. A new tool in mass spectrometric protein interaction analysis., Anal. Chem. 73 (2001) 1927–34.
[34] C. Ihling, A. Schmidt, S. Kalkhof, D.M. Schulz, C. Stingl, K. Mechtler, et al., Isotope-labeled cross-linkers and Fourier transform ion cyclotron resonance mass spectrometry for structural analysis of a protein/peptide complex., J. Am. Soc. Mass Spectrom. 17 (2006) 1100–1113.
[35] E. V Petrotchenko, J.J. Serpa, C.H. Borchers, An isotopically coded CID-cleavable biotinylated cross-linker for structural proteomics., Mol. Cell. Proteomics. 10 (2011) M110.001420.
[36] P.L. Ross, Y.N. Huang, J.N. Marchese, B. Williamson, K. Parker, S. Hattan, et al., Multiplexed protein quantitation in Saccharomyces cerevisiae using amine-reactive isobaric tagging reagents., Mol. Cell. Proteomics. 3 (2004) 1154–69.
[37] R.D. Unwin, A. Pierce, R.B. Watson, D.W. Sternberg, A.D. Whetton, Quantitative proteomic analysis using isobaric protein tags enables rapid comparison of changes in transcript and protein levels in transformed cells., Mol. Cell. Proteomics. 4 (2005) 924–35.

[38] A. Thompson, J. Schäfer, K. Kuhn, S. Kienle, J. Schwarz, G. Schmidt, et al., Tandem mass tags: a novel quantification strategy for comparative analysis of complex protein mixtures by MS/MS., Anal. Chem. 75 (2003) 1895–904.

[39] S.-E. Ong, B. Blagoev, I. Kratchmarova, D.B. Kristensen, H. Steen, A. Pandey, et al., Stable isotope labeling by amino acids in cell culture, SILAC, as a simple and accurate approach to expression proteomics., Mol. Cell. Proteomics. 1 (2002) 376–86.

[40] S. Pepke, T. Kinzer-Ursem, S. Mihalas, M.B. Kennedy, A dynamic model of interactions of Ca2+, calmodulin, and catalytic subunits of Ca2+/calmodulin-dependent protein kinase II., PLoS Comput. Biol. 6 (2010) e1000675.

[41] M. Zhang, T. Tanaka, M. Ikura, Calcium-induced conformational transition revealed by the solution structure of apo calmodulin., Nat. Struct. Biol. 2 (1995) 758–67.

[42] Y.S. Babu, C.E. Bugg, W.J. Cook, Structure of calmodulin refined at 2.2 A resolution., J. Mol. Biol. 204 (1988) 191–204.

[43] J.L. Fallon, F.A. Quiocho, A closed compact structure of native Ca(2+)-calmodulin., Structure. 11 (2003) 1303–7.

[44] D.M. Schulz, C. Ihling, G.M. Clore, A. Sinz, Mapping the topology and determination of a low-resolution three-dimensional structure of the calmodulin-melittin complex by chemical cross-linking and high-resolution FTICRMS: direct demonstration of multiple binding modes., Biochemistry. 43 (2004) 4703–4715.

[45] J.D. Chavez, N.L. Liu, J.E. Bruce, Quantification of protein-protein interactions with chemical cross-linking and mass spectrometry., J. Proteome Res. 10 (2011) 1528–37.

[46] P. Novak, V. Havlicek, P.J. Derrick, K. a Beran, S. Bashir, A.E. Giannakopulos, Monitoring conformational changes in protein complexes using chemical cross-linking and Fourier transform ion cyclotron resonance mass spectrometry: the effect of calcium binding on the calmodulin-melittin complex., Eur. J. Mass Spectrom. (Chichester, Eng). 13 (2007) 281–90.

[47] J. Cox, M. Mann, MaxQuant enables high peptide identification rates, individualized p.p.b.-range mass accuracies and proteome-wide protein quantification., Nat. Biotechnol. 26 (2008) 1367–72.
[48] M. Strohalm, M. Hassman, B. Kosata, M. Kodícek, mMass data miner: an open source alternative for mass spectrometric data analysis., Rapid Commun. Mass Spectrom. 22 (2008) 905–8.
[49] D.M. Horn, R.A. Zubarev, F.W. McLafferty, Automated reduction and interpretation of high resolution electrospray mass spectra of large molecules., J. Am. Soc. Mass Spectrom. 11 (2000) 320–32.
[50] M. Strohalm, D. Kavan, P. Novák, M. Volný, V. Havlícek, mMass 3: a cross-platform software environment for precise analysis of mass spectrometric data., Anal. Chem. 82 (2010) 4648–51.
[51] M.M. Bradford, A rapid and sensitive method for the quantitation of microgram quantities of protein utilizing the principle of protein-dye binding., Anal. Biochem. 72 (1976) 248–254.
[52] C.M. Wilson, Staining of proteins on gels: Comparisons of dyes and procedures, Methods Enzymol. 91 (1983) 236–247.
[53] B. Schilling, R.H. Row, B.W. Gibson, X. Guo, M.M. Young, MS2Assign, automated assignment and nomenclature of tandem mass spectra of chemically crosslinked peptides, J. Am. Soc. Mass Spectrom. 14 (2003) 834–850.
[54] T.H.J. Niedermeyer, M. Strohalm, mMass as a software tool for the annotation of cyclic peptide tandem mass spectra., PLoS One. 7 (2012) e44913.
[55] S. Peri, H. Steen, A. Pandey, GPMAW – a software tool for analyzing proteins and peptides, Trends Biochem. Sci. 26 (2001) 687–689.
[56] K. a Kellersberger, E. Yu, G.H. Kruppa, M.M. Young, D. Fabris, Top-down characterization of nucleic acids modified by structural probes using high-resolution tandem mass spectrometry and automated data interpretation., Anal. Chem. 76 (2004) 2438–45.

Fig. 1. Chemical cross-linking-mass spectrometry workflow for quantification of protein conformational changes.

Fig. 2. SDS-PAGE of calmodulin after cross-linking reaction with DSGd0/d4. M: protein marker. Lane1: Calmodulin calcium-free state without cross-linker. Lane 2: Calmodulin calcium-containing state without cross-linker. Lane 3: calmodulin cross-linked with 10 molar excess of mixture DSGd0/d4 (1:1) in calciumfree state. Lane 4: calmodulin cross-linked with 30 molar excess of mixture DSGd0/d4 (1:1) in calciumfree state. Lane 5: Mixture of calmodulin cross-linked by DSGd0 in calcium-containing state and calmodulin cross-linked by DSGd4 in calcium-free state (10 molar excess). Lane 6: mixture of calmodulin cross-linked by DSGd0 in calcium-containing state and calmodulin cross-linked by DSGd4 in calcium-free state (30 molar excess). Lane 7: Calmodulin cross-linked with 10 molar excess mixture DSGd0/d4 (1:1) in calcium-containing state. Lane 8: Calmodulin cross-linked with 30 molar excess mixture DSGd0/d4 (1:1) in calcium-containing state.

Fig. 3. Comparison of LC-MS chromatograms. (A) Chromatogram of calmodulin in the calcium-free state after digestion at 55°C trypsin: protein ratio 1:10. (B) Chromatogram of calmodulin in the calcium-containing state after digestion at 37°C trypsin: protein ratio 1:20. (C) Chromatogram of calmodulin in the calcium-containing samples after digestion at 37°C trypsin: protein ratio 1:10. (D) Chromatogram of calmodulin in calcium-containing state after digestion at 55°C trypsin: protein ratio 1:10. Zoom of the selected region corresponding to calmodulin that was not cleaved after digestion. Signals originating from unmodified protein (star), protein with one cross-linker (filled circle), and protein with two cross-linkers (square) are indicated.

Fig. 4. Product ion spectrum of the signal at m/z 766.73 ([M+4H]4+) corresponding to a cross-linked peptide 75-77 and 91-106 using DSSd0/d4.

Fig. 5. Quantification of cross-links by mMass 5.5. Comparision of *in-silico* simulation (yellow points and isotopic pattern) and measured data (blue points).

Fig. 6. Mass spectra of the intra-peptide cross-link 75-86 modified by a 1:1 mixture of DSGd0/DSGd4 in the calcium-containing state (A) and in the calcium-free state (C). The mass spectrum of the same cross-

link identified in samples prepared for quantification of conformational changes, modified by DSGd0 in the calcium-containing state and by DSGd4 in the calcium-free state (B).

Fig. 7. Visualization of the identified cross-links. Three different structures of calmodulin. (A) NMR structure of calcium-free state (1DMO/4)[41]. (B) X-Ray structure of calcium-containing state (1PRW)[43]. (C) X-Ray structure of calcium-containing state (3CLN)[42]. Side chains of modified lysines are visualized and colored. Lines indicate distances between alpha carbons. The color of the lines correspond to quantifying ratio (blue=ratio 0-20, dark violet=ratio 20-40, violet=ratio 40-60, dark red=ratio 60-80 and red=ratio 80-100)

Table 1 Summary of identified cross-links as well as their quantifying ratios. Data obtained for digestion condition 2.6B (cleavage in solution by trypsin at 55°C).

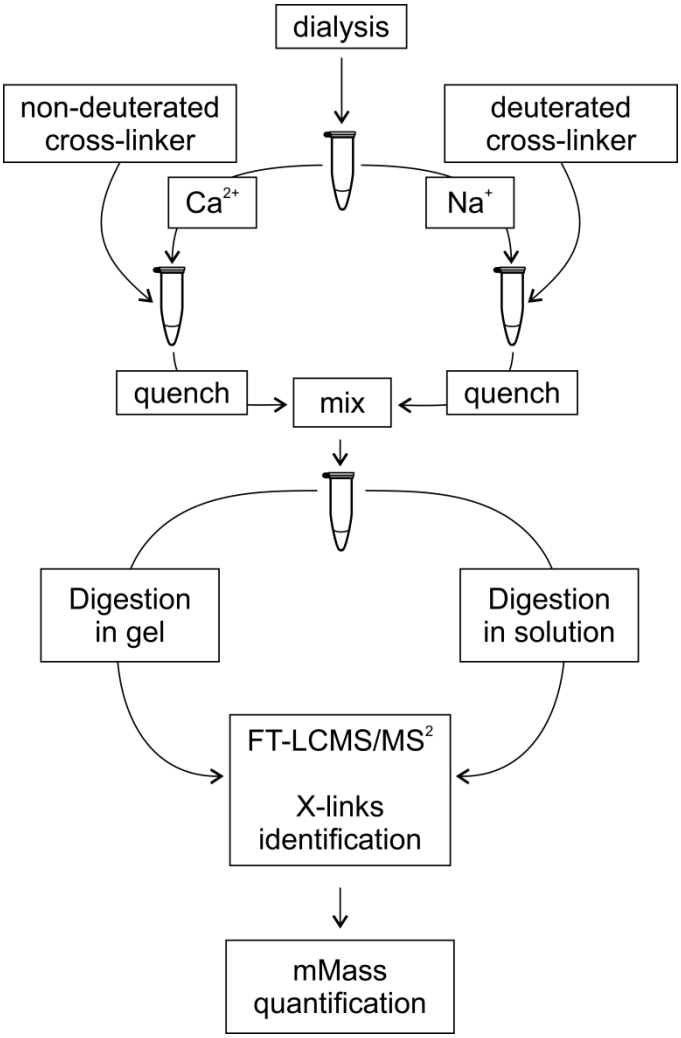

Fig. 1. Chemical cross-linking-mass spectrometry workflow for quantification of protein conformational changes.

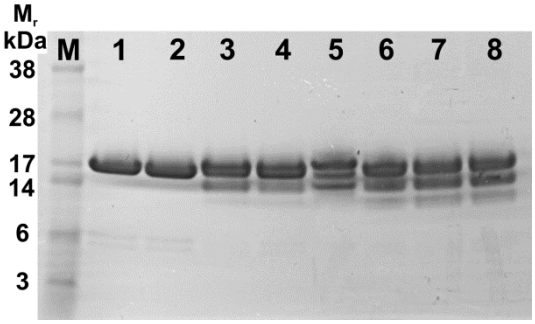

Fig. 2. SDS-PAGE of calmodulin after cross-linking reaction with DSGd0/d4. M: protein marker. Lane1: Calmodulin calcium-free state without cross-linker. Lane 2: Calmodulin calcium-containing state without cross-linker. Lane 3: calmodulin cross-linked with 10 molar excess of mixture DSGd0/d4 (1:1) in calcium-free state. Lane 4: calmodulin cross-linked with 30 molar excess of mixture DSGd0/d4 (1:1) in calcium-free state. Lane 5: Mixture of calmodulin cross-linked by DSGd0 in calcium-containing state and calmodulin cross-linked by DSGd4 in calcium-free state (10 molar excess). Lane 6: mixture of calmodulin cross-linked by DSGd0 in calcium-containing state and calmodulin cross-linked by DSGd4 in calcium-free state (30 molar excess). Lane 7: Calmodulin cross-linked with 10 molar excess mixture DSGd0/d4 (1:1) in calcium-containing state. Lane 8: Calmodulin cross-linked with 30 molar excess mixture DSGd0/d4 (1:1) in calcium-containing state.

Table 1 Summary of identified cross-links as well as their quantifying ratios. Data obtained for digestion condition 2.6B (cleavage in solution by trypsin at 55°C).

Peptide	Modified AA	DSG Ca^{2+}:Na^{+}	DSS Ca^{2+}:Na^{+}
91-106x76-86	K94-K77	11:89 ± 0	9:91 ± 1
91-106x75-77	K94-K75	88:12 ± 0	76:24 ± 0
91-106x22-37	K94-K30	16:84 ± 1	21:79 ± 0
91-106x14-30	K94-K21	37:63 ± 1	71:29 ± 1
75-77x22-37	K75-K30	87:13 ± 0	51:49 ± 2
75-77x14-30	K75-K21	87:13 ± 0	76:24 ± 0
75-77x1-21	K75-K13	34:56 ± 1	4:96 ± 1
75-90	K77-K75	81:19 ± 1	76:24 ± 0
75-86	K77-K75	60:40 ± 2	71:29 ± 0
14-37	K30-K75	52:48 ± 1	48:52 ± 1

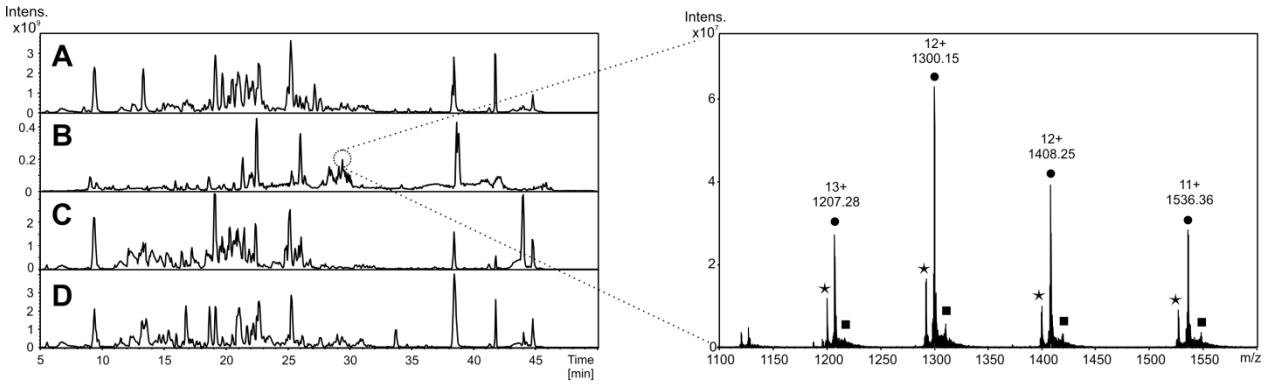

Fig. 3. Comparison of LC-MS chromatograms. (A) Chromatogram of calmodulin in the calcium-free state after digestion at 55°C trypsin: protein ratio 1:10. (B) Chromatogram of calmodulin in the calcium-containing state after digestion at 37°C trypsin: protein ratio 1:20. (C) Chromatogram of calmodulin in the calcium-containing samples after digestion at 37°C trypsin: protein ratio 1:10. (D) Chromatogram of calmodulin in calcium-containing state after digestion at 55°C trypsin: protein ratio 1:10. Zoom of the selected region corresponding to calmodulin that was not cleaved after digestion. Signals originating from unmodified protein (star), protein with one cross-linker (filled circle), and protein with two cross-linkers (square) are indicated.

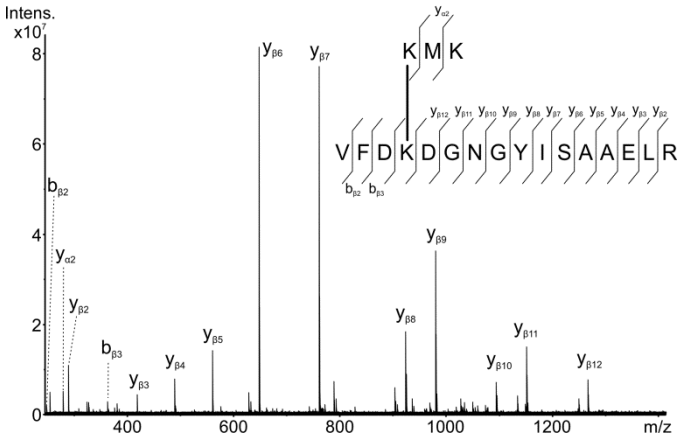

Fig. 4. Product ion spectrum of the signal at m/z 766.73 ($[M+4H]^{4+}$) corresponding to a cross-linked peptide 75-77 and 91-106 using DSSd0/d4.

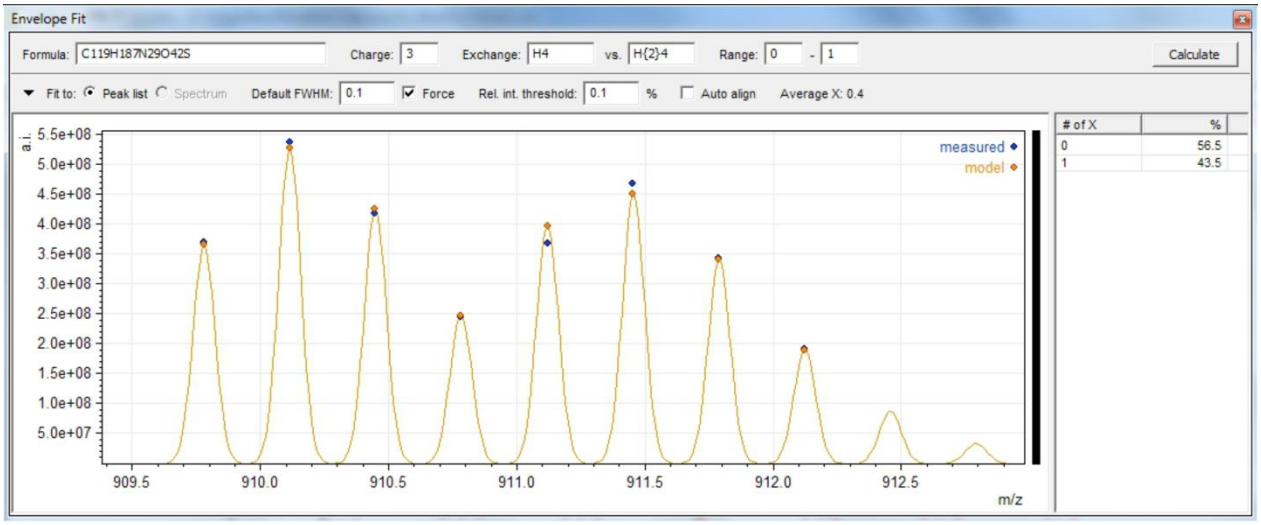

Fig. 5. Quantification of cross-links by mMass 5.5.Comparision of *in-silico* simulation (yellow points and isotopic pattern) and measured data (blue points).

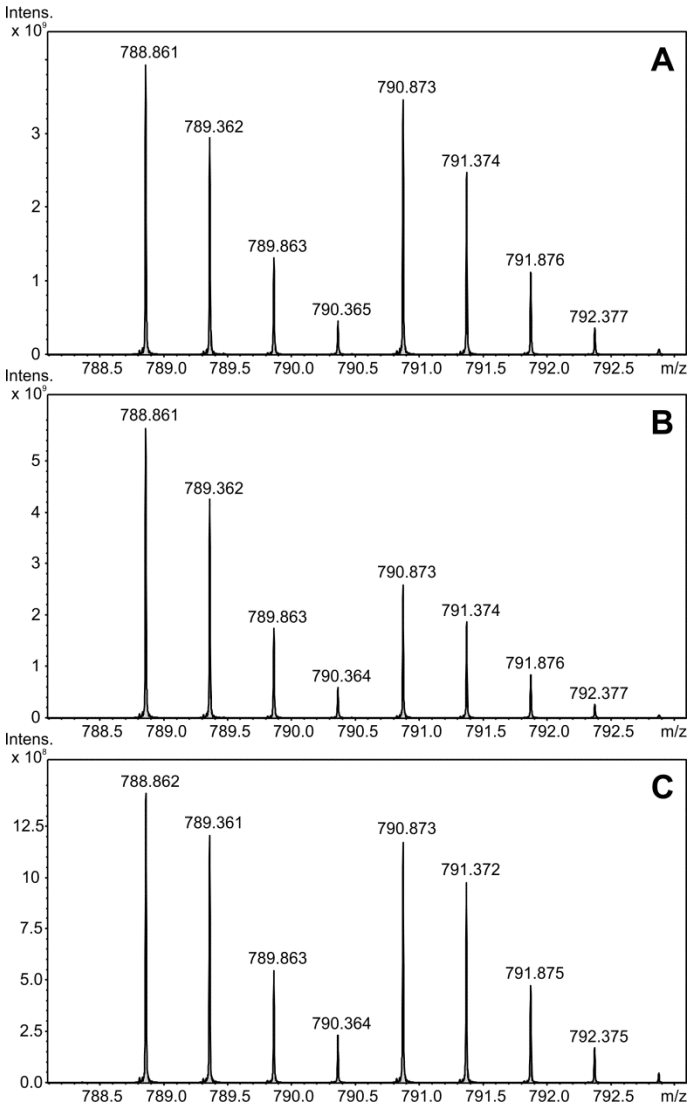

Fig. 6. Mass spectra of the intra-peptide cross-link 75-86 modified by a 1:1 mixture of DSGd0/DSGd4 in the calcium-containing state (A) and in the calcium-free state (C). The mass spectrum of the same cross-link identified in samples prepared for quantification of conformational changes, modified by DSGd0 in the calcium-containing state and by DSGd4 in the calcium-free state (B).

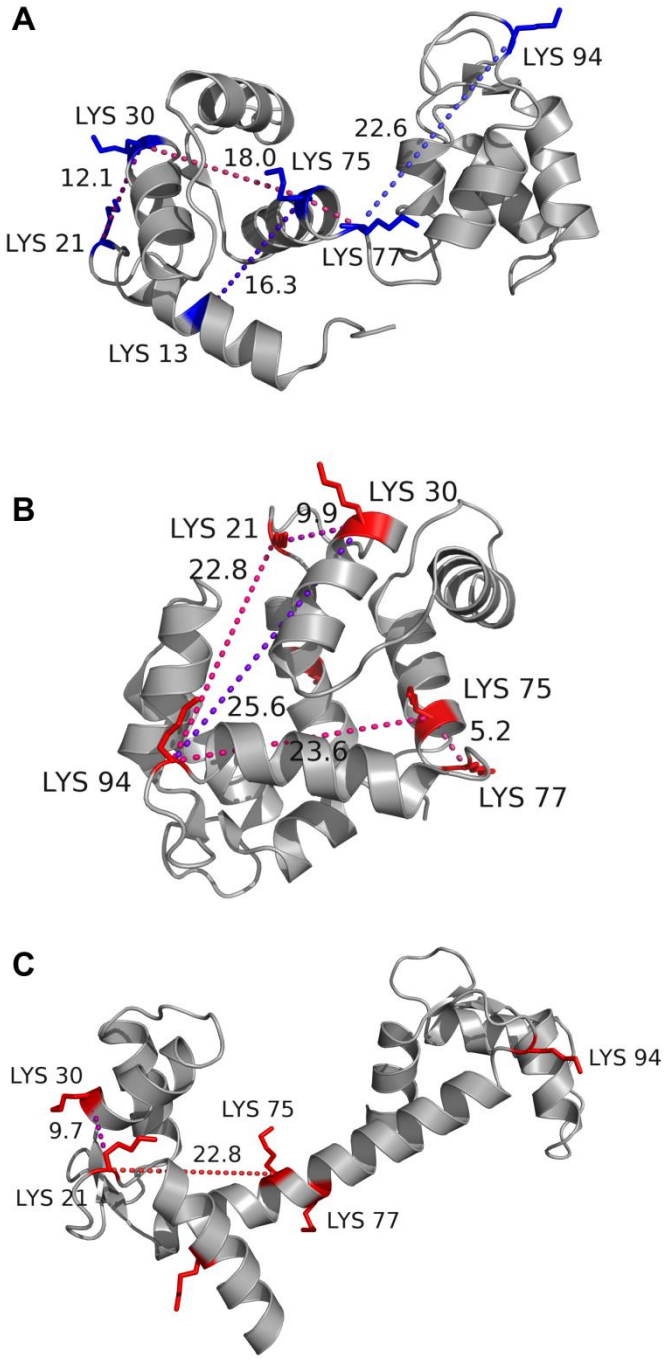

Fig. 7. Visualization of the identified cross-links. Three different structures of calmodulin. (A) NMR structure of calcium-free state (1DMO/4)[41]. (B) X-Ray structure of calcium-containing state (1PRW)[43]. (C) X-Ray structure of calcium-containing state (3CLN)[42]. Side chains of modified lysines are visualized and colored. Lines indicate distances between alpha carbons. The color of the lines correspond to quantifying ratio (blue=ratio 0-20, dark violet=ratio 20-40, violet=ratio 40-60, dark red=ratio 60-80 and red=ratio 80-100).

Paper 2

Macakova, E., Kopecka, M., **Kukacka, Z.**, Veisova, D., Novak, P., Man, P., Obsil. T., Obsilova, V

Structural basis of the 14-3-3 protein/dependent activatio of yeast neutral trehalase Nth1.

Biochim Biophys Acta. 1830, 4491-9 (2013)

My contribution to the publication: *Hydrogen/deuterium exchange experiments and chemical cross-linking experiments*

Biochimica et Biophysica Acta 1830 (2013) 4491–4499

Contents lists available at SciVerse ScienceDirect

Biochimica et Biophysica Acta

journal homepage: www.elsevier.com/locate/bbagen

Structural basis of the 14-3-3 protein-dependent activation of yeast neutral trehalase Nth1

Eva Macakova [a,b,1], Miroslava Kopecka [a,b,1], Zdenek Kukacka [c,d], Dana Veisova [a,b], Petr Novak [c,d], Petr Man [c,d], Tomas Obsil [a,e], Veronika Obsilova [a,*]

[a] Institute of Physiology, Academy of Sciences of the Czech Republic v.v.i., Videnska 1083, 14220 Prague, Czech Republic
[b] 2nd Faculty of Medicine, Charles University, V Uvalu 84, 150 06 Prague, Czech Republic
[c] Institute of Microbiology, Academy of Sciences of the Czech Republic v.v.i., Videnska 1083, 14220 Prague, Czech Republic
[d] Department of Biochemistry, Faculty of Science, Charles University, Hlavova 2030, 12843 Prague, Czech Republic
[e] Department of Physical and Macromolecular Chemistry, Faculty of Science, Charles University, Hlavova 2030, 12843 Prague, Czech Republic

ARTICLE INFO

Article history:
Received 4 April 2013
Received in revised form 8 May 2013
Accepted 20 May 2013
Available online 29 May 2013

Keywords:
14-3-3
Bmh
Neutral trehalase
H/D exchange
Molecular modeling
Circular dichroism

ABSTRACT

Background: Trehalases are highly conserved enzymes catalyzing the hydrolysis of trehalose in a wide range of organisms. The activity of yeast neutral trehalase Nth1 is regulated in a 14-3-3- and a calcium-dependent manner. The Bmh proteins (the yeast 14-3-3 isoforms) recognize phosphorylated Nth1 and enhance its enzymatic activity through an unknown mechanism.
Methods: To investigate the structural basis of interaction between Nth1 and Bmh1, we used hydrogen/deuterium exchange coupled to mass spectrometry, circular dichroism spectroscopy and homology modeling to identify structural changes occurring upon the complex formation.
Results: Our results show that the Bmh1 protein binding affects structural properties of several regions of phosphorylated Nth1: the N-terminal segment containing phosphorylation sites responsible for Nth1 binding to Bmh, the region containing the calcium binding domain, and segments surrounding the active site of the catalytic trehalase domain. The complex formation between Bmh1 and phosphorylated Nth1, however, is not accompanied by the change in the secondary structure composition but rather the change in the tertiary structure.
Conclusions: The 14-3-3 protein-dependent activation of Nth1 is based on the structural change of both the calcium binding domain and the catalytic trehalase domain. These changes likely increase the accessibility of the active site, thus resulting in Nth1 activation.
General significance: The results presented here provide a structural view of the 14-3-3 protein-dependent activation of yeast neutral trehalase Nth1, which might be relevant to understand the process of Nth1 activity regulation as well as the role of the 14-3-3 proteins in the regulation of other enzymes.

1. Introduction

The neutral trehalase Nth1 has been widely studied since its isolation and characterization in the 1990s [1–3]. Nth1 belongs to the glycoside hydrolase family 37 (EC 3.2.1.28) of O-glycosyl hydrolases (EC 3.2.1) which comprises enzymes with a common trehalase activity. The biological function of trehalase consists of the control of trehalase concentration via the degradation of trehalose [α-D-glucopyranosyl-(1-1)-α-D-glucopyranoside] into two molecules of glucose by hydrolyzing one of the two glycosidic bonds in trehalose with the inversion of the anomeric configuration. Trehalose is a naturally occurring non-reducing sugar found in a wide variety of organisms where it protects proteins and membranes from various stress conditions like dehydration, heat, cold, oxidation and desiccation and serves as a carbon and energy source. Trehalose is particularly important for insects as the hydrolyzed glucose is crucial for insect flight. It has also been suggested that in yeast and plants it serves as a regulatory and signaling molecule to direct certain metabolic pathways or to affect growth [4]. Recent studies have revealed that the enzyme activity of *Saccharomyces cerevisiae* Nth1 is regulated through an interesting mechanism involving phosphorylation of several sites by cAMP-dependent protein kinase (PKA), Ca^{2+} and the Bmh protein binding [5–7].

The yeast Bmh proteins belong to the 14-3-3 protein family, a eukaryotic family of highly conserved regulatory molecules, playing an important role in the regulation of signal transduction, apoptosis, cell cycle control, and nutrient-sensing pathways (reviewed in [8–10]). They fold into U-shaped homo- or heterodimers with a 40 Å-wide channel containing two amphipathic binding grooves, by which they bind their ligands mostly in a phosphorylation-dependent manner

Abbreviations: HDX, H/D exchange; HDX–MS, H/D exchange coupled to mass spectrometry; DSS, disuccinimidyl suberate; DSG, disuccinimidyl glutarate; WT, wild type; Nth1, neutral trehalase; pNth1, phosphorylated neutral trehalase; DMSO, dimethyl sulfoxide; TCEP, tris (2-carboxyethyl)phosphine; VDM, validoxylamine; CD, circular dichroism

* Corresponding author. Tel.: +420 241062191; fax: +420 244472269.
E-mail address: obsilova@biomed.cas.cz (V. Obsilova).

[1] The first two authors EM and MK contributed equally to this work.

0304-4165/$ – see front matter © 2013 Elsevier B.V. All rights reserved.
http://dx.doi.org/10.1016/j.bbagen.2013.05.025

[11–14]. Through these binding interactions, the members of the 14-3-3 protein family serve as molecular chaperons that modulate the subcellular localization, the structure or the stability of hundreds of other proteins. Notably, the catalytic activity of several enzymes, including tryptophan and tyrosine hydroxylases, serotonin N-acetyltransferase (AANAT), Raf kinases, ASK1 kinase, plant plasma membrane H^+-ATPase, plant nitrate reductase, plant mitochondrial and chloroplast adenosine 5-triphosphate (ATP) synthases and more, have been shown to be regulated in a 14-3-3 protein-dependent manner (reviewed in [9,10,15]). However, the mechanistic understanding of these regulations is mostly elusive. The 14-3-3 protein-dependent activation of AANAT is one of the few cases where available structural data enabled insight into the mechanism of the 14-3-3 protein action [16]. Regulation of this enzyme is based on a direct structural change where the 14-3-3 protein forces AANAT to adopt a conformation that allows optimal substrate binding.

Recently, we have performed a detailed biochemical characterization of the 14-3-3 protein-dependent activation of *S. cerevisiae* Nth1 and showed that Bmh proteins bind tightly to the phosphorylated N-terminal segment of Nth1 with residues Ser60 and Ser83 being sites primarily responsible for this interaction [6]. The close proximity of these two phosphorylated recognition sites also suggests a synergistic effect on binding as has been shown previously [17,18]. The complex formation strongly enhances the enzymatic activity of Nth1 and this activation is significantly more potent compared to Ca^{2+}-dependent one. Although we have obtained valuable information concerning the activation of Nth1, that study has not yielded sufficient structural insights into these mechanisms of Nth1 activation.

Thus, in this work we employed hydrogen/deuterium exchange coupled with mass spectrometry (HDX–MS) and circular dichroism spectroscopy to perform a structural analysis of a complex formed between the *S. cerevisiae* Nth1 and Bmh1. The HDX–MS method is commonly used to probe interactions within protein–protein and protein–ligand complexes since changes in HDX rates allow identification of binding surfaces and detection of conformational changes [19–21]. Our results show that Bmh1 binding to the phosphorylated Nth1 induces substantial changes in the deuteration kinetics of several Nth1 regions including the N-terminal segment where the 14-3-3 binding motifs are located, the Ca^{2+}-binding domain, and the catalytic trehalase domain. This suggests that these regions form the interaction surface of Nth1. In addition, our data also indicate that the Bmh1 protein binding affects the structural properties of segments surrounding the buried active site of Nth1. This might enable easier substrate and product entry and departure, respectively, and thus results in Nth1 activation. The interaction surface of Bmh1 includes not only the surface of the ligand binding groove where the phosphorylated N-terminal segment of Nth1 binds but also surfaces outside the central cavity of Bmh1 dimer. Circular dichroism measurements confirmed that the interaction between Bmh1 and Nth1 affects their tertiary structure but without the change in their secondary structure composition.

2. Materials and methods

2.1. Expression and purification of Bmh1 protein

DNA encoding *S. cerevisiae* Bmh1 protein was ligated into pET-15b (Novagen) using the NdeI and BamHI sites. The entire coding region was checked by sequencing. The Bmh proteins were expressed and purified as described previously [22].

2.2. Expression, purification, phosphorylation and activity measurement of Nth1

DNA encoding *S. cerevisiae* Nth1 protein was ligated into pET-32b (Novagen) with deletion of 81 base pairs after the sequence (6 × H) SSGLVPRGS using the NcoI and BamHI sites. The entire coding region was checked by sequencing. The Nth1 protein was expressed, purified and phosphorylated as described previously [6]. The enzyme kinetics of the hydrolysis of trehalose by Nth1 was measured using a stopped assay as described previously [6]. Specific activity was determined in μmol of glucose liberated per min per mg of protein.

2.3. Circular dichroism spectroscopy

The far-UV CD spectra were measured in a quartz cuvette with an optical path length of 1 mm (Starna, USA) using a J-810 spectropolarimeter (Jasco, Japan). The conditions of the measurements were as follows: a spectral region of 200–260 nm, a scanning speed of 10 nm/min, a response time of 8 s, a resolution of 1 nm, a bandwidth of 1 nm and a sensitivity of 100 mdeg. The final spectrum was obtained as an average of 5 accumulations. The spectra were corrected for a baseline by subtracting the spectra of the corresponding polypeptide-free solution. The CD measurements were conducted at room temperature (23 °C) in the buffer containing 20 mM Tris–HCl (pH 7.5), 150 mM NaCl, 2 mM 2-mercaptoethanol, 10% (w/v) glycerol buffer. The Bmh1 concentration was 0.089 $mg \cdot mL^{-1}$; the concentration of pNth1 and Nth1 was 0.145 $mg \cdot mL^{-1}$. After baseline correction, the final spectra were expressed as a mean residue elipticities Q_{MRW} ($deg \cdot cm^2 \cdot dmol^{-1}$) and were calculated using the equation

$$[Q]_{MRW} = \frac{\theta_{obs} \times 100 \times M_W}{c \times l \times N_R}, \quad (1)$$

where θ_{obs} is the observed ellipticity in mdeg, c is the protein concentration in $mg \cdot mL^{-1}$, l is the path length in cm, M_w is the protein molecular weight and N_R is the number of amino acids in the protein. Secondary structure content was estimated using tools available at Dichroweb website [23].

The near-UV CD spectra were measured in a quartz cuvette with an optical path length of 1 cm (Starna, USA) in a spectral region of 250–320 nm. The Bmh1 concentration was 0.447 $mg \cdot mL^{-1}$; the concentration of pNth1 and was 0.69 $mg \cdot mL^{-1}$.

2.4. Molecular modeling

Three-dimensional model of the catalytic domain of yeast neutral trehalase Nth1 (sequence 295–721) was generated using the DeepView v4.0.4, the SWISS-MODEL server [24,25] and the crystal structure of trehalase Tre37A from *Escherichia coli* (PDB code 2JF4, sequence 145–533) as a template [26]. The sequence identity and similarity of Nth1 catalytic domain to trehalase Tre37A are 27 and 42%, respectively. The final model was validated by PROCHECK, and bad contacts were corrected manually by Coot program [27]. The three-dimensional model of Bmh1 (sequence 4–236) was generated employing the same procedure and using the crystal structures of several known 14-3-3 protein isoforms as templates: PDB codes 1A4O [11], 1YZ5 [28], 2B05, 2BTP, 2C63 and 2BR9 [29]. Both models were further experimentally validated using the distance constraints derived from chemical cross-linking with homo-bifunctional cross-linkers DSS and DSG (amine–amine coupling) which covalently modify lysine residues.

2.5. Hydrogen/deuterium exchange kinetics coupled to mass spectrometry (HDX–MS)

HDX of the Bmh1 protein, phosphorylated Nth1 (pNth1) protein, and pNth1 in the presence of the Bmh1 protein was initiated by a 10-fold dilution in a deuterated buffer containing 20 mM Tris–HCl (pH/pD 7.5), 1 mM EDTA, 3 mM DTT, 200 mM NaCl and 10% (w/v) glycerol. The final protein concentrations were 3.16 μM for Bmh1 and 1.6 μM for phosphorylated Nth1. The molar ratio between Bmh1 and Nth1 was therefore 2:1. Aliquots (80 μL) were taken after 30 s, 1 min, 3 min,

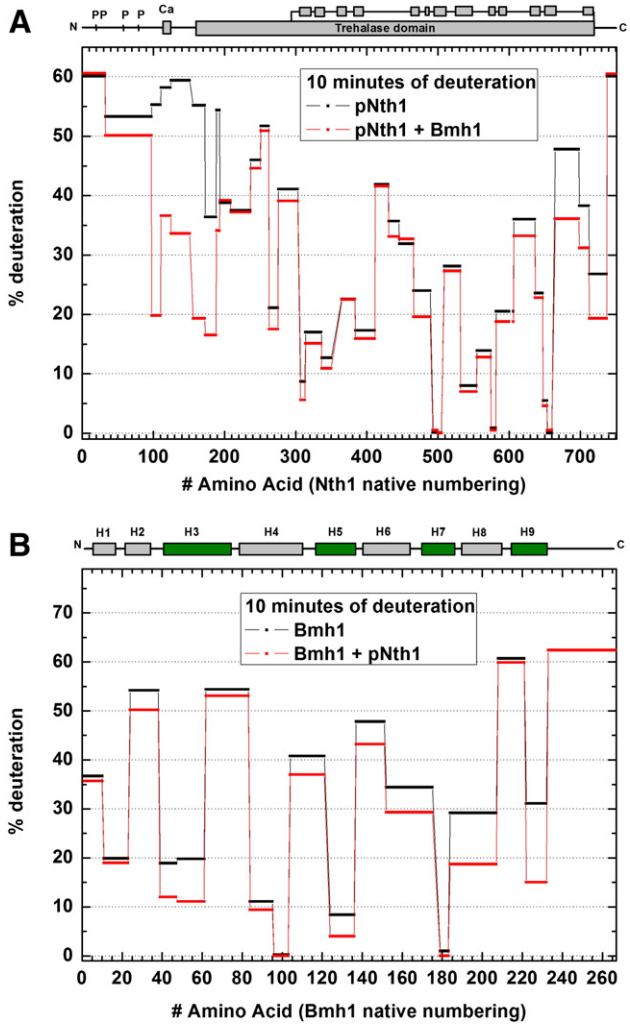

Fig. 1. A. Protection plot showing the deuteration levels of pNth1 both in the presence and absence of Bmh1 after 10 min of deuteration. The domain structure of *S. cerevisiae* Nth1 showing the relative position of PKA-phosphorylation sites and both the calcium and catalytic trehalase binding domains are shown at the top. B. Protection plot showing the deuteration levels of Bmh1 both in the presence and in the absence of pNth1 after 10 min of deuteration. Secondary structure elements are indicated at the top. The helices that form the ligand binding groove are colored green.

Table 1
Distance constraints of Nth1 derived from the cross-linking experiments and their comparison with distance constraints derived from the homology model of the catalytic domain of Nth1.

Cross-linker	Cross-linked residues[a]	Cα–Cα distance from the homology model	Cα–Cα distance constraint from the cross-linking experiments[b]
		Å	Å
DSS/DSSD4	K214–K675, inter	–	≤24
DSS/DSSD4	K214/K221–K563, inter	–	≤24
DSG/DSGD4	K258–K393, inter	–	≤20
DSS/DSSD4	K258–K343, inter	–	≤24
DSG/DSGD4	K393–K396, intra	5.1	≤20
DSS/DSSD4	K385–K517, inter	17.5	≤24
DSG/DSGD4	K385–K517, inter	17.5	≤20
DSS/DSSD4	K371–K718, inter	17.7	≤24
DSS/DSSD4	K537–K584, inter	16.4	≤24
DSG/DSGD4	K589–K593, intra	6.1	≤20
DSS/DSSD4	K589–K593, inter	6.1	≤24
DSG/DSGD4	K461–K561, inter	16.4	≤20
DSS/DSSD4	K461–K561, inter	16.4	≤24
DSS/DSSD4	K456–K458, inter	6.5	≤24
DSG/DSGD4	K456–K458, inter	6.5	≤20
DSS/DSSD4	K458–K461, inter	7.6	≤24
DSG/DSGD4	K458–K461, inter	7.6	≤20

[a] Intra denotes cross-link between residues from the same peptide, inter denotes cross-link between residues from two different peptides.
[b] The Cα–Cα inter-residue distance constraints used were based on the length of the spacer arm which is 7.7 Å for DSG and 11.4 Å for DSS. Concerning the flexibility of the lysine side chains the following cutoffs are generally used: 20 Å for α-carbons of lysine cross-linked with DSG, and 24 Å for α-carbons of lysine cross-linked with DSS[25].

10 min, 30 min, 1 h, 3 h and 5 h of exchange. The exchange was quenched by adding 20 μL of 0.1 M HCl and rapid freezing in liquid nitrogen. Analysis of deuterated samples (HPLC-MS) was done on HPLC (1200 Agilent Technologies, Waldbronn, Germany) connected to ESI–FT-ICR MS (9.4 T APEX-Ultra, Bruker Daltonics, Billerica, MA). The analysis started by a quick thawing of the sample and followed by digestion on a pepsin column (66 μL bed volume, flow rate 100 $\mu L \cdot min^{-1}$). Generated peptides were online desalted on a Peptide MicroTrap (Michrom Bioresources, Auburn, CA) and separated on a C18 reversed phase column (0.5 × 50 mm, Jupiter, Phenomenex) using a linear gradient 10–45% B in 20 min, where solvent A was 2% acetonitrile/0.4% formic acid in water, solvent B 95% acetonitrile/5% water/0.4% formic acid. Injection and switching valve, pepsin column, peptide trap and the analytical column were placed in an ice box to minimize the back-exchange. Peptide identification (mapping, HPLC-MS/MS) was done using the same

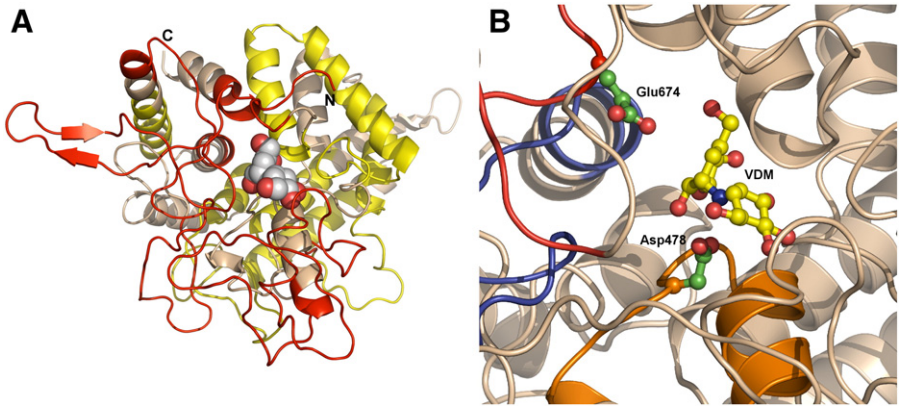

Fig. 2. A. Homology model of the catalytic trehalase domain of Nth1 (sequence 295–721). Regions that show fast deuteration and surround the active site (276–303, 412–465, 607–636 and 665–712) are shown in red. On the other hand, regions that exhibit slow exchange kinetics (307–350, 384–411, 493–505, 532–581 and 648–660) are shown in yellow. The active site contains trehalase inhibitor validoxylamine (shown as spheres) based on the crystal structure of the template (trehalase Tre37A, PDB code 2JF4) used to build this homology model [26]. B. Detailed view of the active site of Nth1 containing the inhibitor validoxylamine with selected residues proposed to act as the acid (Asp478) and base (Glu674) in the hydrolysis mechanism [26]. Both residues and inhibitor are shown in ball-and-stick representation. Regions that show slower deuteration kinetics upon Bmh1 binding are shown in red (peptide 665–698), blue (607–636) and orange (466–489).

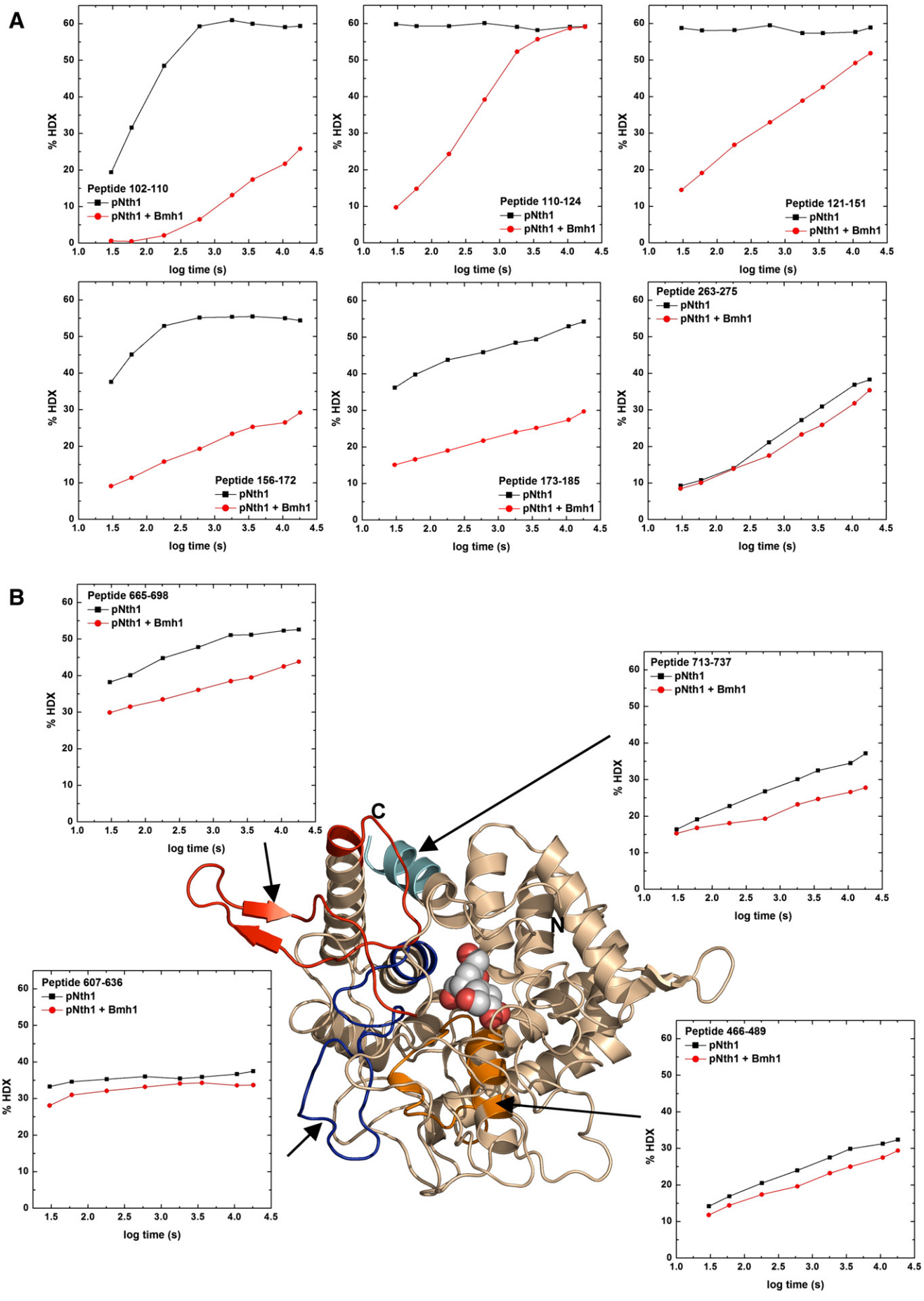
A
Peptide 102-110
pNth1
pNth1 + Bmh1
Peptide 110-124
Peptide 121-151
Peptide 156-172
Peptide 173-185
Peptide 263-275
% HDX
log time (s)
B
Peptide 665-698
Peptide 713-737
Peptide 607-636
Peptide 466-489
C
N

system as described above and the MS/MS spectra were searched by MASCOT against a database containing sequences of Bmh1 and Nth1 (the only allowed partial modification was Ser phosphorylation). Spectra of partially deuterated peptides were exported to txt files using DataAnalysis v 4.0 (Bruker Daltonics, Billerica, MA) and processed using the Java based program ExPro written in our laboratory [14,30].

2.6. Chemical cross-linking

The proteins (pNth1 or Bmh1) were cross-linked with homobifunctional cross-linkers disuccinimidyl suberate (DSS) and disuccinimidyl glutarate (DSG). The concentrations were as follows—Bmh1 0.2 $mg \cdot mL^{-1}$ and pNth1 0.3 $mg \cdot mL^{-1}$. For the cross-linking reaction, the proteins were transferred to 20 mM HEPES buffer (pH 7.5) with 150 mM NaCl and cross-linkers DSS and DSG were used as 1:1 (mol/mol) mixtures of non-deuterated and four-times deuterated compounds (d0/d4). Freshly prepared stock solutions of cross-linkers (10 mg/mL in DMSO) were added in 20× molar excess to pNth1 and reaction mixtures were incubated for 1 h at room temperature. Following cross-linking, proteins were separated on a NuPAGE 4–12% Bis–Tris gel using MES running buffer and the bands corresponding to a monomeric cross-linked protein were excised. The cysteines were reduced with 100 mM TCEP for 5 min at 90 °C and free cysteines were alkylated with 50 mM iodoacetamide for 20 min at room temperature in the dark. Trypsin digestion proceeded overnight at 37 °C with an enzyme/protein ratio of 1:20 (wt/wt). The resulting peptide mixtures were desalted on a peptide MacroTrap column (Michrom Bioresources). After desalting, the peptide mixtures were loaded onto a reverse phased column MAGIC C18 column (0.2 × 150 mm, Michrom Bioresources) and separated on a capillary HPLC system (Agilent Technologies) at a flow rate of 4 $\mu L \cdot min^{-1}$ under the following gradient conditions: 1–10% B in 1 min, 10–45% B in 19 min, 45–95% B in 5 min, where solvent A was 0.2% formic acid, 2.5% acetonitrile and 2.5% isopropanol in water and solvent B was 0.16% formic acid in 90% acetonitrile and 5% isopropanol. The column was connected directly to an Apex-ULTRA Qe FT-ICR mass spectrometer (Bruker Daltonics) equipped with a 9.4 T superconducting magnet using an electrospray ion source. The instrument was calibrated externally using arginine clusters resulting in mass accuracy below 2 ppm. Data acquisition and data processing were performed using ApexControl 3.0.0 and DataAnalysis 4.0 (Bruker Daltonics), respectively. The cross-links were identified using Links software [31]. The Links algorithm was set to consider the carbamidomethylation of cysteine and the possible single oxidation of methionine. The mass error threshold was kept below 2 ppm and all assigned fragments were verified manually.

3. Results

3.1. Preparation and characterization of the complex between yeast Nth1 and Bmh1 for HDX–MS measurements

The main goal of this study was to provide the structural basis for Bmh1 binding-dependent activation of Nth1 from *S. cerevisiae*. The complex between Bmh1 and phosphorylated Nth1 (pNth1) was prepared as described previously [6,22]. The phosphorylation of PKA phosphorylation sites (Ser20, Ser21, Ser60 and Ser83) was checked by mass spectrometry [6]. The interaction between pNth1 and Bmh1 was verified using native gel electrophoresis (see Supplemental data Fig. S1). The specific trehalase activity of pNth1 in the presence of Bmh1 was found to be 66 ± 2 $\mu mol \cdot min^{-1} \cdot mg^{-1}$ (μmol of glucose liberated per min per mg of protein). The circular dichroism (CD) spectroscopy was used to check the native structure of prepared Nth1, pNth1 and Bmh1 proteins. The analysis of measured far-UV CD spectra (Fig. S2) revealed that Nth1 contains ~26% of α-helix, ~24% of β-sheet and ~50% of random coil regions, whereas pNth1 contains ~31% of α-helix, ~17% of β-sheet and ~52% of random coil regions. The Bmh1 protein contains ~84% of α-helix and ~16% of random coil regions in a good agreement with the theoretical prediction.

3.2. HDX kinetics reveals significant structural changes of both pNth1 and Bmh1 upon the complex formation

The HDX–MS is an ideal technique for probing the protein–protein interactions and conformational changes of proteins by measuring the time-dependent increases in the weighted average peptide masses along the entire length of the protein backbone [32]. During the HDX–MS experiment we primarily monitor the backbone amide hydrogens because of the quick back-exchange of side chain and N-terminal amides. The exchange kinetics of the backbone amide hydrogens depends on both the solvent exposure and the hydrogen bonding. Therefore the regions that are exposed to the solvent and/or highly flexible commonly become deuterated quickly. In addition, the backbone amide hydrogens that are involved in the formation of hydrogen bonds in secondary structural elements generally exhibit slower deuteration and their exchange rates reflect structural stability and protein conformational mobility [19,33]. The importance of observed changes in the deuteration kinetics and the corresponding structural change can be "measured" by the difference in the number of deuterons which reflects the number of altered hydrogen bonds or solvent-shielded amides. For example, the average difference in deuteration level of 10% on a peptide with 22 exchangeable amides means 2.2 deuterons reflecting 2–3 amide bonds affected by the structural change or solvent shielding.

In order to identify regions of pNth1 and Bmh1 involved in protein–protein interactions and/or undergoing conformational changes upon the complex formation we studied the exchange kinetics of the pNth1:Bmh1 complex as well as free pNth1 and Bmh1. The exchange kinetics of pNth1 was followed on 255 peptides covering 92% of the Nth1 sequence (Fig. S3) while in the case of Bmh1 we used 61 peptides covering 99% of the Bmh1 sequence (Fig. S4) [30].

3.3. Structural changes of pNth1

To outline the exchange kinetics alongside the whole sequence of pNth1, an exchange profile showing the percentage of deuteration at a given time, in this case 10 min, for the selected non-overlapping peptides covering the entire protein sequence was created (Fig. 1A). The exchange profile of pNth1 alone (shown in black) reveals regions that exhibit relatively fast deuteration kinetics (the extent of the deuteration is higher than 30%) including the N-terminal segment containing all four PKA phosphorylation sites (region 2–110), the segment containing the putative calcium binding domain (region 111–151) and several regions from the trehalase catalytic domain (amino acids 156–262, 276–303, 412–465, 607–636, 665–712 and 738–751). The high rate of the isotope exchange suggests that these regions are either flexible and/or solvent exposed.

In order to obtain the structural interpretation for HDX–MS data we built a homology model of the catalytic domain of Nth1 (sequence 295–721) using the crystal structure of trehalase Tre37A from *E. coli* as a template [26]. The sequence identity and similarity of these two domains are 27% and 42%, respectively. This structural model consists of an $(\alpha/\alpha)_6$ barrel similar to that found for other α-toroidal

Fig. 3. HDX–MS reveals the binding surface of pNth1. Graphs represent HDX kinetics for selected pNth1 regions that show slower deuterium exchange kinetics upon Bmh1 binding. A. Regions from the unstructured N-terminal part of Nth1 that are missing in the homology model of the catalytic domain. B. Regions from the catalytic trehalase domain are mapped on its homology structural model (shown in red, blue, cyan and orange). Deuterium exchange is expressed as percentages relative to the maximum theoretical deuteration level for pNth1 alone (black squares) and pNth1 in the presence of Bmh1 (red circles). Time units are in seconds.

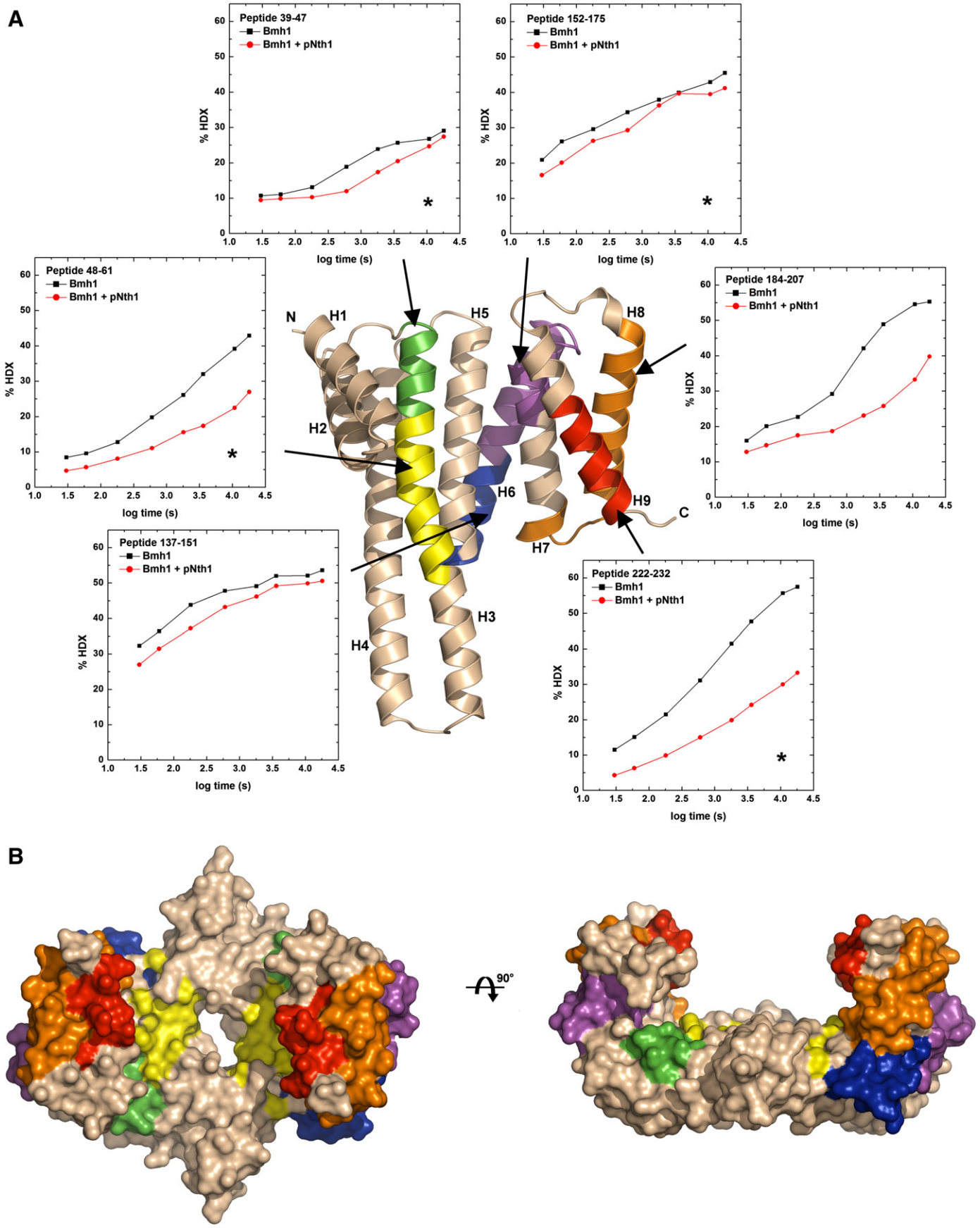

Fig. 4. HDX–MS reveals the binding surface of Bmh1. A. HDX kinetics for Bmh1 regions that show slower deuterium exchange kinetics upon pNth1 binding mapped on the structural model of Bmh1 (shown in red, green, blue, yellow, magenta and orange). Peptides forming the ligand binding groove are labeled by asterisks. Deuterium exchange is expressed as percentages relative to the maximum theoretical deuteration level for Bmh1 alone (black squares) and Bmh1 in the presence of pNth1 (red circles). Time units are in seconds. Only one monomer of Bmh1 is shown for clarity. B. Regions that show slower deuterium exchange upon pNth1 binding mapped on the surface representation of the Bmh1 dimer.

glycosidases with the active site buried within the structure (Fig. 2). The homology model was further experimentally validated using the distance constraints derived from the chemical cross-linking with homo-bifunctional cross-linkers DSS and DSG (amine–amine coupling) which covalently modify lysine residues. The comparison of the Cα–Cα inter-residue distance constraints from the cross-linking experiments and the homology model of Nth1 is shown in Table 1. Concerning the flexibility of the lysine side chains the following cutoffs are usually applied: 20 Å for α-carbons of lysines cross-linked with DSG, and 24 Å for α-carbons of lysines cross-linked with DSS [34]. As can be noticed, the Cα–Cα inter-lysine distances obtained from the cross-linking experiments correspond well with the distances derived from the structural model (Fig. S5). The structural model of Nth1 catalytic domain is also consistent with the results of HDX–MS measurements. Regions that show faster deuteration surround the active site and are solvent accessible (Fig. 2A, shown in red). On the other hand, segments that exhibit slower exchange kinetics (the extent of deuteration is lower than 20%) include regions 307–350, 384–411, 493–505, 532–581, and 648–660 (Fig. 2A, shown in yellow) correspond well with the secondary structural elements (Fig. 1A, shown on top) and/or are buried and have a low solvent accessibility. These results imply that our model based on the homology with Tre37A is a reasonable structural model for the catalytic domain of Nth1.

Bmh1 binding induces substantial reduction of the deuteration kinetics of several Nth1 regions (Fig. 1A, compare black and red profiles). The most profound decrease in exchange kinetics was observed for peptides from the region 98–193 where the deuteration level (at 10 min) dropped from the initial 55–60% in the absence of Bmh1 to 20–35% in its presence (Figs. 1A and 3A). Regions whose deuteration is moderately but significantly decreased upon Bmh1 binding include peptides from the N-terminal segment where the 14-3-3 binding motifs are located (33–97) and the catalytic domain (263–275, 307–313, 431–445, 466–489, 607–636 and 665–737). The decrease in deuterium incorporation can be interpreted as lower solvent exposure and/or the change in hydrogen bonding upon the complex formation, thus strongly suggesting that these regions (or their parts) form the interaction surface of pNth1 and/or undergo a structural rearrangement upon Bmh1 binding. Our structural model of Nth1, unfortunately, contains neither the N-terminal segment nor the putative calcium binding domain because the trehalase Tre37A, which was used as a template, possesses no such regions [26]. Thus, only peptides from the catalytic domain (466–489, 607–636, 665–698, and 713–737) can be mapped to our structural model. As can be seen in Fig. 3B, the structural model suggests that the active site of Nth1 is buried. Therefore, it is reasonable to speculate that the activation of Nth1 requires a conformational change that opens the active site and allows a better substrate and product entry and departure, respectively. It is likely that the observed reduction in the deuteration kinetics of regions that surround the active site of Nth1 (466–489, 607–636, 665–698, and 713–737) (Fig. 3B) reflects such Bmh1-induced structural change.

In addition, Bmh1 binding affects the deuteration kinetics of segments not only surrounding the active site but also containing residues crucial for catalysis (Fig. 2B). Sequence alignment used to prepare the structural model of Nth1 catalytic domain revealed that peptides 466–489 (Fig. 3B, shown in orange) and 665–698 (Fig. 3B, shown in red) contain residues Asp478 and Glu674 that are equivalent to Asp312 and Glu496 of *E. coli* trehalase Tre37A, which were suggested to function as the catalytic acid and base, respectively [26]. Thus, it seems that Bmh1 binding also affects the structural properties of residues that form the active site of Nth1.

A minor Bmh1-dependent decrease in deuteration level (~4% in 10 min) was also observed for the N-terminal part of pNth1 (33–97) containing both phosphorylation sites Ser60 and Ser83 that are crucial for Nth1 binding to the Bmh proteins. These changes likely reflect the binding of this segment of pNth1 into the ligand binding grooves of the Bmh1 protein [6]. In addition, the high level of deuteration of this segment (~50–60% in the absence of Bmh1) is consistent with the prediction that this region is disordered and highly flexible. This is also a reason why Bmh1 binding-dependent changes in the deuteration level in this region of pNth1 are not so evident. Such flexible regions undergo fast exchange and the information is then nearly or completely lost during the analysis.

3.4. Structural changes of Bmh1

The same approach was used to investigate the binding surface of the Bmh1 protein. The isotopic exchange profiles for Bmh1 alone and upon the binding to pNth1 are shown in Fig. 1B (compare black and red profiles). The profile observed for Bmh1 alone contains periodically alternating regions with fast and slow deuteration kinetics, thus corresponding well with the known structure of the 14-3-3 proteins.

To obtain structural interpretation for HDX–MS data we also built a homology model of the Bmh1 protein (Fig. 4). This model was also further experimentally validated using the distance constraints derived from the chemical cross-linking with homo-bifunctional cross-linkers DSS and DSG. The comparison of the Cα–Cα inter-residue distance constraints from the cross-linking experiments again corresponds well with the model (Table S1 and Fig. S6) and validates mainly the dimeric nature of Bmh1.

The highest deuteration was detected for helix H6, loops between helices H2 and H3, H3 and H4, H4 and H5, H8–H9, and the C-terminal tail. On the other hand, the lowest deuteration was observed for peptides from helices H1, H3, H4, H5, H7 and H9. Regions where we observed a significant decrease in the exchange kinetics upon pNth1 binding include peptides 39–47 and 48–61 from helix H3, peptides 137–151 from helix H6, peptides 152–175 from helices H6 and H7, peptides 184–207 from helices H7 and H8 and peptides 222–232 from the C-terminus of helix H9 (Fig. 4A). Again, the slower deuterium incorporation can be interpreted as decreased accessibility to the solvent upon the complex formation, thus strongly suggesting that these regions (or their parts) form the interaction surface of Bmh1. It is interesting that these peptides map not only to the surface of the ligand binding groove formed by helices H3, H5, H7 and H9 (where the phosphorylated N-terminal segment of pNth1 binds) but also to the surface of helices H6 and H8 outside the central cavity of the Bmh1 dimer (Fig. 4B).

3.5. Circular dichroism measurements

The circular dichroism (CD) is a standard technique for examining the structure of proteins in a solution [35]. Both far- and near-UV CD spectra were measured to investigate the possible structural changes of Bmh1 and pNth1 upon the complex formation. The comparison of far-UV CD spectra of the Bmh1:pNth1 complex (with the 2:1 molar stoichiometry) and the sum of the individual CD spectra of Bmh1 and pNth1 show no significant differences in the secondary structure composition (Fig. 5A). However, the comparison of near-UV CD spectra revealed significant changes in the region from 260 to 310 nm (Fig. 5B). The CD signal in this region reflects changes in the mobility, the nature of the environment and the spatial disposition of the aromatic amino acids [35]. Therefore, observed changes in the near-UV CD spectrum suggest that the complex formation between Bmh1 and pNth1 affects their tertiary structure in a good agreement with results of HDX–MS measurements.

Thus, the enhancement of the pNth1 enzyme activity upon Bmh1 binding as well as the decrease in the deuteration kinetics of several pNth1 and Bmh1 regions do not result from the change in the secondary structure composition but rather reflect the changes in the protein's tertiary structure.

4. Discussion

The aim of the current study is to provide a mechanistic insight into the activation of yeast neutral trehalase Nth1 by means of the 14-3-3-protein binding. Trehalases catalyze the hydrolysis of one of the two glycosidic bonds in trehalose with inversion of the anomeric

configuration. The only available crystal structure of trehalase (periplasmic enzyme Tre37A from *E. coli*) revealed that the active site is buried, thus suggesting that a significant conformational change would be required for the substrate and product entry and departure, respectively [26]. Comparison of sequences of yeast neutral trehalase Nth1 and *E. coli* trehalase Tre37A suggests that a similar mechanism might also apply for the yeast Nth1. The hypothesis that the active site of Nth1 is inaccessible is further supported by the fact that the enzyme by itself is catalytically inactive and its full activation requires its binding to the regulatory Bmh proteins (yeast 14-3-3 isoforms) known to modulate another protein's structure [6].

The 14-3-3 proteins are known to regulate the catalytic activity of several other enzymes including AANAT, plant plasma membrane H^+-ATPase, tyrosine and tryptophan hydroxylases, Raf kinases and more [16,36–38]. The mechanisms behind these processes are mostly elusive with the exception of AANAT and H^+-ATPase where the available structural data provided the insight into their regulations. In the case of AANAT, the 14-3-3 protein modulates its activity and affinity for substrates by changing the structure of a region involved in substrate binding [16]. The activation of H^+-ATPase is based on the binding of the 14-3-3 protein to its phosphorylated C-terminus inducing both the conformational change and the change of its oligomeric state [36]. In addition, it has recently been shown that the 14-3-3 protein-dependent structural modulation is also involved in the regulation of phosducin and the regulator of G-protein signaling 3 [13,39]. Therefore, it is reasonable to assume that similar mechanism might also be involved in the regulation of Nth1 activity.

In this work, we used HDX–MS and CD to investigate the interaction between the 14-3-3 protein and Nth1. These techniques enable the mapping of the interaction surfaces as well as the conformational changes of proteins in solution. Our results from HDX–MS experiments revealed that Bmh1 binding to the phosphorylated pNth1 decreases the isotope exchange kinetics for peptides from: (i) the N-terminal segment containing both phosphorylation sites Ser60 and Ser83 that are crucial for Nth1 binding to Bmh; (ii) the region 102–185, that corresponds to the Ca^{2+}-binding domain; and (iii) several peptides from the catalytic trehalase domain that surround the active site (Figs. 1A and 3). This strongly suggests that these regions are either in direct physical contact with the Bmh1 protein or undergo a structural change upon the complex formation. However, this structural change doesn't involve the change in the secondary structure composition within the complex but rather the change in the protein's tertiary structure, as indicated by far- and near-UV CD spectra (Fig. 5). Since the structure of the 14-3-3 protein dimer is very rigid [10,40], we believe that the tertiary structure of pNth1 is affected upon the complex formation. On the basis of these results we propose a model of the Bmh-dependent activation of Nth1 (Fig. 6). In the non-phosphorylated state, the active site of Nth1 is buried within the structure of the catalytic domain and the enzyme is inactive. The phosphorylation of Nth1 by PKA creates two 14-3-3 binding sites within the N-terminal segment of the enzyme. These motifs are recognized by yeast 14-3-3 isoforms (Bmh) and the Bmh1:pNth1 complex with the stoichiometry 2:1 is formed [6]. The Bmh binding affects the structural properties of both the Ca^{2+}-binding and the catalytic domains of pNth1. These structural changes enhance the enzymatic activity of pNth1 likely by increasing the accessibility of its active site, thus allowing the entry and departure of trehalose and glucose, respectively.

As far as the binding surface of the 14-3-3 protein is concerned, our results show that the interaction between Bmh1 and pNth1 extends beyond its binding groove. As can be seen in Fig. 4, the binding surface of Bmh1 protein includes less-conserved regions of helixes H6 and H8 outside the central channel of the 14-3-3 dimer. A similar binding surface was recently described for the human 14-3-3ζ in its complex with the regulator of G-protein signaling 3 using HDX–MS and small angle X-ray scattering [14]. In addition, a recently solved crystal structure of the complex between florigen Hd3a and the 14-3-3 protein revealed that this region is an important part of the binding interface [41]. Thus, it seems that this region outside the central channel is a common interaction surface in various 14-3-3 protein complexes and its sequence variability can contribute to the 14-3-3 isoform-binding specificity [10,40,42].

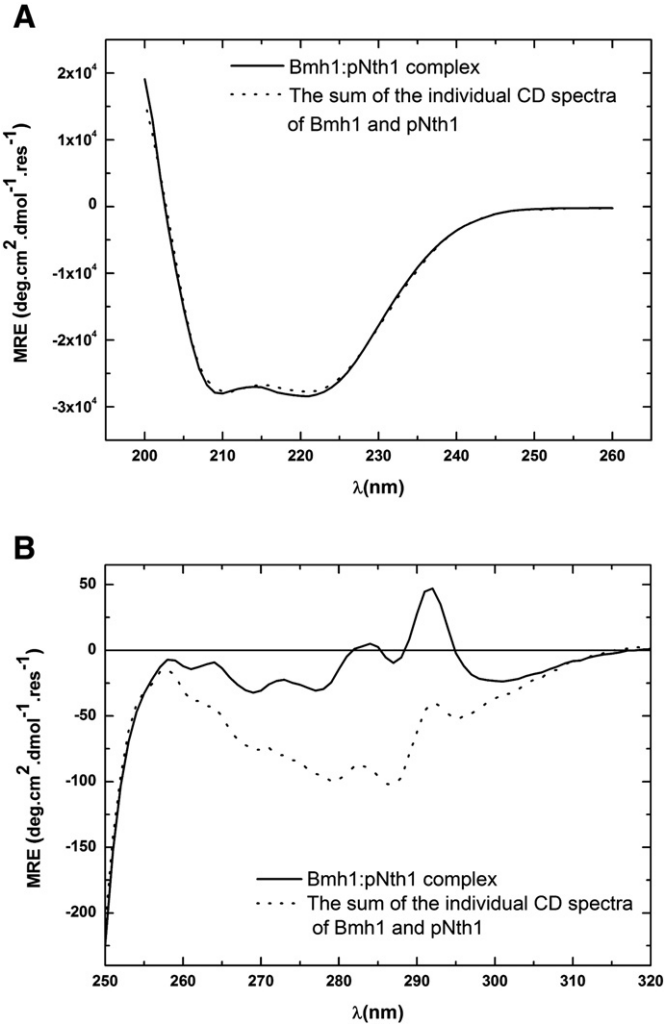

Fig. 5. A. The comparison of the far-UV CD spectrum of the Bmh1:pNth1 complex (solid line) with the sum of the individual far-UV CD spectra of Bmh1 and pNth1 (dotted line). B. The comparison of the near-UV CD spectrum of the Bmh1:pNth1 complex (solid line) with the sum of the individual near-UV CD spectra of Bmh1 and pNth1 (dotted line). Proteins were mixed with the 2:1 molar stoichiometry (Bmh1:Nth1). The mean residue ellipticity (MRE) is plotted as a function of the wavelength.

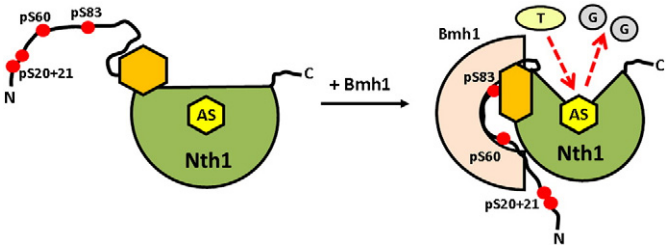

Fig. 6. Proposed mechanism for Bmh-dependent activation of Nth1. The active site of Nth1 in the absence of Bmh is buried within the structure of the trehalase domain and the enzyme is catalytically inactive [26]. Phosphorylated Nth1 is recognized by Bmh protein (yeast 14-3-3 isoform) and its binding to the N-terminal pSer60 and pSer83 induces conformational change within both the Ca^{2+}-binding domain and the catalytic domain in close proximity to the active site. This structural change enables substrate and product entry and departure, respectively, hence the enzyme activation. AS denotes the active site, T and G denotes trehalose and glucose, respectively, serines that are phosphorylated by PKA are shown as red circles, Ca^{2+}-binding domain is shown in orange, catalytic trehalase domain in green and the Bmh protein in pink.

In conclusion, in this work we provide structural insight into the 14-3-3 protein-dependent activation of yeast neutral trehalase Nth1 using HDX–MS and CD. Our results show that Bmh1 induces substantial changes in the deuteration kinetics of several Nth1 regions including the N-terminal segment where the 14-3-3 binding motifs are located, the Ca^{2+}-binding domain, and the catalytic trehalase domain. Our data also suggest that regions surrounding the buried active site are affected by Bmh1 binding and, thus, potentially undergo a structural change upon the complex formation. Such conformational change might enable easier substrate and product entry and departure, respectively, and thus results in Nth1 activation. The interaction surface of Bmh1 includes not only the surface of the ligand binding groove where the phosphorylated N-terminal segment of Nth1 binds but also surfaces outside the central cavity of Bmh1 dimer.

Acknowledgements

This work was supported by the Czech Science Foundation (Project P207/11/0455); Grant Agency of Charles University (Grants 644313 and 350111); Academy of Sciences of the Czech Republic (Research Projects RVO: 67985823 of the Institute of Physiology and RVO: 61388971 of the Institute of Microbiology) and Ministry of Education, Youth and Sports of the Czech Republic (Research Project MSM0021620857).

We wish to thank P. Novotna from the Department of Physics and Measurements, Institute of Chemical Technology, Prague for measuring the CD spectra.

Appendix A. Supplementary data

Supplementary data to this article can be found online at http://dx.doi.org/10.1016/j.bbagen.2013.05.025.

References

[1] H. App, H. Holzer, Purification and characterization of neutral trehalase from the yeast ABYS1 mutant, J. Biol. Chem. 264 (1989) 17583–17588.
[2] M. Kopp, H. Muller, H. Holzer, Molecular analysis of the neutral trehalase gene from *Saccharomyces cerevisiae*, J. Biol. Chem. 268 (1993) 4766–4774.
[3] M. Kopp, S. Nwaka, H. Holzer, Corrected sequence of the yeast neutral trehalase-encoding gene (NTH1): biological implications, Gene 150 (1994) 403–404.
[4] A.D. Elbein, Y.T. Pan, I. Pastuszak, D. Carroll, New insights on trehalose: a multifunctional molecule, Glycobiology 13 (2003) 17R–27R.
[5] S. Panni, C. Landgraf, R. Volkmer-Engert, G. Cesareni, L. Castagnoli, Role of 14-3-3 proteins in the regulation of neutral trehalase in the yeast *Saccharomyces cerevisiae*, FEMS Yeast Res. 8 (2008) 53–63.
[6] D. Veisova, E. Macakova, L. Rezabkova, M. Sulc, P. Vacha, H. Sychrova, T. Obsil, V. Obsilova, Role of individual phosphorylation sites for the 14-3-3-protein-dependent activation of yeast neutral trehalase Nth1, Biochem. J. 443 (2012) 663–670.
[7] W. Schepers, G. Van Zeebroeck, M. Pinkse, P. Verhaert, J.M. Thevelein, In vivo phosphorylation of SER21 and SER83 during nutrient-induced activation of the yeast PKA target trehalase, J. Biol. Chem. 287 (2012) 44130–44142.
[8] H. Fu, R.R. Subramanian, S.C. Masters, 14-3-3 proteins: structure, function, and regulation, Annu. Rev. Pharmacol. Toxicol. 40 (2000) 617–647.
[9] C. Mackintosh, Dynamic interactions between 14-3-3 proteins and phosphoproteins regulate diverse cellular processes, Biochem. J. 381 (2004) 329–342.
[10] T. Obsil, V. Obsilova, Structural basis of 14-3-3 protein functions, Semin. Cell Dev. Biol. 22 (2011) 663–672.
[11] D. Liu, J. Bienkowska, C. Petosa, R.J. Collier, H. Fu, R. Liddington, Crystal structure of the zeta isoform of the 14-3-3 protein, Nature 376 (1995) 191–194.
[12] J. Silhan, P. Vacha, P. Strnadova, J. Vecer, P. Herman, M. Sulc, J. Teisinger, V. Obsilova, T. Obsil, 14-3-3 protein masks the DNA binding interface of forkhead transcription factor FOXO4, J. Biol. Chem. 284 (2009) 19349–19360.
[13] L. Rezabkova, E. Boura, P. Herman, J. Vecer, L. Bourova, M. Sulc, P. Svoboda, V. Obsilova, T. Obsil, 14-3-3 protein interacts with and affects the structure of RGS domain of regulator of G protein signaling 3 (RGS3), J. Struct. Biol. 170 (2010) 451–461.
[14] L. Rezabkova, P. Man, P. Novak, P. Herman, J. Vecer, V. Obsilova, T. Obsil, Structural basis for the 14-3-3 protein-dependent inhibition of the regulator of G protein signaling 3 (RGS3) function, J. Biol. Chem. 286 (2011) 43527–43536.
[15] G. Tzivion, J. Avruch, 14-3-3 proteins: active cofactors in cellular regulation by serine/threonine phosphorylation, J. Biol. Chem. 277 (2002) 3061–3064.
[16] T. Obsil, R. Ghirlando, D.C. Klein, S. Ganguly, F. Dyda, Crystal structure of the 14-3-3zeta:serotonin N-acetyltransferase complex. a role for scaffolding in enzyme regulation, Cell 105 (2001) 257–267.
[17] B. Kostelecky, A.T. Saurin, A. Purkiss, P.J. Parker, N.Q. McDonald, Recognition of an intra-chain tandem 14-3-3 binding site within PKCepsilon, EMBO Rep. 10 (2009) 983–989.
[18] M. Molzan, C. Ottmann, Synergistic binding of the phosphorylated S233- and S259-binding sites of C-RAF to one 14-3-3zeta dimer, J. Mol. Biol. 423 (2012) 486–495.
[19] J.R. Engen, Analysis of protein conformation and dynamics by hydrogen/deuterium exchange MS, Anal. Chem. 81 (2009) 7870–7875.
[20] A. Aitken, Post-translational modification of 14-3-3 isoforms and regulation of cellular function, Semin. Cell Dev. Biol. 22 (2011) 673–680.
[21] H. Frauenfelder, G. Chen, J. Berendzen, P.W. Fenimore, H. Jansson, B.H. McMahon, I.R. Stroe, J. Swenson, R.D. Young, A unified model of protein dynamics, Proc. Natl. Acad. Sci. U. S. A. 106 (2009) 5129–5134.
[22] D. Veisova, L. Rezabkova, M. Stepanek, P. Novotna, P. Herman, J. Vecer, T. Obsil, V. Obsilova, The C-terminal segment of yeast BMH proteins exhibits different structure compared to other 14-3-3 protein isoforms, Biochemistry 49 (2010) 3853–3861.
[23] L. Whitmore, B.A. Wallace, DICHROWEB, an online server for protein secondary structure analyses from circular dichroism spectroscopic data, Nucleic Acids Res. 32 (2004) W668–W673.
[24] T. Schwede, J. Kopp, N. Guex, M.C. Peitsch, SWISS-MODEL: an automated protein homology-modeling server, Nucleic Acids Res. 31 (2003) 3381–3385.
[25] K. Arnold, L. Bordoli, J. Kopp, T. Schwede, The SWISS-MODEL workspace: a web-based environment for protein structure homology modelling, Bioinformatics 22 (2006) 195–201.
[26] R.P. Gibson, T.M. Gloster, S. Roberts, R.A. Warren, I. Storch de Gracia, A. Garcia, J.L. Chiara, G.J. Davies, Molecular basis for trehalase inhibition revealed by the structure of trehalase in complex with potent inhibitors, Angew. Chem. Int. Ed Engl. 46 (2007) 4115–4119.
[27] P. Emsley, B. Lohkamp, W.G. Scott, K. Cowtan, Features and development of Coot, Acta Crystallogr. D Biol. Crystallogr. 66 (2010) 486–501.
[28] A. Benzinger, G.M. Popowicz, J.K. Joy, S. Majumdar, T.A. Holak, H. Hermeking, The crystal structure of the non-liganded 14-3-3sigma protein: insights into determinants of isoform specific ligand binding and dimerization, Cell Res. 15 (2005) 219–227.
[29] X. Yang, W.H. Lee, F. Sobott, E. Papagrigoriou, C.V. Robinson, J.G. Grossmann, M. Sundstrom, D.A. Doyle, J.M. Elkins, Structural basis for protein–protein interactions in the 14-3-3 protein family, Proc. Natl. Acad. Sci. U. S. A. 103 (2006) 17237–17242.
[30] D. Kavan, P. Man, MSTools-Web based application for visualization and presentation of HXMS data, Int. J. Mass Spectrom. 302 (2011) 53–58.
[31] M.M. Young, N. Tang, J.C. Hempel, C.M. Oshiro, E.W. Taylor, I.D. Kuntz, B.W. Gibson, G. Dollinger, High throughput protein fold identification by using experimental constraints derived from intramolecular cross-links and mass spectrometry, Proc. Natl. Acad. Sci. U. S. A. 97 (2000) 5802–5806.
[32] A.N. Hoofnagle, K.A. Resing, N.G. Ahn, Protein analysis by hydrogen exchange mass spectrometry, Annu. Rev. Biophys. Biomol. Struct. 32 (2003) 1–25.
[33] R.E. Iacob, J.R. Engen, Hydrogen exchange mass spectrometry: are we out of the quicksand? J. Am. Soc. Mass Spectrom. 23 (2012) 1003–1010.
[34] D. Rozbesky, P. Man, D. Kavan, J. Chmelik, J. Cerny, K. Bezouska, P. Novak, Chemical cross-linking and H/D exchange for fast refinement of protein crystal structure, Anal. Chem. 84 (2012) 867–870.
[35] S.M. Kelly, T.J. Jess, N.C. Price, How to study proteins by circular dichroism, Biochim. Biophys. Acta 1751 (2005) 119–139.
[36] C. Ottmann, S. Marco, N. Jaspert, C. Marcon, N. Schauer, M. Weyand, C. Vandermeeren, G. Duby, M. Boutry, A. Wittinghofer, J.L. Rigaud, C. Oecking, Structure of a 14-3-3 coordinated hexamer of the plant plasma membrane H+-ATPase by combining X-ray crystallography and electron cryomicroscopy, Mol. Cell 25 (2007) 427–440.
[37] V. Obsilova, E. Nedbalkova, J. Silhan, E. Boura, P. Herman, J. Vecer, M. Sulc, J. Teisinger, F. Dyda, T. Obsil, The 14-3-3 protein affects the conformation of the regulatory domain of human tyrosine hydroxylase, Biochemistry 47 (2008) 1768–1777.
[38] H. Fu, K. Xia, D.C. Pallas, C. Cui, K. Conroy, R.P. Narsimhan, H. Mamon, R.J. Collier, T.M. Roberts, Interaction of the protein kinase Raf-1 with 14-3-3 proteins, Science 266 (1994) 126–129.
[39] L. Rezabkova, M. Kacirova, M. Sulc, P. Herman, J. Vecer, M. Stepanek, V. Obsilova, T. Obsil, Structural modulation of phosducin by phosphorylation and 14-3-3 protein binding, Biophys. J. 103 (2012) 1960–1969.
[40] V. Obsilova, J. Silhan, E. Boura, J. Teisinger, T. Obsil, 14-3-3 proteins: a family of versatile molecular regulators, Physiol. Res. 57 (Suppl. 3) (2008) S11–S21.
[41] K. Taoka, I. Ohki, H. Tsuji, K. Furuita, K. Hayashi, T. Yanase, M. Yamaguchi, C. Nakashima, Y.A. Purwestri, S. Tamaki, Y. Ogaki, C. Shimada, A. Nakagawa, C. Kojima, K. Shimamoto, 14-3-3 proteins act as intracellular receptors for rice Hd3a florigen, Nature 476 (2011) 332–U397.
[42] A.K. Gardino, S.J. Smerdon, M.B. Yaffe, Structural determinants of 14-3-3 binding specificities and regulation of subcellular localization of 14-3-3–ligand complexes: a comparison of the X-ray crystal structures of all human 14-3-3 isoforms, Semin. Cancer Biol. 16 (2006) 173–182.

Paper 3

Kopecka M, Kosek D, **Kukacka Z**, Rezabkova L, Man P, Novak P, Obsil T, Obsilova V.

Role of the EF-hand-like Motif in the 14-3-3 Protein-mediated Activation of Yeast Nth1.

J Biol Chem. 289, 13948-61 (2014)

My contribution to the publication: *Hydrogen/deuterium exchange experiments and chemical cross-linking experiments*

Protein Structure and Folding:

Role of the EF-hand-like Motif in the 14-3-3 Protein-mediated Activation of Yeast Neutral Trehalase Nth1

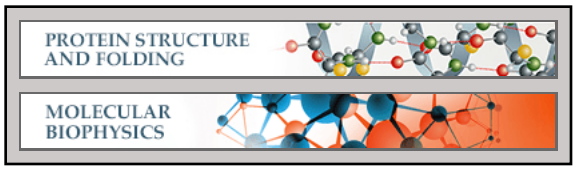

Miroslava Kopecka, Dalibor Kosek, Zdenek Kukacka, Lenka Rezabkova, Petr Man, Petr Novak, Tomas Obsil and Veronika Obsilova

J. Biol. Chem. 2014, 289:13948-13961.
doi: 10.1074/jbc.M113.544551 originally published online April 8, 2014

THE JOURNAL OF BIOLOGICAL CHEMISTRY VOL. 289, NO. 20, pp. 13948–13961, May 16, 2014

Role of the EF-hand-like Motif in the 14-3-3 Protein-mediated Activation of Yeast Neutral Trehalase Nth1*

Received for publication, December 27, 2013, and in revised form, March 20, 2014 Published, JBC Papers in Press, April 8, 2014, DOI 10.1074/jbc.M113.544551

Miroslava Kopecka[‡§], Dalibor Kosek[‡¶], Zdenek Kukacka[‖], Lenka Rezabkova[‡¶], Petr Man[‖**], Petr Novak[‖**], Tomas Obsil[‡¶], and Veronika Obsilova[‡1]**

*From the [‡]Institute of Physiology and the [‖]Institute of Microbiology, Academy of Sciences of the Czech Republic v.v.i., Videnska 1083, 14220 Prague, Czech Republic, the [§]Second Faculty of Medicine, Charles University, V Uvalu 84, 150 06 Prague, Czech Republic, and the Departments of [¶]Physical and Macromolecular Chemistry and **Biochemistry, Faculty of Science, Charles University, Hlavova 2030, 12843 Prague, Czech Republic*

Background: The yeast neutral trehalase Nth1 is activated by the 14-3-3 protein binding.
Results: The 14-3-3 protein induces a structural rearrangement of Nth1 with changes within the EF-hand like motif being essential for the activation process.
Conclusion: The EF-hand-like motif-containing domain is crucial for the 14-3-3-dependent activation of Nth1.
Significance: Structural basis of the mechanism of Nth1 activation.

Trehalases hydrolyze the non-reducing disaccharide trehalose amassed by cells as a universal protectant and storage carbohydrate. Recently, it has been shown that the activity of neutral trehalase Nth1 from *Saccharomyces cerevisiae* is mediated by the 14-3-3 protein binding that modulates the structure of both the catalytic domain and the region containing the EF-hand-like motif, whose role in the activation of Nth1 is unclear. In this work, the structure of the Nth1·14-3-3 complex and the importance of the EF-hand-like motif were investigated using site-directed mutagenesis, hydrogen/deuterium exchange coupled to mass spectrometry, chemical cross-linking, and small angle x-ray scattering. The low resolution structural views of Nth1 alone and the Nth1·14-3-3 complex show that the 14-3-3 protein binding induces a significant structural rearrangement of the whole Nth1 molecule. The EF-hand-like motif-containing region forms a separate domain that interacts with both the 14-3-3 protein and the catalytic trehalase domain. The structural integrity of the EF-hand like motif is essential for the 14-3-3 protein-mediated activation of Nth1, and calcium binding, although not required for the activation, facilitates this process by affecting its structure. Our data suggest that the EF-hand like motif-containing domain functions as the intermediary through which the 14-3-3 protein modulates the function of the catalytic domain of Nth1.

Trehalose (α-D-glucopyranosyl-(1-1)-α-D-glucopyranoside) is a non-reducing disaccharide of glucose found in a broad variety of organisms, including bacteria, yeast, fungi, insects, and plants, with the exception of mammalian cells. The generation of trehalose is triggered by stresses, such as heat, drying, or oxidative stress, indicating that the accumulated trehalose protects proteins and membranes from these stress conditions. Moreover, it can also act as a signaling or regulatory molecule in some cells, connecting the trehalose metabolism to glucose transport and glycolysis (1).

Hydrolysis of trehalose into two glucose subunits is carried out by trehalases (2). Trehalase was first described in *Aspergillus niger* and then in *Saccharomyces cerevisiae* and subsequently in many other organisms, including plants and animals (3–6). It has been shown that the yeast *S. cerevisiae* possesses several different trehalases: the vacuolar acid trehalase Ath1 with a lower pH optimum of about 4.5, and the cytoplasmic neutral trehalases Nth1 and Nth2 with a pH optimum of about 7 (7–10). The sequence comparison revealed that neutral trehalases from yeast *S. cerevisiae* and *Kluyveromyces lactis* possess, compared with other organisms, an N-terminal extension that contains several protein kinase A (PKA) phosphorylation sites as well as the EF-hand-like calcium binding motif, suggesting that this region is involved in the regulation of these enzymes' activity (11–13). Indeed, it has recently been shown that the activity of *S. cerevisiae* Nth1 is regulated by PKA phosphorylation, Ca^{2+}, and the 14-3-3 protein binding (14–16).

In yeast *S. cerevisiae*, two 14-3-3 protein isoforms (Bmh1 and Bmh2) with a great degree of homology have been identified (17). Bmh1 and Bmh2 were shown to be essential in most laboratory yeast strains (18). As in higher eukaryotes, yeast 14-3-3 proteins bind to and modulate the activity of plenty of proteins involved in crucial cellular processes (19). In our previous study, we identified two key phosphorylation sites within the N-terminal segment of *S. cerevisiae* Nth1 that are responsible for the 14-3-3 protein-mediated activation of Nth1 (15). This activation is significantly more potent compared with the Ca^{2+} only-dependent activation, which is more common among trehalases from other organisms. Subsequently, we showed that the 14-3-3 protein binding affects the conformation of both the region containing the EF-hand-like motif and the catalytic trehalase domain (Fig. 1), with changes in the EF-hand-like motif being, surprisingly, most profound (20). Thus, these data sug-

* This work was supported by Czech Science Foundation Project P207/11/0455; Grant Agency of Charles University Grants 644313 and 800413; and Academy of Sciences of the Czech Republic Research Projects RVO: 67985823 of the Institute of Physiology and RVO: 61388971 of the Institute of Microbiology. Access to MS facilities was supported by Academy of Sciences of the Czech Republic Project OPPK CZ.2.16/3.1.00/24023.
[1] To whom correspondence should be addressed. Tel.: 420-241062191; Fax: 420-244472269; E-mail: obsilova@biomed.cas.cz.

gested that this motif plays an important, although unclear, role in the activation of *S. cerevisiae* Nth1.

In this work, the structure of the Nth1·14-3-3 complex and the importance of the EF-hand-like motif located between residues 114 and 125 in the activation of Nth1 were investigated using the site-directed mutagenesis, the hydrogen/deuterium exchange (HDX)[2] coupled to mass spectrometry (HDX-MS), chemical cross-linking, and small angle x-ray scattering (SAXS). The low resolution structural views of Nth1 alone and the Nth1·14-3-3 complex show that the 14-3-3 protein binding induces a significant structural rearrangement of the whole Nth1 molecule. The EF-hand-like motif-containing region forms a separate domain that interacts with both the 14-3-3 protein and the catalytic trehalase domain. The structural integrity of the EF-hand-like motif is essential for the 14-3-3 protein-mediated activation of Nth1, and calcium binding, although not required for the activation, facilitates this process by affecting its structure. Our data suggest that the EF-hand like motif-containing domain functions as the intermediary through which the 14-3-3 protein modulates the function of the catalytic domain of Nth1.

EXPERIMENTAL PROCEDURES

Expression and Purification of Bmh1—DNA encoding *S. cerevisiae* Bmh1 protein was ligated into pET-15b (Novagen) using the NdeI and BamHI sites (21). The histidine-tagged protein was expressed by isopropyl 1-thio-β-D-galactopyranoside induction for 5 h at 37 °C and purified from *E. coli* BL21(DE3) using chelating Sepharose® Fast Flow (GE Healthcare) using the standard protocol. Next, Bmh1 was purified by anion exchange chromatography using Q Sepharose® Fast Flow (GE Healthcare). The protein was eluted using a linear gradient of NaCl (50–1000 mM). Fractions containing Bmh1 were concentrated and further purified using size exclusion chromatography on a Superdex 75 10/300 GL column (GE Healthcare) in a buffer containing 20 mM Tris/HCl (pH 7.5), 150 mM NaCl, 1 mM EDTA, 1 mM DTT, and 10% (w/v) glycerol. The protein concentration of purified Bmh1 was determined from UV absorption at 280 nm using an extinction coefficient value of 28,880 $M^{-1}\cdot cm^{-1}$ (22).

Expression, Purification, and Phosphorylation of Nth1—Nth1 from *S. cerevisiae* was expressed, purified, and phosphorylated as described previously (15). To ensure that prepared Nth1 is calcium-free, the final purification step (the size exclusion chromatography) was done in the presence of either 1 mM EDTA or EGTA (in a buffer containing 20 mM Tris/HCl (pH 7.5), 150 mM NaCl, 1 mM EDTA or 1 mM EGTA, 1 mM DTT, and 10% (w/v) glycerol). The protein concentration of purified Nth1 was determined from UV absorption at 280 nm using an extinction coefficient value of 142,560 $M^{-1}\cdot cm^{-1}$ (22).

Mutants of Nth1 (D103L, D114L, D114E, D116L, K117L, N118L, I121L, D125L, D125E, and D173L) were created by using the QuikChange™ approach (Stratagene). All mutations were confirmed by sequencing, and phosphorylation was checked by mass spectrometry.

Differential Scanning Fluorimetry—The thermofluor assay was performed using a real-time PCR LightCycler 480 II (Roche Applied Science). The proteins at a concentration of 0.2 mg/ml were tested in the presence of 8× concentrated Sypro Orange (Sigma-Aldrich) in a total reaction volume of 25 μl in the LightCycler 480 Multiwell Plate 96 (Roche Applied Science). The plate was sealed with the LightCycler 480 Sealing Foil (Roche Applied Science), and a temperature gradient from 20 to 95 °C with a rate of 0.01 °C/s was applied. The wavelengths for fluorescence excitation and emission were 465 and 580 nm, respectively. The melting temperature values, T_m, corresponding to the inflection points of the melting curves, were determined as the minima of the negative first derivative using the Roche LightCycler 480 SW 1.5 software (23, 24).

Enzyme Activity Measurements—The trehalase activity of phosphorylated Nth1 (pNth1) WT and mutants was measured by estimating the glucose produced by hydrolysis of trehalose using a stopped assay as described previously (15, 25). Specific trehalase activity of pNth1 was measured in the presence and in the absence of Bmh1 and/or Ca^{2+}. The final concentrations of pNth1, Bmh1, and Ca^{2+} were 100 nM, 15 μM, and 10 mM, respectively. The calcium was added to the 50 μl of reaction mixture from the 200 mM stock solution of $CaCl_2$. The assay was performed at 30 °C in buffer containing 20 mM Tris-HCl (pH 7.5), 150 mM NaCl, 10% (w/v) glycerol, and 30 mM trehalose. Experiments performed in the absence of Ca^{2+} also contained 1 mM EDTA or EGTA. The production of glucose was detected using the Amplex® Red glucose/glucose oxidase assay kit (Invitrogen). The specific activity of trehalase was determined as μmol of glucose liberated/min/mg of protein at 571 nm.

Near-UV Circular Dichroism (CD) Spectroscopy—The near-UV ECD spectra were measured in a quartz cuvette with an optical path length of 1 cm (Starna) using a J-810 spectropolarimeter (Jasco, Japan). The conditions of the measurements were as follows: a spectral region of 250–320 nm, a scanning speed of 10 $nm\cdot min^{-1}$, a response time of 8 s, a resolution of 1 nm, a bandwidth of 1 nm, and a sensitivity of 100 millidegrees. The final spectrum was obtained as an average of five accumulations. The spectra were corrected for a base line by subtracting the spectra of the corresponding polypeptide-free solution. The ECD measurements were conducted at room temperature (23 °C) in buffer containing 20 mM Tris-HCl (pH 7.5), 150 mM NaCl, 2 mM 2-mercaptoethanol, 10% (w/v) glycerol buffer. The Bmh1 concentration was 0.45 $mg\cdot ml^{-1}$, and the concentration of pNth1 WT and mutants was 0.69 $mg\cdot ml^{-1}$. After baseline correction, the final spectra were expressed as mean residue ellipticities, Q_{MRW} (degrees·cm^2·$dmol^{-1}$·number of $residues^{-1}$) and were calculated using the equation,

$$[Q]_{MRW} = \frac{\theta_{obs} M_r}{c l N_R 10} \quad \text{(Eq. 1)}$$

[2] The abbreviations used are: HDX, H/D exchange; HDX-MS, H/D exchange coupled to mass spectrometry; SV, sedimentation velocity; DSG, disuccinimidyl glutarate; DSS, disuccinimidyl suberate; DSS(G)D0 and DSS(G)D4, non-deuterated and four-times deuterated cross-linkers disuccinimidyl suberate (disuccinimidyl glutarate), respectively; pNth1, phosphorylated Nth1; SAXS, small angle x-ray scattering; Nth1, yeast enzyme neutral trehalase; Bmh1, yeast 14-3-3 protein isoform.

where θ_{obs} is the observed ellipticity in millidegrees, c is the protein concentration in mg·ml^{-1}, l is the path length in cm, M_r is the protein molecular weight, and N_R is the number of amino acids in the protein (26).

Analytical Ultracentrifugation Measurements—Sedimentation velocity (SV) experiments were performed using a ProteomLab^{TM} XL-I analytical ultracentrifuge (Beckman Coulter). SV experiments of Bmh1 and pNth1 were conducted at loading concentrations of 0.2–20 μM, 20 °C, and 42,000 or 48,000 revolutions/min rotor speed (An-50 Ti rotor, Beckman Coulter). All data were collected with absorbance optics at 280 nm. Samples were dialyzed against the buffer containing 20 mM Tris-HCl (pH 7.5), 150 mM NaCl, and 2 mM 2-mercaptoethanol before analysis. To study the effect of Ca^{2+} on the interaction, the dilution series of Bmh1 with constant concentration of pNth1 were analyzed with and without 10 mM $CaCl_2$ in the buffer solution. The $c(S)$ distributions were calculated from the raw absorbance data using the software package SEDFIT followed by fitting the chemical equilibrium using the Lamm equation modeling implemented in the software package SEDPHAT with the previously known s values of each component (27, 28). Loading concentrations were slightly corrected in the process of fitting.

Hydrogen/Deuterium Exchange Kinetics Coupled to Mass Spectrometry (HDX-MS)—HDX of the Bmh1 protein, pNth1 protein, both proteins in the presence and in the absence of 10 mM Ca^{2+}, and pNth1 in the presence of the Bmh1 protein and/or 10 mM Ca^{2+} was initiated by a 10-fold dilution in a deuterated buffer containing 20 mM Tris-HCl (pH/pD 7.5), 1 mM EDTA, 3 mM DTT, 150 mM NaCl, and 10% (w/v) glycerol. The final protein concentrations were 3.16 μM for Bmh1 and 1.6 μM for phosphorylated Nth1. The molar ratio between Bmh1 and Nth1 was therefore 2:1. Aliquots (80 μl) were taken after 30 s, 1 min, 3 min, 10 min, 30 min, 1 h, 3 h, and 5 h of exchange. The exchange was quenched by adding 20 μl of 0.1 M HCl and rapid freezing in liquid nitrogen. Analysis was done as described previously (20, 29).

Chemical Cross-linking Combined with Mass Spectrometry—Both Bmh1 and pNth1 alone and pNth1 in the complex with Bmh1 were cross-linked using cross-linkers disuccinimidyl suberate (DSS) or disuccinimidyl glutarate (DSG). For the cross-linking reaction, all proteins were dialyzed against buffer containing 20 mM HEPES (pH 7.5), 150 mM NaCl, 1 mM EGTA, and the protein concentrations were as follows: pNth1, 0.25 mg·ml^{-1}; Bmh1, 0.25 mg·ml^{-1}. All proteins were cross-linked in the presence of 10 mM Ca^{2+} using non-deuterated cross-linkers (DSSD0 and DSGD0) and in the absence of Ca^{2+} using four-times deuterated cross-linkers (DSSD4 and DSGD4). Freshly prepared stock solutions of cross-linkers (5 mg·ml^{-1} in DMSO) were added in a 15× and 30× molar excess to each protein alone or in a 50× and 100× molar excess to the pNth1·Bmh1 complex. The reaction mixtures were incubated for 2 h at room temperature. After that, samples that were cross-linked in the presence of Ca^{2+} with non-deuterated compounds were mixed with identical samples that were cross-linked in the absence of Ca^{2+} with deuterated compounds in a 1:1 molar ratio, and their analysis was performed as described previously (20, 30).

SAXS—SAXS data were collected on the European Molecular Biology Laboratory P12 beamline on the storage ring DORIS III (Deutsches Elektronen Synchrotron, Hamburg, Germany). The pNth1·Bmh1 protein complex and Nth1 were measured in a concentration range of 1.8–15 mg·ml^{-1}. Bmh1 was measured in a concentration range of 2.2–16.3 mg·ml^{-1}. Data analysis was performed using the ATSAS software suite (31). The data were averaged after normalization to the intensity of the transmitted beam, and the scattering of the buffer was subtracted using PRIMUS (32). The forward scattering ($I(0)$) and the radius of gyration (R_g) were evaluated using the Guinier approximation. The distance distribution function ($P(r)$) and the maximum particle dimension (D_{max}) were determined by the indirect Fourier transformation of the scattering data $I(s)$ using GNOM (33). The solute apparent molecular mass (MM_{exp}) was estimated by comparison of the forward scattering with that from reference solutions of bovine serum albumin (molecular mass 66 kDa). *Ab initio* molecular envelopes were computed using DAMMIN (34), which represents the protein by a collection of dummy atoms in a constrained volume with a maximum diameter defined experimentally by D_{max}. For each protein, 10 surfaces were generated and averaged using DAMAVER (35). The averaged surfaces were then used as the final SAXS three-dimensional structure.

RESULTS

The Integrity of the EF-hand-like Motif-containing Region Is Crucial for the 14-3-3 Protein-dependent Activation of Nth1—The catalytic activity of *S. cerevisiae* Nth1 is regulated by PKA-mediated phosphorylation followed by 14-3-3 binding, with Ca^{2+} playing an unclear regulatory role (14–16). Fig. 2*A* shows the activity of phosphorylated Nth1 (pNth1) in the presence of Ca^{2+}, Mg^{2+}, and Bmh1 (yeast 14-3-3 protein isoform). Samples with Bmh1 only also contained additional 1 mM EDTA or EGTA to ensure that no traces of metals were present. As can be seen, the Ca^{2+} only-dependent activity of pNth1 is very small, whereas Bmh1- and Bmh1 + Ca^{2+}-dependent activities are significantly higher, with the last one being a little bit more profound. No significant difference was observed for the Bmh1 only-dependent activity of pNth1 in the presence of either 1 mM EDTA or 1 mM EGTA; thus, only the activity in the presence of EDTA is shown. This activity (54 ± 1 μmol·min^{-1}·mg^{-1}) is somewhat lower compared with the activity measured in the absence of EDTA (64–66 μmol·min^{-1}·mg^{-1} (20)). In addition, no significant activation was observed in the presence of Mg^{2+} alone, and the effect of Bmh1 + Mg^{2+} on pNth1 activity was similar to that of Bmh1 alone.

Franco *et al.* (13) showed that the Ca^{2+}-dependent activation of Nth1 from *Schizosaccharomyces pombe* is mediated by a conserved Ca^{2+}-binding EF-hand-like motif that is also present in *S. cerevisiae* Nth1 (sequence ^{114}DTDKNYQITIED^{125}). To investigate the importance of this motif in *S. cerevisiae* pNth1 activation, we performed site-directed mutagenesis of several residues that correspond to both conserved and non-conserved positions from EF-hand motifs of numerous Ca^{2+}-binding proteins (Fig. 1*B*) (36, 37). We mutated residues Asp^{114}, Asp^{116}, Asn^{118}, and Asp^{125}, which correspond to conserved positions 1, 3, 5, and 12 in EF-hand motifs participating in metal coordina-

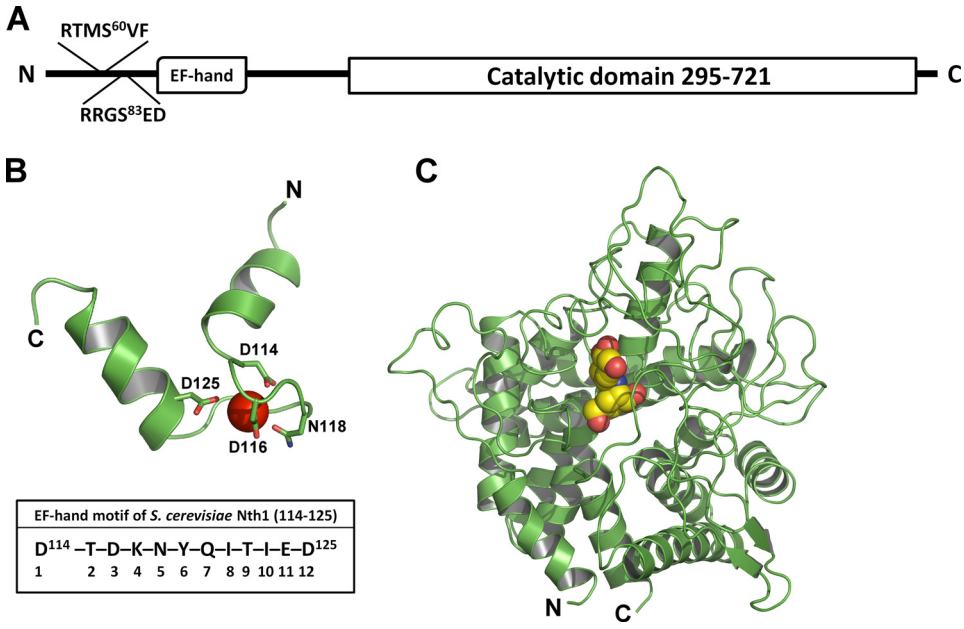

FIGURE 1. *A*, domain structure of *S. cerevisiae* Nth1. Relative positions of the 14-3-3 protein binding sites (Ser^{60} and Ser^{83}), the EF-hand like motif (sequence 114–125), and the catalytic domain (sequence 295–721) are shown. *B*, the sequence and the model of the EF-hand like motif (sequence 114–125) of Nth1. Mutated residues important for metal coordination at positions 1, 3, 5, and 12 are shown in *red*. The structural model of the EF-hand like motif of Nth1 was created using Modeler version 9.12 (46) and the structure of the EF-hand motif of calmodulin (Protein Data Bank code 1EXR) as a template (47). *C*, three-dimensional model of the catalytic domain of yeast neutral trehalase Nth1 (sequence 295–721) was generated as described previously using the crystal structure of trehalase Tre37A from *E. coli* (Protein Data Bank code 2JF4, sequence 145–533) as a template. The active site contains trehalase inhibitor validoxylamine (shown as *spheres*), which was present in the structure of the template (20, 40).

tion, and residues Lys^{117} and Ile^{121} at non-conserved positions 4 and 8, respectively, which are not involved in metal coordination (36, 37). In addition, we also mutated residues Asp^{103} and Asp^{173} from regions bordering the EF-hand-like motif.

To verify that the introduced mutations did not result in an overall destabilization of the Nth1 structure, the stability of all prepared mutants was checked by measuring the thermally induced protein denaturation using differential scanning fluorimetry. No significant differences in the temperature of the unfolding transition (T_m) were observed for all Nth1 mutants with the exception of the I121L variant (Table 1). The slightly lower T_m of I121L mutant might reflect different conformation of the EF-hand-like motif because this residue (position) is known to be important for the proper conformation of the motif (36). The binding of selected phosphorylated Nth1 mutants to Bmh1 was also checked by using analytical ultracentrifugation, and no significant differences compared with pNth1 WT were observed (data not shown). Thus, all prepared Nth1 mutants were found to be suitable for trehalase activity measurements.

Next, the Bmh1-mediated activity of prepared pNth1 mutants in the absence and the presence of Ca^{2+} was measured (Fig. 2*B*). Although all mutants, with the exception of D116L, showed either significantly or totally suppressed Bmh1-mediated activity in the absence of Ca^{2+} (Fig. 2*B*, *white bars*), the presence of Ca^{2+} (Fig. 2*B*, *gray bars*) rescued the activity of all but the D114L, N118L, and D125L mutants. These three residues are located at positions crucial for metal coordination, and their replacement with Leu had the most profound effect on pNth1 activity both in the absence and the presence of Ca^{2+}. On the other hand, mutations D114E and D125E, which should rescue the Ca^{2+} binding, showed high Bmh1-mediated activity

TABLE 1

Midpoint temperatures of the protein-unfolding transition (T_m) for Nth1 WT and mutants as determined using differential scanning fluorimetry

Uncertainties are the S.E. values calculated from three experiments.

Nth1 variant	T_m
	℃
WT	53.6 ± 0.3
D103L	52.3 ± 0.2
D114L	52.7 ± 0.2
D114E	53.4 ± 0.2
D116L	53.1 ± 0.1
K117L	53.6 ± 0.1
N118L	52.8 ± 0.5
I121L	50.4 ± 0.3
D125L	52.6 ± 0.2
D125E	53.3 ± 0.1
D173L	52.5 ± 0.1

but only in the presence of Ca^{2+}. These data suggested not only that the structural integrity of the EF-hand like motif is essential for the Bmh1-mediated activation of pNth1 but also that calcium binding helps to mediate the activation process, probably through the structural stabilization of the EF-hand-like motif.

pNth1 Mutants D114L and D125L Show Conformational Behavior Similar to That of Wild Type—Trehalase activity measurements revealed that pNth1 mutants D114L and D125L are unable to get activated in the presence of Bmh1 (Fig. 2*B*), although their binding affinities for Bmh1 remain unchanged. To compare the conformational behavior of these two inactive mutants with pNth1 WT, near-UV CD spectra, which are sensitive to certain aspects of protein tertiary structure, of the pNthl D114L·Bmh1, pNth1 D125L·Bmh1, and pNth1 WT·Bmh1 complexes (with 1:2 molar stoichiometry) were measured. The comparison of spectra of complexes with sums of the individual CD spectra of pNth variants and Bmh1 revealed no

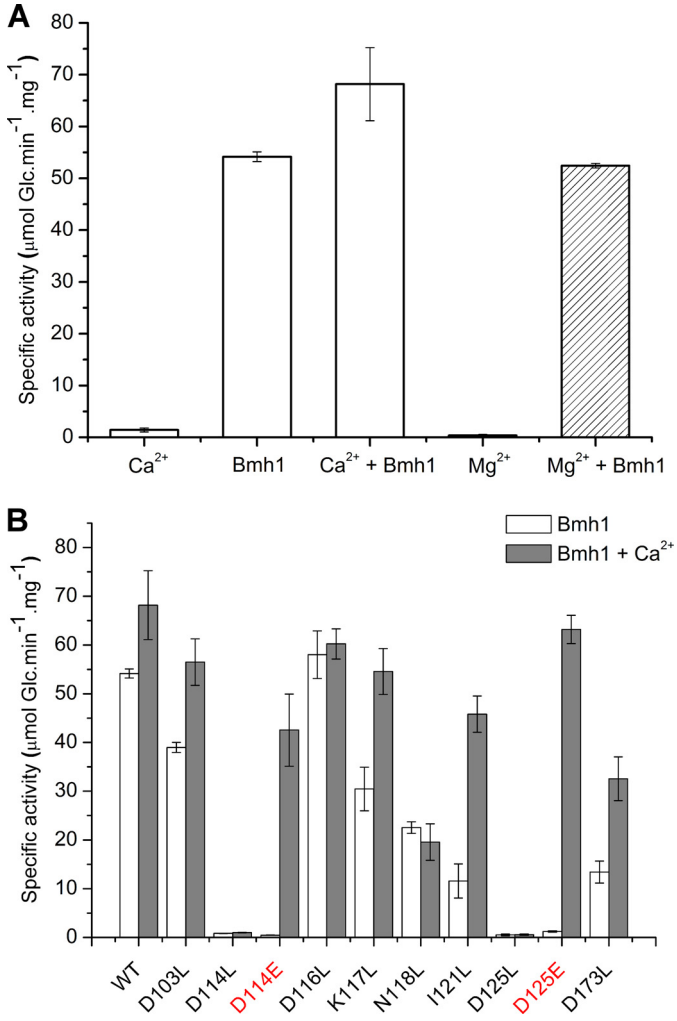

FIGURE 2. *A*, comparison of specific trehalase activities of pNth1 WT under different conditions. Data in the presence of 30 mM trehalose are shown. Specific activity of trehalase is expressed as μmol of glucose liberated/min/mg of protein. Results shown are means ± S.D. from three experiments. *B*, specific trehalase activities of pNth1 WT, and mutants in the presence of Bmh1 (*white bars*) or Bmh1 + Ca^{2+} (*gray bars*). Data in the presence of 30 mM trehalose are shown. Specific activity of trehalase is expressed as μmol of glucose liberated/min/mg of protein. Results are means ± S.D. (*error bars*) from three experiments.

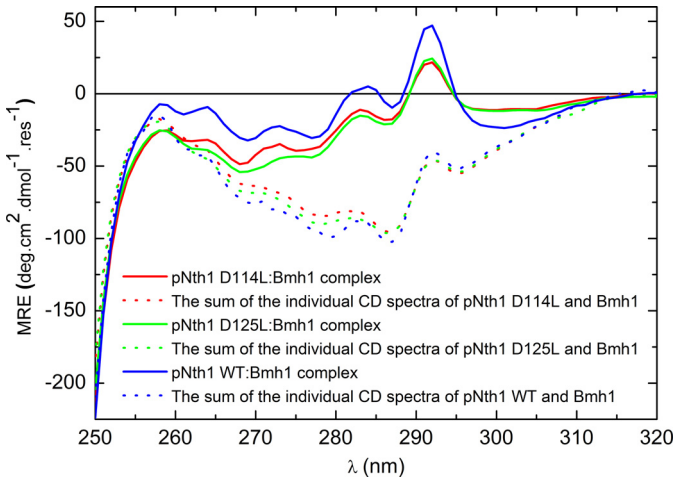

FIGURE 3. **The comparison of the near-UV CD spectra of pNth1 D114L·Bmh1 (*solid red line*), pNth1 D125L·Bmh1 (*solid green line*), and pNth1 WT·Bmh1 (*solid blue line*) complexes with the sums of the individual CD spectra of pNth1 variants and Bmh1 (corresponding *colored dotted lines*).** The mean residue ellipticity (*MRE*) is plotted as a function of wavelength in degrees·cm^2·dmol^{-1}·number of residues^{-1}).

significant differences between mutants D114L and D125L and pNth1 WT (Fig. 3). This suggested that the inability of these two mutants to become activated by Bmh1 is not due to the lack of the Bmh1-mediated conformational change (or interaction) but rather results from subtle differences in the conformation of the EF-hand-like motif-containing region that cannot be observed by this method.

Ca^{2+} Ions Do Not Affect the Dissociation Constant of the pNth1·Bmh1 Complex—Trehalase activity measurements revealed that several pNth1 mutants exhibit significantly higher activity in the presence of Bmh1 + Ca^{2+} compared with the presence of Bmh1 only (Fig. 2*B*). Therefore, we checked whether the presence of Ca^{2+} increases the stability of the pNth1·Bmh1 complex using analytical ultracentrifugation (sedimentation velocity method). Continuous distributions of sedimentation coefficients, $c(s)$, for mixtures of pNth1 and Bmh1 at five different molar ratios (from 5:1 to 1:20) both in the absence and the presence of Ca^{2+} are shown in Fig. 4. These distributions (normalized on the peak height) showed that Bmh1 and pNth1 form a complex with a weight-averaged sedimentation coefficient ($s_{w,20}$) of 7.2 S, whereas Bmh1 and pNth1 alone show single peaks with $s_{w,20}$ values of 3.6 and 5.1 S, respectively. The low abundance of the complex formation at 7.2 S for samples containing the lowest and the highest concentration of Bmh1 (0.2 and 20 μM, respectively) is due to the large excess of either pNth1 or Bmh1 in these mixtures (the concentration of pNth1 was 1 μM).

The analysis of sedimentation velocity data revealed no significant effect of Ca^{2+} on the apparent equilibrium dissociation constant (K_d) of the pNth1·Bmh1 complex because K_d values of 10×10^{-9} were determined both in the presence and the absence of 10 mM Ca^{2+}. Thus, the more potent activation of pNth1 WT and mutants in the presence of Bmh1 + Ca^{2+} compared with that with Bmh1 only (Fig. 2*B*) cannot be explained by the increase in the binding affinity of pNth1 for Bmh1.

The EF-hand-like Motif of pNth1 Adopts Different Conformations in the Presence of Ca^{2+}, Bmh1, and Bmh1 + Ca^{2+}—Many proteins containing the EF-hand motif undergo a conformational change upon the Ca^{2+} binding (37). To investigate whether the same also holds true for pNth1, HDX-MS measurements were performed. HDX-MS experiments are based on monitoring the deuteration kinetics of backbone amides and enable characterization of protein dynamics and conformational changes because the rate of exchange of deuterium for hydrogen depends on both the solvent exposure and the hydrogen bonding of the studied region (38, 39). Results of these experiments are presented in Figs. 5 and 6. For the sake of comparison, these figures also show previously published data obtained in the absence of Ca^{2+} for pNth1 alone, Bmh1 alone, and the pNth1·Bmh1 complex (20).

Structural Changes within the EF-hand-like Motif-containing Region—The comparison of HDX-MS data for pNth1 in the presence of Ca^{2+}, Bmh1, and Bmh1 + Ca^{2+} revealed large differences in the deuteration kinetics for five peptides from the region containing the EF-hand-like motif under all conditions

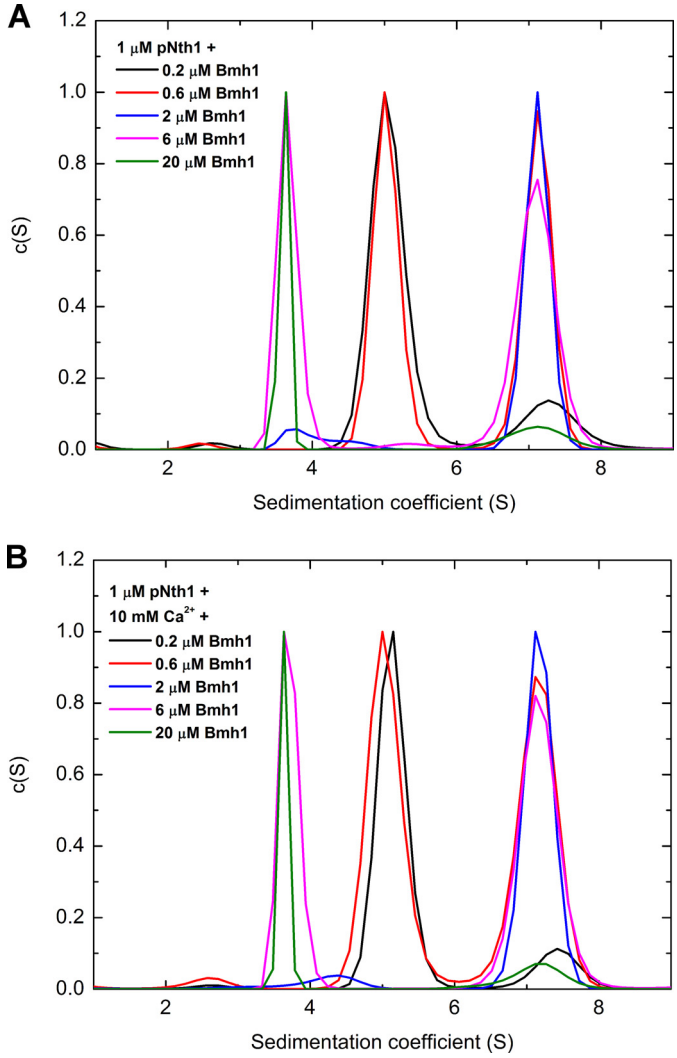

FIGURE 4. **Sedimentation velocity analysis reveals that the binding affinity of pNth1 for Bmh1 is unchanged in the presence of Ca^{2+}.** Continuous distributions of sedimentation coefficients, *c*(*s*), for mixtures containing constant concentration of pNth1 (1 μM) and different concentrations of Bmh1 (0.2–20 μM) reveal no significant differences in the absence (*A*) and in the presence (*B*) of Ca^{2+}. All distributions are normalized on the peak height. The Lamm equation modeling of SV data was performed using the SEDPHAT software package (27, 28). Data without Ca^{2+} (*A*) and with 10 mM Ca^{2+} (*B*) were fitted using the model, A + B ⇌ AB. Bmh1 was modeled as a tight dimer that interacts with pNth1 in 1:1 stoichiometry. Both series can be fitted with nearly identical $K_D < 21$ nM with 95% confidence level (the best fitted value was 10 nM). Loading concentrations were slightly corrected in the fit (up to 10%).

tested. Peptides 102–110, 110–124, and 156–172 exhibit significantly slower deuteration in the presence of Ca^{2+} (compare *black* and *red lines* in Fig. 5*A*), with the peptide 110–124 (which contains the EF-hand-like motif) showing the slower isotope exchange only in short incubation times. In addition, an even more profound decrease in the rate of deuteration was observed for all pNth1 peptides between residues 102 and 185 in the presence of Bmh1 (*blue line*) or Bmh1 + Ca^{2+} (*green line*). Observed changes in HDX kinetics might reflect additional conformational change and/or decreased accessibility to the solvent. Interestingly, only the peptide 110–124 showed significant differences in isotope exchange kinetics when comparing peptides from the pNth1·Bmh1 complex with or without Ca^{2+}. These results suggest that the region 102–185 of pNth1, especially the peptide 110–124 (the EF-hand like motif), adopts three different structural states (and/or positions) in the presence of Ca^{2+}, Bmh1, and Bmh1 + Ca^{2+}.

Structural Changes within the Catalytic Trehalase Domain of pNth1—Exchange kinetics for four peptides from the vicinity of the pNth1 active site whose deuteration was moderately but significantly decreased upon the Bmh1 protein binding is shown in Fig. 5*B* (20). It can be noticed that only the peptide 665–698 showed some decrease in the deuteration kinetics in the presence of Ca^{2+} (compare *black* and *red lines*). In addition, the presence of Ca^{2+} had no significant effect on isotope exchange kinetics of these four peptides in the presence of Bmh1 (compare *blue* and *green lines*).

Thus, HDX-MS data suggested that the Ca^{2+} binding affects mainly the structure of the EF-hand-like motif-containing region, whereas its effect on the catalytic domain is less profound.

Ca^{2+}-mediated Structural Changes of Bmh1 Molecule—We also investigated whether the presence of Ca^{2+} affects the deuterium exchange kinetics of Bmh1 peptides. A significant decrease in the deuteration level in the presence of Ca^{2+} was observed for several peptides, with the strongest effect being observed for helices H3 (peptides 39–47 and 48–61), H8 (peptide 184–207), and H9 (peptide 227–232) (compare *black* and *red lines* in Fig. 6). Only two peptides (184–207 and 222–232 from helices H8 and H9, respectively) showed significantly decreased exchange kinetics when comparing peptides from the pNth1·Bmh1 complex with or without Ca^{2+} (compare *green* and *blue lines* in Fig. 6), suggesting that these helices might interact with and thus be affected by changes within the EF-hand-like motif of bound pNth1.

Binding to Bmh1 Affects the Relative Position of the N-terminal Region and the Catalytic Domain of pNth1—Site-directed mutagenesis and HDX-MS suggested that the structural integrity of the EF-hand-like motif is crucial for pNth1 activation and that its conformational change is an integral part of the activation process. This also implied that this region might be adjacent to the catalytic domain and that its conformational changes affect the structure (or the accessibility) of the active site and hence enable the activation. The crystallographic structural data are available only for trehalase Tre37A from *E. coli* (40) which shows homology with the catalytic domain of *S. cerevisiae* Nth1 (sequence 295–721). We used this homology to build a structural model of the catalytic domain of Nth1, which, however, does not include either the region containing the EF-hand like motif or the N-terminal segment containing PKA phosphorylation sites (and the 14-3-3 protein-binding motifs) (20). Therefore, we used chemical cross-linking combined with mass spectrometry and SAXS to obtain structural information concerning the relative position of the region containing the EF-hand-like motif and the catalytic domain as well as additional information about structural changes induced by Ca^{2+} and the 14-3-3 protein binding.

To enable easier distinction of changes induced by Ca^{2+}, both pNth1 alone and the pNth1·Bmh1 complex were cross-linked by non-deuterated cross-linking agents (DSS and DSG) in the presence of Ca^{2+} and by four-times deuterated agents in

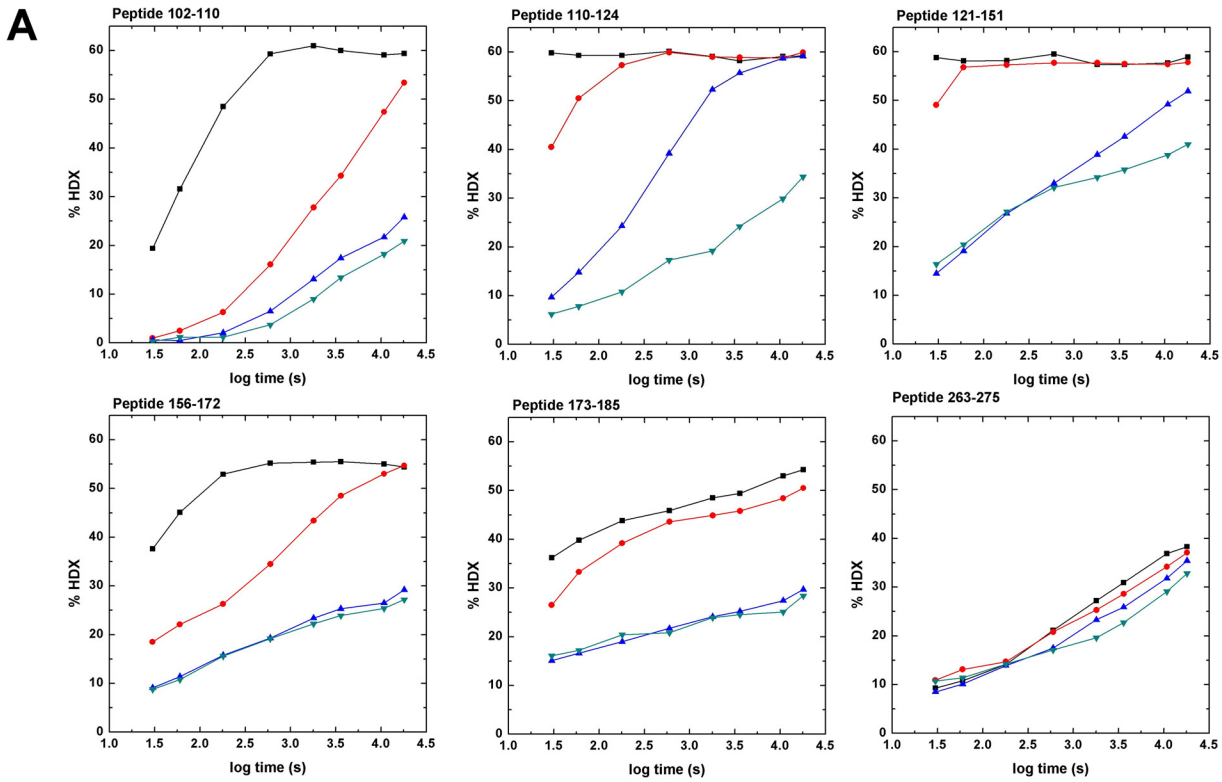

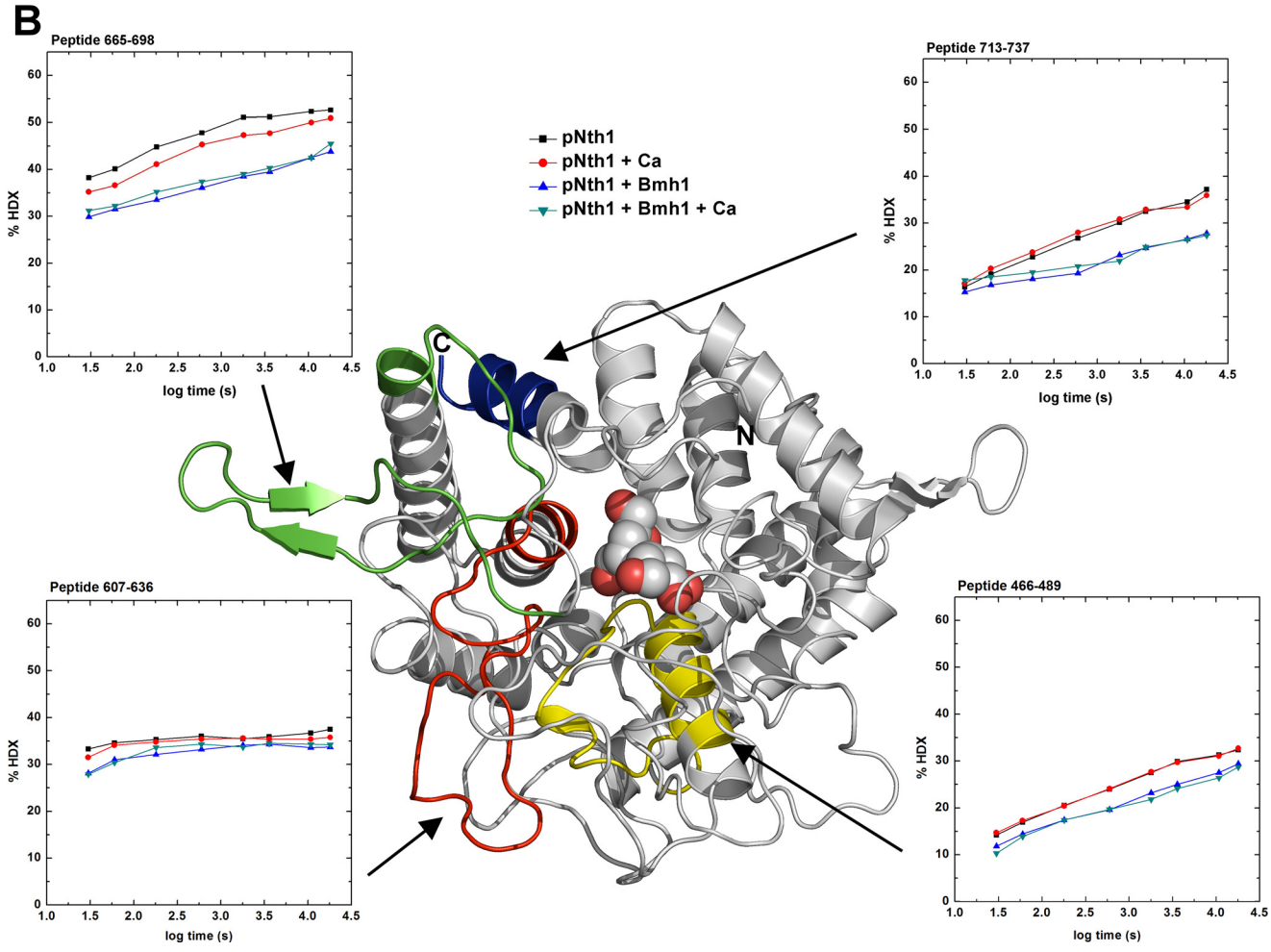

the absence of Ca^{2+} (see "Experimental Procedures" for details). The cross-linking experiments with pNth1 alone revealed 33 intramolecular distance constraints (Table 2), from which 17 can be compared with Cα–Cα distance constraints derived from the homology model of the catalytic domain (data not shown). No cross-links between the N-terminal region (sequence 1–250) and the catalytic domain (sequence 300–720) were observed, suggesting that in the absence of Bmh1, these two domains are not in contact with one another. Quantification of obtained cross-links (last two columns in Table 2) revealed that the ratio between non-deuterated and deuterated cross-links is close to 1:1 for all but two of them. The two exceptions are for the peptide from the region containing the EF-hand like motif whose residues Lys-132 and Lys-142 are cross-linked only in the presence of Ca^{2+} (the abundances of DSG and DSS cross-links are ~78 and ~90%, respectively). This suggests that in the presence of Ca^{2+}, these two lysines are close enough to form a cross-link. However, in the absence of Ca^{2+}, this region possesses different conformation and/or flexibility, and the distance between these two residues is too large to form a cross-link.

The list of pNth1 cross-links from the pNth1·Bmh1 complex is shown in Table 3. In this case, the presence of Ca^{2+} changed the abundances of significantly more cross-links compared with pNth1 alone. This confirmed that pNth1 (when bound to Bmh1) adopts a different conformation that is more sensitive to Ca^{2+} binding compared with free pNth1. The most profound changes were observed for intramolecular cross-links Lys^{211}–Lys^{214}, Lys^{214}–Lys^{563}, Lys^{257}–Lys^{258}, Lys^{258}–Lys^{393}, Lys^{385}–Lys^{517}, Lys^{456}–Lys^{458}, and Lys^{589}–Lys^{593}. The presence of the cross-link Lys^{214}–Lys^{563}, which was not observed for pNth1 alone, suggested that the part containing residue Lys^{214} and the catalytic domain (containing Lys^{563}) of pNth1 are much closer to one another in the Bmh1-bound form. In addition, the differences between conformations of pNth1 bound to Bmh1 in the presence and the absence of Ca^{2+} are also supported by intermolecular cross-links between pNth1 and Bmh1 peptides (Table 4). Although in the presence of Ca^{2+} the intramolecular cross-link between pNth1 residues Lys^{214} and Lys^{563} is preferentially formed (Table 3), in the absence of Ca^{2+}, these two residues preferentially form intermolecular cross-links with Bmh1 residues Lys^{127} and Lys^{76}, respectively (Table 4). A similar effect was also observed for pNth1 residue Lys^{393}, which forms in the presence of a Ca^{2+} intramolecular cross-link with Lys^{258}, whereas in the absence of Ca^{2+}, prefers an intermolecular cross-link with Bmh1 residue Lys^{145} (Tables 3 and 4). The results of chemical cross-linking for the Bmh1 alone correspond well with the distance restraints derived from the homology model of the Bmh1 molecule (data not shown).

Low Resolution Structure of the pNth1·Bmh1 Protein Complex—SAXS offers information about the dimension and shape of a protein in solution and was thus used here to gain visual insight into the global architecture of Nth1, Bmh1, and their complex. The experimental SAXS curves from Nth1, Bmh1, and the pNth1·Bmh1 complex are shown in Fig. 7*A*. The apparent molecular mass of the pNth1·Bmh1 protein complex was estimated by comparison of the forward scattering intensity $I(0)$ with that from reference solutions of bovine serum albumin. The estimated molecular mass of ~147 kDa corresponds well to 2:1 molar stoichiometry, in good agreement with our previously published results (15). The Guinier analysis revealed that Nth1 alone has a significantly larger radius of gyration (R_g of 52.0 ± 0.4 Å) compared with Bmh1 alone (R_g of 32.6 ± 0.1 Å) and the pNth1·Bmh1 complex (R_g of 40.5 ± 0.1 Å), suggesting that the complex is a more compact particle than Nth1 alone.

This was further confirmed by the distance distribution function, $P(r)$, which revealed maximal dimensions (D_{max}) of Bmh1, Nth1, and the pNth1·Bmh1 complex to be of 92, 183, and 127 Å, respectively (Fig. 7*B*). These values of D_{max} corroborated a more extended and asymmetric shape of free Nth1 compared with the complex.

The calculated low resolution *ab initio* envelopes for Nth1 alone, Bmh1 alone, and the pNth1·Bmh1 complex are shown in Fig. 7, *C–E*. The envelope of Bmh1 alone shows a characteristic cuplike shape of the 14-3-3 dimer molecule and agrees well with the theoretical model of Bmh1 dimer (Fig. 7*C*). The envelope for Nth1 alone (Fig. 7*D*) shows that the enzyme adopts an extended rodlike conformation, in good agreement with the results of cross-linking experiments, where no cross-links between the N-terminal region and the catalytic domain were observed (Table 2). The narrower half probably represents the flexible and unstructured N-terminal segment containing all PKA phosphorylation sites and the 14-3-3-binding motifs, whereas the thicker half would correspond to the rest of the enzyme (the EF-hand like motif-containing region and the catalytic domain).

The envelope of the complex is, as expected, more spherical and shows that pNth1 adopts significantly different conformation when bound to Bmh1 (Fig. 7*E*). The shape of the envelope suggests that the cuplike-shaped Bmh1 dimer is located within the wide central part of the particle. The rigid body modeling of the pNth1·Bmh1 complex was performed using homology models of Bmh1 and the catalytic domain of Nth1 (sequence 295–721). The rigid body model of the Nth1(295–721)·Bmh1 complex displayed good agreement with both the low resolution molecular envelope and the results of cross-linking experiments (Table 4). The *inset* in Fig. 7*E* shows the detailed view of the binding interface between Nth1(295–721) and Bmh1, where two of three observed intermolecular cross-links

FIGURE 5. **HDX-MS reveals conformational changes of pNth1 upon the Ca^{2+} binding.** Graphs represent HDX kinetics for selected pNth1 regions that show different deuterium exchange kinetics in the presence of Ca^{2+}, Bmh1, and Bmh1 + Ca^{2+} (for the sake of comparison, these figures also show previously published data obtained in the absence of Ca^{2+} for pNth1 alone and when bound to Bmh1 (20)). *A*, peptides from the N-terminal part of Nth1 that are missing in the homology model of the catalytic domain. *B*, peptides from the catalytic trehalase domain (shown in *yellow*, *red*, *green*, and *blue*) are mapped on its homology structural model covering the sequence 295–721. Deuterium exchange is expressed as percentages relative to the maximum theoretical deuteration level for pNth1 alone (*black squares*), pNth1 in the presence of Ca^{2+} (*red circles*), pNth1 in the presence of Bmh1 (*blue triangles*), and pNth1 in the presence of Bmh1 + Ca^{2+} (*green triangles*). Time units are in seconds.

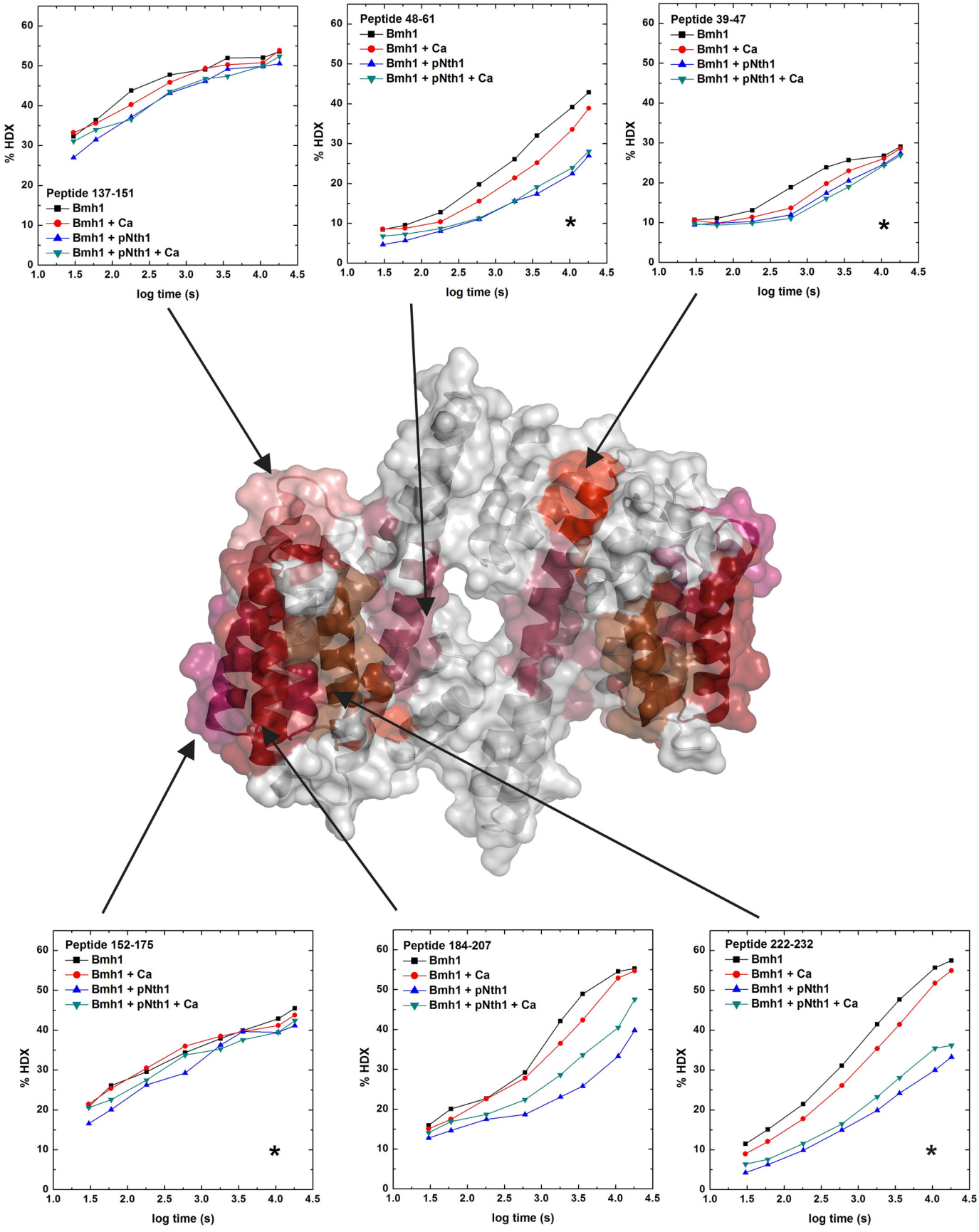

TABLE 2
Intramolecular distance constraints of pNth1 derived from the cross-linking experiments in the presence and the absence of Ca^{2+} and their comparison with distance constraints derived from the homology model of the catalytic domain of Nth1

Cross-linker	Cross-linked residues	Cα-Cα distance from the homology model	Cα-Cα distance constraint from the cross-linking experiments[a]	pNth1 (DSS(G)/DSS(G)D4)[b]	
				$+Ca^{2+}$	$-Ca^{2+}$
		Å	Å	%	%
DSG/DSGD4	Lys^{49}–Lys^{584}		≤20	49.8	50.2
DSG/DSGD4	Lys^{49}–Lys^{69}		≤20	55.7	44.3
DSS/DSSD4	Lys^{52}–Lys^{104}		≤24	42.2	57.8
DSS/DSSD4	Lys^{52}–Lys^{584}		≤24	48.4	51.6
DSG/DSGD4	Lys^{70}–Lys^{75}		≤20	45.1	54.9
DSS/DSSD4	Lys^{70}–Lys^{75}		≤24	53.4	46.6
DSG/DSGD4	Lys^{132}–Lys^{142}		≤20	77.6	22.4
DSS/DSSD4	Lys^{132}–Lys^{142}		≤24	89.8	10.2
DSG/DSGD4	Lys^{211}–Lys^{214}		≤20	51	49
DSS/DSSD4	Lys^{211}–Lys^{214}		≤24	45.4	54.6
DSG/DSGD4	Lys^{257}–Lys^{258}		≤20	47	53
DSS/DSSD4	Lys^{257}–Lys^{258}		≤24	50.3	49.7
DSG/DSGD4	Lys^{258}–Lys^{343}		≤20	47.8	52.2
DSS/DSSD4	Lys^{258}–Lys^{343}		≤24	55.6	44.4
DSG/DSGD4	Lys^{258}–Lys^{393}		≤20	51	49
DSS/DSSD4	Lys^{258}–Lys^{393}		≤24	51.3	48.7
DSG/DSGD4	Lys^{370}–Lys^{371}	3.9	≤20	49.7	50.3
DSS/DSSD4	Lys^{370}–Lys^{371}	3.9	≤24	45.4	54.6
DSG/DSGD4	Lys^{371}–Lys^{718}	17.7	≤20	50.1	49.9
DSS/DSSD4	Lys^{371}–Lys^{718}	17.7	≤24	48.9	51.1
DSG/DSGD4	Lys^{385}–Lys^{517}	17.5	≤20	48.8	51.2
DSS/DSSD4	Lys^{385}–Lys^{517}	17.5	≤24	45.5	54.5
DSG/DSGD4	Lys^{456}–Lys^{458}	6.5	≤20	46.4	53.6
DSS/DSSD4	Lys^{456}–Lys^{458}	6.5	≤24	51.4	48.6
DSS/DSSD4	Lys^{458}–Lys^{461}	7.6	≤24	41.3	58.7
DSG/DSGD4	Lys^{461}–Lys^{561}	16.4	≤20	48.1	51.9
DSS/DSSD4	Lys^{461}–Lys^{561}	16.4	≤24	48.8	51.2
DSS/DSSD4	Lys^{537}–Lys^{584}	16.4	≤24	44.9	55.1
DSG/DSGD4	Lys^{561}–Lys^{563}	5.6	≤20	52.4	47.6
DSG/DSGD4	Lys^{589}–Lys^{593}	6.1	≤20	46.2	53.8
DSS/DSSD4	Lys^{589}–Lys^{593}	6.1	≤24	46.9	53.1
DSG/DSGD4	Lys^{593}–Lys^{597}	6.3	≤20	46.9	53.1
DSS/DSSD4	Lys^{593}–Lys^{597}	6.3	≤24	47.7	52.3

[a] The Cα–Cα interresidue distance constraints used were based on the length of the spacer arm, which is 7.7 Å for DSG and 11.4 Å for DSS. Concerning the flexibility of the lysine side chains, the following cut-offs are generally used: 20 Å for α-carbons of lysine cross-linked with DSG and 24 Å for α-carbons of lysine cross-linked with DSS (30).
[b] Representation (%) of individual cross-link isoform (the ratio between the abundance of non-deuterated and deuterated cross-links). pNth1 was cross-linked by non-deuterated cross-linking agents (DSS and DSG) in the presence of Ca^{2+} and by four-times deuterated agents in the absence of Ca^{2+}.

(Lys^{76}(Bmh1)–Lys^{563}(Nth1) and Lys^{145}(Bmh1)–Lys^{393}(Nth1)) are located. The third intermolecular cross-link (Lys^{127}-(Bmh1)–Lys^{214}(Nth1)) involves Nth1 residue Lys^{214} outside of the modeled catalytic domain. The molecular envelope also suggested locations of the N-terminal segment and the EF-hand like motif-containing region of pNth1. The central part of the envelope is significantly wider than the maximum width of the Bmh1 dimer envelope and more bulky on one side just next to α-helices H5, H6, and H8 of Bmh1 and close to the catalytic domain of Nth1. We believe that this bulky part represents the EF-hand-like motif-containing region of pNth1. Peptides from α-helices H6, H8, and H9 of Bmh1 showed significantly decreased exchange kinetics and the highest sensitivity to the presence of Ca^{2+} upon the binding of pNth1 (Fig. 6). In addition, the intermolecular cross-link Lys^{127}(Bmh1)–Lys^{214}(Nth1) connects residues Lys^{127} from the α-helix H5 of Bmh1 and Lys^{214} from the EF-hand-like motif-containing region of Nth1 (Table 4). Thus, these data suggested that the EF-hand-like motif-containing region of pNth1 forms a separate domain that interacts with both the outer surface of the Bmh1 dimer (outside its central channel involving helices H5, H6, H8, and H9) and the catalytic trehalase domain.

The narrow protrusion located just in front of one ligand binding groove of Bmh1 probably represents the very N-terminal segment of pNth1, whereas the rest of the N-terminal part, which contains both phosphorylated 14-3-3 binding motifs ($Ser(P)^{60}$ and $Ser(P)^{83}$; Fig. 1*A*), would be docked within the ligand binding grooves of the Bmh1 molecule, as has been observed in other structures of the 14-3-3 protein complexes (41–45).

DISCUSSION

The helix-loop-helix EF-hand Ca^{2+}-binding motif is a widespread and versatile sequence found in a large number of protein families (36, 37). The N-terminal part of *S. cerevisiae* contains sequence that closely resembles such an EF-hand motif (Fig. 1), suggesting the possibility that this sequence and the calcium binding play a role in the regulation of this enzyme activity (13). In this work, various techniques of structural biology, including HDX-

FIGURE 6. **HDX-MS reveals regions of Bmh1 that are affected by Ca^{2+} and pNth1 binding.** HDX kinetics for Bmh1 regions that show slower deuterium exchange kinetics upon pNth1 binding mapped on the surface representation of the structural model of Bmh1 dimer (shown in *different shades* of *red*). For the sake of comparison, these figures also show previously published data obtained in the absence of Ca^{2+} for Bmh1 alone and when bound to pNth1 (20). Deuterium exchange is expressed as percentages relative to the maximum theoretical deuteration level for Bmh1 alone (*black squares*), Bmh1 in the presence of Ca^{2+} (*red circles*), Bmh1 in the presence of pNth1 (*green triangles*), and Bmh1 in the presence of pNth1 + Ca^{2+} (*blue triangles*). Time units are in seconds. Peptides forming the ligand binding groove are marked with an *asterisk*.

TABLE 3

Intramolecular distance constraints of pNth1 bound to Bmh1 derived from the cross-linking experiments in the presence and the absence of Ca^{2+} and their comparison with distance constraints derived from the homology model of the catalytic domain of Nth1

Cross-linker	Cross-linked residues	Cα–Cα distance from the homology model	Cα–Cα distance constraint from the cross-linking experiments[a]	pNth1 (DSS(G)/DSS(G)D4)[b]	
				$+Ca^{2+}$	$-Ca^{2+}$
		Å	Å	%	%
DSG/DSGD4	Lys^{70}–Lys^{75}		≤20	55.5	44.5
DSS/DSSD4	Lys^{70}–Lys^{75}		≤24	49.0	51.0
DSG/DSGD4	Lys^{132}–Lys^{142}		≤20	56.8	43.2
DSS/DSSD4	Lys^{132}–Lys^{142}		≤24	52.9	47.1
DSG/DSGD4	Lys^{211}–Lys^{214}		≤20	65.3	34.7
DSS/DSSD4	Lys^{211}–Lys^{214}		≤24	58.8	41.2
DSG/DSGD4	Lys^{214}–Lys^{563}		≤20	80.0	20
DSS/DSSD4	Lys^{214}–Lys^{563}		≤24	60.1	39.9
DSG/DSGD4	Lys^{257}–Lys^{258}		≤20	66.7	33.3
DSS/DSSD4	Lys^{257}–Lys^{258}		≤24	59.3	40.7
DSG/DSGD4	Lys^{258}–Lys^{393}		≤20	68.3	31.7
DSS/DSSD4	Lys^{258}–Lys^{393}		≤24	71.2	28.8
DSG/DSGD4	Lys^{370}–Lys^{371}	3.9	≤20	54.9	45.1
DSS/DSSD4	Lys^{370}–Lys^{371}	3.9	≤24	47.9	52.1
DSG/DSGD4	Lys^{385}–Lys^{517}	17.5	≤20	70.2	29.8
DSS/DSSD4	Lys^{385}–Lys^{517}	17.5	≤24	50.8	49.2
DSG/DSGD4	Lys^{393}–Lys^{396}	5.1	≤20	51.1	48.9
DSS/DSSD4	Lys^{393}–Lys^{396}	5.1	≤24	49.5	50.5
DSG/DSGD4	Lys^{456}–Lys^{458}	6.5	≤20	68.8	31.2
DSS/DSSD4	Lys^{456}–Lys^{458}	6.5	≤24	63.7	36.3
DSS/DSSD4	Lys^{458}–Lys^{461}	7.6	≤24	50.2	49.8
DSS/DSSD4	Lys^{537}–Lys^{584}	16.4	≤24	51.1	48.9
DSG/DSGD4	Lys^{589}–Lys^{593}	6.1	≤20	71.1	28.9
DSS/DSSD4	Lys^{589}–Lys^{593}	6.1	≤24	55.1	44.9

[a] The Cα–Cα interresidue distance constraints used were based on the length of the spacer arm, which is 7.7 Å for DSG and 11.4 Å for DSS. Concerning the flexibility of the lysine side chains, the following cut-offs are generally used: 20 Å for α-carbons of lysine cross-linked with DSG and 24 Å for α-carbons of lysine cross-linked with DSS (30).
[b] Representation (%) of individual cross-link isoform (the ratio between the abundance of non-deuterated and deuterated cross-links). pNth1 bound to Bmh1 was cross-linked by non-deuterated cross-linking agents (DSS and DSG) in the presence of Ca^{2+} and by four-times deuterated agents in the absence of Ca^{2+}.

TABLE 4

Intermolecular distance constraints between pNth1 and Bmh1 derived from the cross-linking experiments in the presence and the absence of Ca^{2+}

Cross-linker	Cross-linked residues	Cα-Cα distance constraint from the cross-linking experiments[a]	Bmh1·pNth1 (DSS(G)/DSS(G)D4)[b]	
			$+Ca^{2+}$	$-Ca^{2+}$
		Å	%	%
DSG/DSGD4	Lys^{127a}-Lys^{214b}	≤20	28.8	71.2
DSS/DSSD4	Lys^{127a}-Lys^{214b}	≤24	40.2	59.8
DSG/DSGD4	Lys^{76a}-Lys^{563b}	≤20	34.7	65.3
DSS/DSSD4	Lys^{76a}-Lys^{563b}	≤24	42.2	57.8
DSG/DSGD4	Lys^{145a}-Lys^{393b}	≤20	31.3	68.7
DSS/DSSD4	Lys^{145a}-Lys^{393b}	≤24	30.7	69.3

[a] The Cα–Cα interresidue distances constraints used were based on the length of the spacer arm, which is 7.7 Å for DSG and 11.4 Å for DSS. Concerning the flexibility of the lysine side chains, the following cut-offs are generally used: 20 Å for α-carbons of lysine cross-linked with DSG and 24 Å for α-carbons of lysine cross-linked with DSS (30).
[b] Representation (%) of individual cross-link isoform (the ratio between the abundance of non-deuterated and deuterated cross-links). The pNth1·Bmh1 complex was cross-linked by non-deuterated cross-linking agents (DSS and DSG) in the presence of Ca^{2+} and by four-times deuterated agents in the absence of Ca^{2+}.
[c] Residues from the Bmh1 peptide.
[d] Residues from the pNth1 peptide.

MS, chemical cross-linking, and SAXS, were used to investigate the mechanism of the 14-3-3 protein-mediated activation of Nth1 and, especially, the role of EF-hand like motif in this process.

Site-directed mutagenesis of residues located at important positions within the EF-hand like motif significantly affected the Bmh1-mediated activation of pNth1 (Fig. 2*B*, *white bars*), thus suggesting the essential role of this region in the activation process. This is in a good agreement with our previous HDX-MS experiments that revealed significant 14-3-3 protein-mediated structural changes not only within the catalytic trehalase domain but mainly in this region (20). Interestingly, the presence of Ca^{2+} recovered the Bmh1-mediated trehalase activity of most of the studied mutants (Fig. 2*B*, *gray bars*), with the exception of those where we mutated conserved positions 1, 5, and 12 of the EF-hand motif (mutants D114L, N118L, and D125L) that are directly involved in metal coordination (36, 37). The inability of the D114L and D125L mutants to become activated was not due to the lack of the Bmh1-mediated structural change, as documented by near-UV CD spectra (Fig. 3), but rather resulted from different conformation of the EF-hand like motif. In support of that, Ca^{2+}-binding rescue mutants D114E and D125E showed high Bmh1-mediated activity but only in the presence of Ca^{2+}. These data suggested that the calcium binding to the EF-hand like motif facilitates the 14-3-3 protein-mediated activation of pNth1 because it enabled activation of mutants that are catalytically inactive in the absence of Ca^{2+}.

The key role of the EF-hand like motif-containing region in the activation of pNth1 was further confirmed by results obtained from HDX-MS and chemical cross-linking. These experiments showed that this region adopts different conformational states depending on the presence of Ca^{2+}, Bmh1, or both (Fig. 5 and Tables 2–4). We suggest that these different structural states are reflected by different trehalase activities under these conditions. Consistently, the comparison of SAXS-based low resolution molecular envelopes of both Nth1 alone and the pNth1·Bmh1 complex (Fig. 7, *D* and 7*E*) revealed a dramatic structural change of pNth1 upon its binding to Bmh1. The low resolution *ab initio* shape of the pNth1·Bmh1 complex also suggested that the EF-hand-like-containing region of Nth1 forms a separate domain that interacts with both the outer surface of the Bmh1 dimer and the

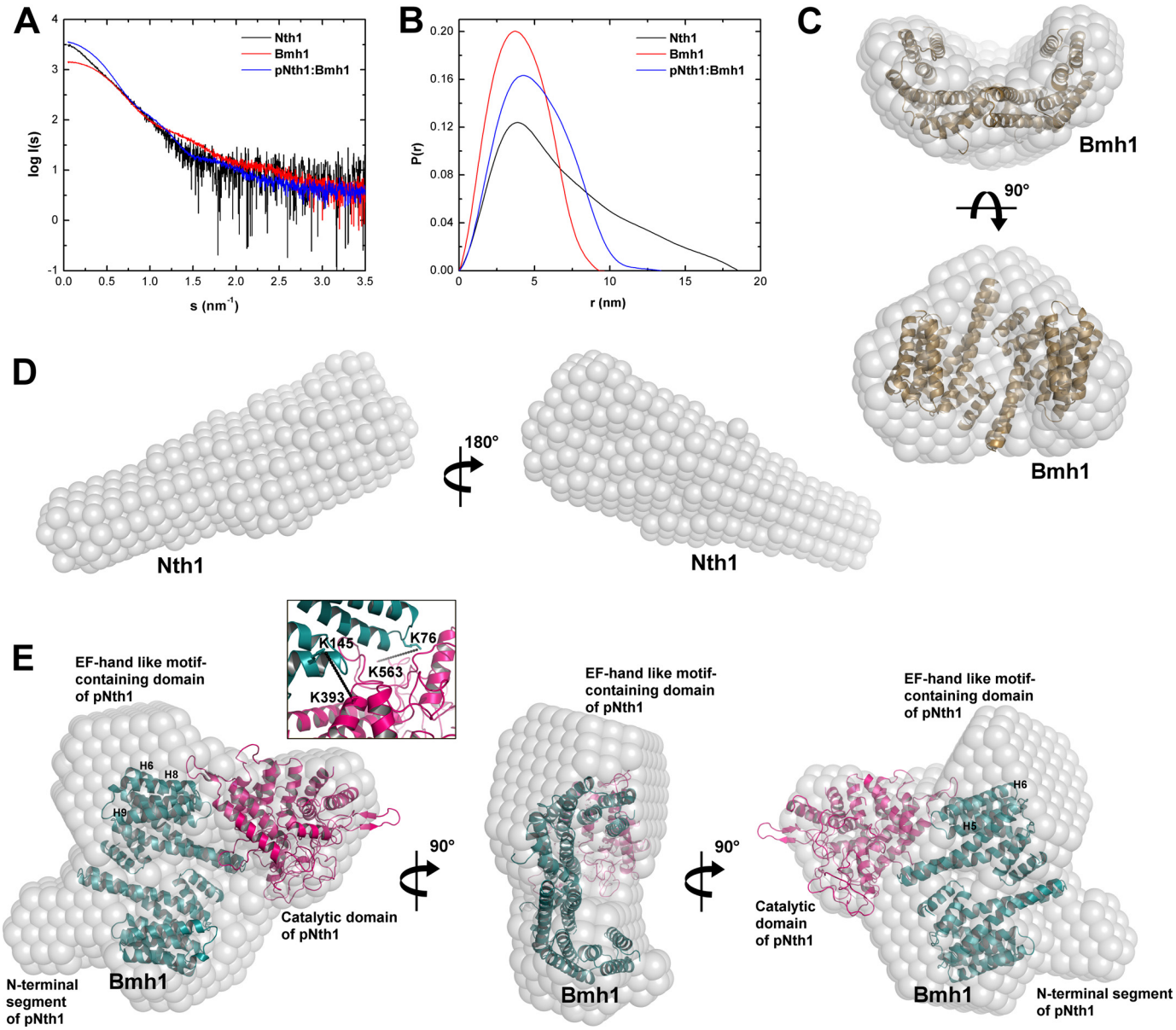

FIGURE 7. **SAXS scattering data and the low resolution structure of Nth1, Bmh1, and pNth1·Bmh1 complex.** *A*, solution scattering pattern for Nth1, Bmh1, and the pNth1·Bmh1 complex. Scattering intensity $I(s)$ is plotted in relation to the scattering vector s ($s = 4\pi\sin(\theta)/\lambda$, where 2θ is the scattering angle and λ is the wavelength). *B*, plot of the distance distribution functions $P(r)$ with the maximum particle dimensions (D_{max}) of 92, 183, and 127 Å for Bmh1, Nth1, and the pNth1·Bmh1 complex, respectively. *C*, superposition of the SAXS-based envelope (*spheres* represent the dummy residues) of Bmh1 with the theoretical model of Bmh1 (sequence 4–236). *D*, SAXS-based envelope of Nth1 alone. *E*, overlay of the rigid body model of the Nth1(295–721)·Bmh1 complex with SAXS-based envelope. The envelope is shown in *gray*, the catalytic domain of Nth1 (sequence 295–721) is shown in *magenta*, and Bmh1 dimer (sequence 4–236) is shown in *cyan*. A rigid body model was prepared using homology models of the catalytic domain of Nth1(295–721) and Bmh1 (20). The *inset* shows the binding interface between Nth1(295–721) and Bmh1, where two of three observed intermolecular cross-links (Lys^{76}(Bmh1)–Lys^{563}(Nth1) and Lys^{145}(Bmh1)–Lys^{393}(Nth1)) are located.

catalytic trehalase domain, thus supporting our hypothesis that the conformation of this region modulates the 14-3-3-mediated structural changes within the catalytic trehalase domain and thus the resulting enzyme activity.

Therefore, based on our data, we suggest the following model of Nth1 activation. In the absence of the 14-3-3 protein, Nth1 adopts an extended rodlike conformation, and the trehalase activity is very small, probably as a result of the inaccessibility of the active site, as shown by the crystal structure of the homologous domain of the trehalase Tre37A from *E. coli* (Fig. 5*B*) (40). The 14-3-3 protein binding to the phosphorylated N-terminal segment of pNth1 induces a significant structural rearrangement of the whole Nth1 molecule. This conformational change probably increases the accessibility of the active site and thus activates the enzyme. The EF-hand-like motif-containing region forms a separate domain that interacts with both the 14-3-3 protein and the catalytic trehalase domain. The structural integrity of the EF-hand like motif is essential for the 14-3-3 protein-mediated activation of Nth1, and calcium binding, although not required for the activation, facilitates this process by affecting its structure. Our data suggest that the EF-hand-like motif-containing domain functions as the intermediary through which the 14-3-3 protein modulates the function of the catalytic domain of Nth1.

Acknowledgments—We thank P. Novotna and M. Urbanova (Institute of Chemical Technology, Prague) for measuring the CD spectra and J. Pisackova (Institute of Organic Chemistry and Biochemistry, Academy of Sciences of the Czech Republic v.v.i.) for help with the thermofluor method.

REFERENCES

1. Elbein, A. D., Pan, Y. T., Pastuszak, I., and Carroll, D. (2003) New insights on trehalose: a multifunctional molecule. *Glycobiology* **13,** 17R–27R
2. Nwaka, S., and Holzer, H. (1998) Molecular biology of trehalose and the trehalases in the yeast *Saccharomyces cerevisiae*. *Prog. Nucleic Acid Res. Mol. Biol.* **58,** 197–237
3. Kopp, M., Müller, H., and Holzer, H. (1993) Molecular analysis of the neutral trehalase gene from *Saccharomyces cerevisiae*. *J. Biol. Chem.* **268,** 4766–4774
4. Becker, A., Schlöder, P., Steele, J. E., and Wegener, G. (1996) The regulation of trehalose metabolism in insects. *Experientia* **52,** 433–439
5. Behm, C. A. (1997) The role of trehalose in the physiology of nematodes. *Int. J. Parasitol.* **27,** 215–229
6. Oesterreicher, T. J., Markesich, D. C., and Henning, S. J. (2001) Cloning, characterization and mapping of the mouse trehalase (Treh) gene. *Gene* **270,** 211–220
7. Alizadeh, P., and Klionsky, D. J. (1996) Purification and biochemical characterization of the ATH1 gene product, vacuolar acid trehalase, from *Saccharomyces cerevisiae*. *FEBS Lett.* **391,** 273–278
8. Amaral, F. C., Van Dijck, P., Nicoli, J. R., and Thevelein, J. M. (1997) Molecular cloning of the neutral trehalase gene from *Kluyveromyces lactis* and the distinction between neutral and acid trehalases. *Arch. Microbiol.* **167,** 202–208
9. Nwaka, S., Mechler, B., Destruelle, M., and Holzer, H. (1995) Phenotypic features of trehalase mutants in *Saccharomyces cerevisiae*. *FEBS Lett.* **360,** 286–290
10. Jules, M., Beltran, G., François, J., and Parrou, J. L. (2008) New insights into trehalose metabolism by *Saccharomyces cerevisiae*: NTH2 encodes a functional cytosolic trehalase, and deletion of TPS1 reveals Ath1p-dependent trehalose mobilization. *Appl. Environ. Microbiol.* **74,** 605–614
11. Uno, I., Matsumoto, K., Adachi, K., and Ishikawa, T. (1983) Genetic and biochemical evidence that trehalase is a substrate of cAMP-dependent protein kinase in yeast. *J. Biol. Chem.* **258,** 10867–10872
12. Ortiz, C. H., Maia, J. C., Tenan, M. N., Braz-Padrão, G. R., Mattoon, J. R., and Panek, A. D. (1983) Regulation of yeast trehalase by a monocyclic, cyclic AMP-dependent phosphorylation-dephosphorylation cascade system. *J. Bacteriol.* **153,** 644–651
13. Franco, A., Soto, T., Vicente-Soler, J., Paredes, V., Madrid, M., Gacto, M., and Cansado, J. (2003) A role for calcium in the regulation of neutral trehalase activity in the fission yeast *Schizosaccharomyces pombe*. *Biochem. J.* **376,** 209–217
14. Panni, S., Landgraf, C., Volkmer-Engert, R., Cesareni, G., and Castagnoli, L. (2008) Role of 14-3-3 proteins in the regulation of neutral trehalase in the yeast *Saccharomyces cerevisiae*. *FEMS Yeast Res.* **8,** 53–63
15. Veisova, D., Macakova, E., Rezabkova, L., Sulc, M., Vacha, P., Sychrova, H., Obsil, T., and Obsilova, V. (2012) Role of individual phosphorylation sites for the 14-3-3-protein-dependent activation of yeast neutral trehalase Nth1. *Biochem. J.* **443,** 663–670
16. Schepers, W., Van Zeebroeck, G., Pinkse, M., Verhaert, P., and Thevelein, J. M. (2012) *In vivo* phosphorylation of Ser^{21} and Ser^{83} during nutrient-induced activation of the yeast protein kinase A (PKA) target trehalase. *J. Biol. Chem.* **287,** 44130–44142
17. van Heusden, G. P., Griffiths, D. J., Ford, J. C., Chin-A-Woeng, T. F., Schrader, P. A., Carr, A. M., and Steensma, H. Y. (1995) The 14-3-3 proteins encoded by the BMH1 and BMH2 genes are essential in the yeast *Saccharomyces cerevisiae* and can be replaced by a plant homologue. *Eur. J. Biochem.* **229,** 45–53
18. van Heusden, G. P. (2009) 14-3-3 proteins: insights from genome-wide studies in yeast. *Genomics* **94,** 287–293
19. Mackintosh, C. (2004) Dynamic interactions between 14-3-3 proteins and phosphoproteins regulate diverse cellular processes. *Biochem. J.* **381,** 329–342
20. Macakova, E., Kopecka, M., Kukacka, Z., Veisova, D., Novak, P., Man, P., Obsil, T., and Obsilova, V. (2013) Structural basis of the 14-3-3 protein-dependent activation of yeast neutral trehalase Nth1. *Biochim. Biophys. Acta* **1830,** 4491–4499
21. Veisova, D., Rezabkova, L., Stepanek, M., Novotna, P., Herman, P., Vecer, J., Obsil, T., and Obsilova, V. (2010) The C-terminal segment of yeast BMH proteins exhibits different structure compared to other 14-3-3 protein isoforms. *Biochemistry* **49,** 3853–3861
22. Goodwin, T. W., and Morton, R. A. (1946) The spectrophotometric determination of tyrosine and tryptophan in proteins. *Biochem. J.* **40,** 628–632
23. Niesen, F. H., Berglund, H., and Vedadi, M. (2007) The use of differential scanning fluorimetry to detect ligand interactions that promote protein stability. *Nat. Protoc.* **2,** 2212–2221
24. Pisackova, J., Prochazkova, K., Fabry, M., and Rezacova, P. (2012) Crystallization of the effector-binding domain of repressor DeoR from *Bacillus subtilis*. *Crystal Growth Des.* **13,** 844–848
25. Pernambuco, M. B., Winderickx, J., Crauwels, M., Griffioen, G., Mager, W. H., and Thevelein, J. M. (1996) Glucose-triggered signalling in Saccharomyces cerevisiae: different requirements for sugar phosphorylation between cells grown on glucose and those grown on non-fermentable carbon sources. *Microbiology* **142,** 1775–1782
26. Whitmore, L., and Wallace, B. A. (2004) DICHROWEB, an online server for protein secondary structure analyses from circular dichroism spectroscopic data. *Nucleic Acids Res.* **32,** W668–W673
27. Schuck, P. (2000) Size-distribution analysis of macromolecules by sedimentation velocity ultracentrifugation and Lamm equation modeling. *Biophys. J.* **78,** 1606–1619
28. Dam, J., Velikovsky, C. A., Mariuzza, R. A., Urbanke, C., and Schuck, P. (2005) Sedimentation velocity analysis of heterogeneous protein-protein interactions: Lamm equation modeling and sedimentation coefficient distributions *c*(*s*). *Biophys. J.* **89,** 619–634
29. Rezabkova, L., Man, P., Novak, P., Herman, P., Vecer, J., Obsilova, V., and Obsil, T. (2011) Structural basis for the 14-3-3 protein-dependent inhibition of the regulator of G protein signaling 3 (RGS3) function. *J. Biol. Chem.* **286,** 43527–43536
30. Young, M. M., Tang, N., Hempel, J. C., Oshiro, C. M., Taylor, E. W., Kuntz, I. D., Gibson, B. W., and Dollinger, G. (2000) High throughput protein fold identification by using experimental constraints derived from intramolecular cross-links and mass spectrometry. *Proc. Natl. Acad. Sci. U.S.A.* **97,** 5802–5806
31. Konarev, P. V., Volkov, V. V., Petoukhov, M. V., and Svergun, D. I. (2006) ATSAS 2.1, a program package for small-angle scattering data analysis. *J. Appl. Crystallogr.* **39,** 277–286
32. Konarev, P. V., Volkov, V. V., Sokolova, A. V., Koch, M. H. J., and Svergun, D. I. (2003) PRIMUS: a Windows PC-based system for small-angle scattering data analysis. *J. Appl. Crystallogr.* **36,** 1277–1282
33. Svergun, D. I. (1992) Determination of the regularization parameter in indirect-transform methods using perceptual criteria. *J. Appl. Crystallogr.* **25,** 495–503
34. Svergun, D. I. (1999) Restoring low resolution structure of biological macromolecules from solution scattering using simulated annealing. *Biophys. J.* **76,** 2879–2886
35. Volkov, V. V., and Svergun, D. I. (2003) Uniqueness of *ab initio* shape determination in small-angle scattering. *J. Appl. Crystallogr.* **36,** 860–864
36. Rashidi, H. H., Bauer, M., Patterson, J., and Smith, D. W. (1999) Sequence motifs determine structure and Ca++-binding by EF-hand proteins. *J. Mol. Microbiol. Biotechnol.* **1,** 175–182
37. Lewit-Bentley, A., and Réty, S. (2000) EF-hand calcium-binding proteins. *Curr. Opin. Struct. Biol.* **10,** 637–643
38. Engen, J. R. (2009) Analysis of protein conformation and dynamics by hydrogen/deuterium exchange MS. *Anal. Chem.* **81,** 7870–7875
39. Iacob, R. E., and Engen, J. R. (2012) Hydrogen exchange mass spectrometry: are we out of the quicksand? *J. Am. Soc. Mass Spectrom.* **23,** 1003–1010
40. Gibson, R. P., Gloster, T. M., Roberts, S., Warren, R. A., Storch de Gracia, I., García, A., Chiara, J. L., and Davies, G. J. (2007) Molecular basis for trehalase inhibition revealed by the structure of trehalase in complex with potent inhibitors. *Angew Chem. Int. Ed. Engl.* **46,** 4115–4119

41. Rittinger, K., Budman, J., Xu, J., Volinia, S., Cantley, L. C., Smerdon, S. J., Gamblin, S. J., and Yaffe, M. B. (1999) Structural analysis of 14-3-3 phosphopeptide complexes identifies a dual role for the nuclear export signal of 14-3-3 in ligand binding. *Mol. Cell* **4,** 153–166
42. Yaffe, M. B., Rittinger, K., Volinia, S., Caron, P. R., Aitken, A., Leffers, H., Gamblin, S. J., Smerdon, S. J., and Cantley, L. C. (1997) The structural basis for 14-3-3:phosphopeptide binding specificity. *Cell* **91,** 961–971
43. Obsil, T., Ghirlando, R., Klein, D. C., Ganguly, S., and Dyda, F. (2001) Crystal structure of the 14-3-3ζ:serotonin *N*-acetyltransferase complex. a role for scaffolding in enzyme regulation. *Cell* **105,** 257–267
44. Ottmann, C., Marco, S., Jaspert, N., Marcon, C., Schauer, N., Weyand, M., Vandermeeren, C., Duby, G., Boutry, M., Wittinghofer, A., Rigaud, J. L., and Oecking, C. (2007) Structure of a 14-3-3 coordinated hexamer of the plant plasma membrane H^+-ATPase by combining x-ray crystallography and electron cryomicroscopy. *Mol. Cell* **25,** 427–440
45. Yang, X., Lee, W. H., Sobott, F., Papagrigoriou, E., Robinson, C. V., Grossmann, J. G., Sundström, M., Doyle, D. A., and Elkins, J. M. (2006) Structural basis for protein-protein interactions in the 14-3-3 protein family. *Proc. Natl. Acad. Sci. U.S.A.* **103,** 17237–17242
46. Eswar, N., Webb, B., Marti-Renom, M. A., Madhusudhan, M. S., Eramian, D., Shen, M. Y., Pieper, U., and Sali, A. (2007) Comparative protein structure modeling using MODELLER. *Curr. Protoc. Protein Sci.* **50,** 2.9.1–2.9.31.
47. Wilson, M. A., and Brunger, A. T. (2000) The 1.0 Å crystal structure of Ca^{2+}-bound calmodulin: an analysis of disorder and implications for functionally relevant plasticity. *J. Mol. Biol.* **301,** 1237–1256